

2007-12

Spikes, Synchrony, and Attentive Learning by Laminar Thalamocortical Circuits

<https://hdl.handle.net/2144/1961>

"Downloaded from OpenBU. Boston University's institutional repository."

Spikes, synchrony, and attentive learning by laminar thalamocortical circuits

Stephen Grossberg and Massimiliano Versace¹

Department of Cognitive and Neural Systems
Center for Adaptive Systems
Center for Excellence in Education, Science, and Technology
Boston University
677 Beacon Street, Boston, MA 02215, USA

Submitted: December 7, 2007
CAS/CNS Technical Report 2007-023

All correspondence should be addressed to
Professor Stephen Grossberg
Department of Cognitive and Neural Systems
Boston University
677 Beacon Street
Boston, MA 02215
Phone: 617-353-7858
Fax: 617-353-7755
Email: steve@bu.edu

Keywords: attention; learning; STDP; bottom-up filter; top-down expectation; match; prediction; mismatch; LGN; pulvinar; V1; V2; spikes; gamma oscillations; beta oscillations; synchronization; local field potentials; mismatch negativity; acetylcholine; cortical layers; Adaptive Resonance Theory

¹ Authors in alphabetical order. MV was supported in part by the Air Force Office of Scientific Research (AFOSR F49620-01-1-0397), the National Science Foundation (NSF SBE-0354378), and the Office of Naval Research (ONR N00014-01-1-0624). SG was supported in part by the National Science Foundation (NSF SBE-0354378) and the Office of Naval Research (ONR N00014-01-1-0624).

Copyright © 2007

Permission to copy without fee all or part of this material is granted provided that: 1. The copies are not made or distributed for direct commercial advantage; 2. the report title, author, document number, and release date appear, and notice is given that copying is by permission of the BOSTON UNIVERSITY CENTER FOR ADAPTIVE SYSTEMS AND DEPARTMENT OF COGNITIVE AND NEURAL SYSTEMS. To copy otherwise, or to republish, requires a fee and / or special permission.

ABSTRACT

This article develops the Synchronous Matching Adaptive Resonance Theory (SMART) neural model to explain how the brain may coordinate multiple levels of thalamocortical and corticocortical processing to rapidly learn, and stably remember, important information about a changing world. The model clarifies how bottom-up and top-down processes work together to realize this goal, notably how processes of learning, expectation, attention, resonance, and synchrony are coordinated. The model hereby clarifies, for the first time, how the following levels of brain organization coexist to realize cognitive processing properties that regulate fast learning and stable memory of brain representations: single cell properties, such as spiking dynamics, spike-timing-dependent plasticity (STDP), and acetylcholine modulation; detailed laminar thalamic and cortical circuit designs and their interactions; aggregate cell recordings, such as current-source densities and local field potentials; and single cell and large-scale inter-areal oscillations in the gamma and beta frequency domains. In particular, the model predicts how laminar circuits of multiple cortical areas interact with primary and higher-order specific thalamic nuclei and nonspecific thalamic nuclei to carry out attentive visual learning and information processing. The model simulates how synchronization of neuronal spiking occurs within and across brain regions, and triggers STDP. Matches between bottom-up adaptively filtered input patterns and learned top-down expectations cause gamma oscillations that support attention, resonance, and learning. Mismatches inhibit learning while causing beta oscillations during reset and hypothesis testing operations that are initiated in the deeper cortical layers. The generality of learned recognition codes is controlled by a vigilance process mediated by acetylcholine.

SUGGESTED SECTION

Computational and Theoretical Neuroscience

1. INTRODUCTION

1.1 The link between learning, expectation, attention, resonance, and synchrony

This article proposes how the brain coordinates multiple levels of thalamocortical and corticocortical processing to rapidly learn, and stably remember, important information about the world. The Synchronous Matching Adaptive Resonance Theory (SMART) model that is presented here shows how bottom-up and top-down pathways work together to accomplish this goal by coordinating processes of learning, attention, expectation, resonance, and synchrony. In particular, SMART explains how attentive learning requirements are realized by detailed brain circuits, notably the layered organization of cells in neocortical circuits and how they interact with first-order (e.g., the lateral geniculate nucleus, LGN) and higher-order (e.g., the pulvinar nucleus, PULV; Sherman and Guillery, 2001; Shipp, 2003), and nonspecific thalamic nuclei (van Der Werf et al., 2002).

Corticothalamocortical pathways work in parallel with corticocortical routes (Maunsell and Van Essen, 1991; Salin and Bullier, 1995; Sherman and Guillery, 2002). Specific first-order thalamic nuclei relay sensory information to the cerebral cortex, whereas specific second-order thalamic nuclei receive their main input from layer 5 of lower-order cortical areas and relay this information to higher-order cortical areas (Sherman and Guillery, 2002, Figure 1a).

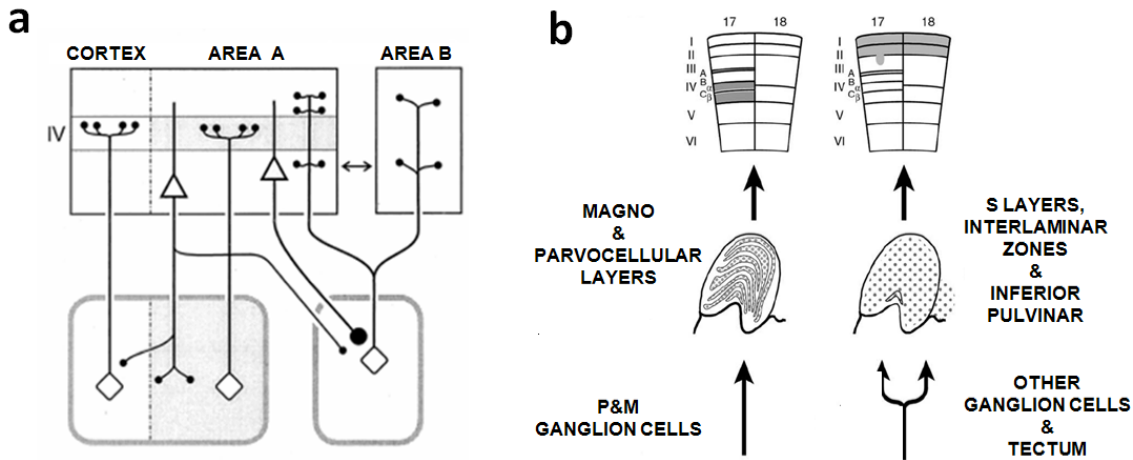


Figure 1 (a) A cortical area A receives thalamocortical inputs from the corresponding thalamic sector (thalamocortical neuron in the gray zone). Layer 6 neurons from cortical area A send modulatory feedback projections (small endings) to the corresponding and to nearby thalamic sectors, as well as a modulatory projection to the thalamic nucleus of a higher-order thalamocortical loop (area B), where driving connections (giant endings) originating in layer 5 neurons of cortical area A are found. These driving connections can activate the thalamocortical pathway to layer IV in area B. This corticothalamocortical indirect pathway supplements the direct corticocortical pathway (double-headed arrow) from A to B. Dashed lines correspond to the border of each thalamocortical loop. [Modified and reprinted with permission from Rouiller and Welcher (2000)]. (b) Schematic views of the diffuse and specific subcortical inputs that terminate in the matrix and core compartments of the dorsal lateral geniculate nuclei of macaque monkeys, and the layer-specific and diffuse or focused projections of these compartments to the cerebral cortex. Cortical areas are indicated by schematic vertical sections with the layers indicated. [Modified and reprinted with permission from Jones (2002)].

The SMART model clarifies how a *match* at the specific first-order and higher-order thalamic nuclei may induce fast learning and stable memory of neural representations in the thalamocortical system (cf., Gove et al., 1995; Grossberg, 1980, 2003). Such a match may occur, for example, at LGN cells in response to bottom-up driving retinal inputs and top-down modulatory expectations from layer 6 of cortical area V1 (Sillito et al., 1994). At a higher level of brain organization, a match may occur at

pulvinar cells in response to driving bottom-up inputs from layer 5 of V1 (Rockland et al., 1999) and top-down modulatory cortical inputs from layer 6 of V2. The model proposes how this bottom-up/top-down matching process can allow bottom-up and top-down feedback loops to cause a persistent resonant state which supports spike synchronization in the gamma frequency range (20 – 70 Hz). Such an oscillation frequency is fast enough to support spike-timing-dependent plasticity (STDP; Levy and Steward, 1983; Markram et al., 1997; Bi and Poo, 2001), since STDP is maximal when pre-synaptic and post-synaptic cells fire within 10-20 ms of each other (Taub et al., 1998; Wespata et al., 2004). In contrast, during a mismatch, slower beta frequency (4 – 20 Hz) oscillations are caused. STDP is disabled at this lower frequency. The model hereby proposes how thalamocortical matching, resonant feedback, synchronous oscillations, and STDP learning may be coordinated, notably how match-sensitive differences in oscillation frequency can enable or disable learning.

The matching process is carried out by a top-down, modulatory on-center, off-surround circuit (Carpenter and Grossberg, 1987; Grossberg, 1995, 1999) which selects a *critical feature pattern* of attended features, while inhibiting unattended features. This process clarifies how attention carries out a form of “biased competition” (Desimone, 1998). The attended feature patterns are the ones that can be rapidly learned in the adaptive weights of bottom-up adaptive filters and top-down expectations. In the case of a partial mismatch, there may simultaneously be cells at which matching and learning occurs, as well as other cells at which mismatch, inhibition, and suppression of learning occurs. Thus, in describing match vs. mismatch states, one needs to understand that there may be cells at which bottom-up and top-down signals mismatch, even though there is a good enough partial match for a synchronous resonant state to persist long enough for STDP to occur at the matched features.

If a mismatch between bottom-up and top-down signal patterns is large enough, it prevents such a synchronous resonant state from developing. Within the model, resonance is prevented when mismatch causes a rapid *reset* of ongoing information processing, and triggers a memory search, or hypothesis testing, for uncommitted cells, or an already familiar recognition category, that can better match bottom-up data. In particular, such a memory search can either enable a totally new recognition category to be learned, or a learned refinement of the critical features that can activate an already familiar recognition category. Thus, the model proposes that there are cycles of resonance and reset, with resonance supporting learning, and reset driving hypothesis testing that leads away from poorly matched states to better ones.

Such a memory search is controlled by an interaction between specific thalamic nuclei, nonspecific thalamic nuclei, and the cerebral cortex. Nonspecific thalamic nuclei, such as the midline and intralaminar nuclei (van der Werf et al., 2002), as well as “matrix” cells in the specific thalamic nuclei (Jones, 2002), derive their name from the fact that they receive diffuse innervations from the sensory periphery and the reticular formation, and project diffusely to the superficial layers of the cerebral cortex (Figure 1b).

In particular, the nonspecific thalamic nuclei are responsible for generating reset signals during mismatch episodes. The model (Figures 2 and 3) suggests how a big enough mismatch at a specific thalamic nucleus can generate a novelty-sensitive burst of activation at a nonspecific thalamic nucleus. This burst is broadcast nonspecifically to the superficial layers of the cerebral cortex, notably layer 1. The nonspecific burst is sensed by dendrites in layer 1 of cortical layer 5 cells. The model explains how the burst leads to a reset event by propagating from layer 1 dendrites via their layer 5 cells to layer 6 and then on to layer 4, shutting down previously active cells there, and thereby enabling a different pattern of activation to take hold in layer 4. It is this reset event that causes the slower beta oscillation frequency. Thus the reset event prevents learning of poorly matched bottom-up and top-down information, both by inhibiting the active learned categorical representations whose top-down

expectations led to the mismatch, and also by creating a slower oscillation frequency to which STDP is insensitive. The details of how this works will be described below.

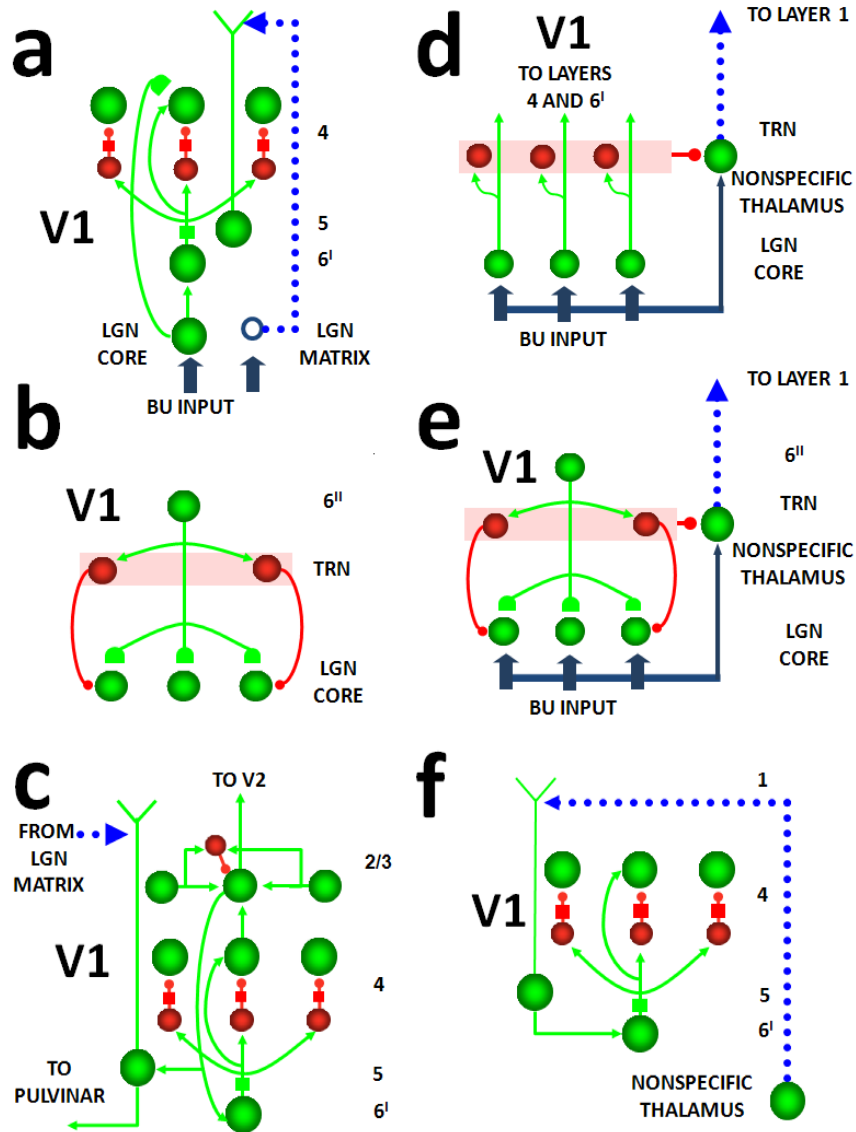


Figure 2 (a) LGN core cells in the specific pathway activate layer 4. LGN core cells also send axons to layer 6' cells, and thereby also activate layer 4 via a 6'→4 modulatory on-center, off-surround network that implements divisive contrast normalization of LGN inputs in layer 4. Layer 4 cells, in turn, activate cells in layer 2/3. In parallel, LGN matrix cell activation in the nonspecific pathway primes layer 5 cortical cells via excitatory connections to cortical layer 1, where layer 5 apical dendrites terminate. Layer 5 cells fire only when *both* matrix cells and layer 2/3 cells fire. Matrix cells hereby enable layer 5 cells to fire in response to layer 2/3 inputs, thereby closing the intracortical 4→2/3→5→6'→4 resonant loop while activating driving inputs from layer 5 to the PULV. **(b)** Top-down feedback from V1 layer 6'' has a dual effect on LGN core cells: excitation via adaptive synapses (hemi-disks at ends of axonal pathways) and broad inhibition via the thalamic reticular nucleus (TRN) pathway. **(c)** Layer 2/3 cell outputs feed back to layer 5 cells, which can fire if matrix cells also input to the layer 1 apical dendrites of layer 5 cells. Layer 5 cell firing can, in turn, activate layer 6' cells that activate layer 4 cells. Matrix cells hereby enable layer 5 cells to close the intracortical 4→2/3→5→6'→4 resonant loop, even while they activate driving inputs from layer 5 to the PULV. **(d)** During bottom-up processing, bottom-up inputs send convergent excitatory signals to the nonspecific thalamus. In parallel, LGN core cells send specific inputs to layers 4 and 6' of the cortex, as well as to TRN cells. The TRN cells, in turn, send convergent inhibition to the nonspecific thalamus. During bottom-up processing, the total excitatory and inhibitory signals are balanced, so that the nonspecific thalamus is not activated by the bottom-up input. **(e)** During top-down matching, layer 6'' cells excite TRN cells which, in turn, send

inhibitory signals via a broad off-surround to LGN core cells. This inhibition helps to prevent cells that receive only bottom-up or top-down signals from firing, but not cells that receive both. Only LGN cells that receive *matching* bottom-up input and top-down cortical feedback cross the spiking threshold and propagate their activity to V1, while also (see (d)) exciting the TRN and inhibiting the nonspecific thalamus. (f) If a bottom-up/top-down mismatch is too great, then the decrease of LGN excitation reduces TRN inhibition to the nonspecific thalamus. The firing rate of the nonspecific thalamus hereby increases, which propagates via the apical dendrites of layer 5 cortical cells to cause a reset of active coding cells in layer 4 (see text).

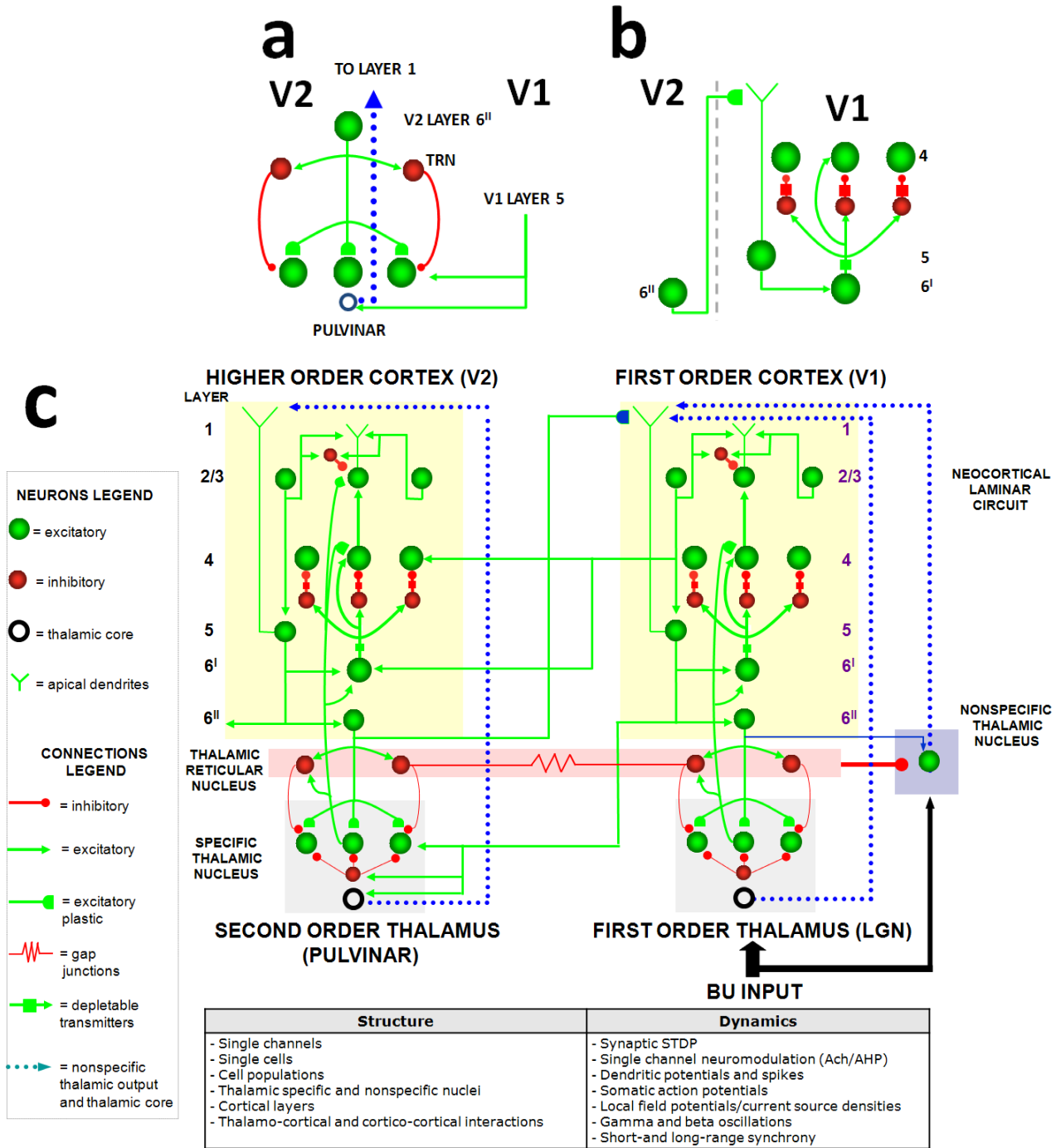


Figure 3 (a) Layer 5 of V1 provides a driving bottom-up input to the pulvinar (PULV), which is matched against top-down signals from layer 6'' of V2. This circuit is homologous to the bottom-up driving input from the retina to the LGN, which is

matched against top-down signals from layer 6^{II} of V1 (see Figure 2). Layer 5 of V1 also excites PULV matrix cells, which provide nonspecific priming input to layer 5 cells in V2. **(b)** Layer 6^{II} of V2 also provides top-down corticocortical feedback to layer 4 of V1 via layer 1 apical dendrites of layer 5 cells that project to layer 6^I and then to 4 via a modulatory on-center, off-surround circuit. **(c)** The entire SMART model circuit includes thalamic nuclei and laminar cortical circuits. The thalamus is subdivided into specific first-order and second-order nuclei, nonspecific nucleus, and thalamic reticular nucleus (TRN). The first-order thalamic matrix cells (1 cell population at each specific thalamic nucleus, shown as an open ring) provide nonspecific excitatory priming to layer 1 in response to bottom-up input, priming layer 5 cells and allowing them to respond to layer 2/3 input. This allows layer 5 to close the intracortical loop and activate the PULV. V1 layer 4 receives inputs from two parallel bottom-up thalamocortical pathways: a direct LGN→4 excitatory input, and a 6^I→4 modulatory on-center, off-surround network that contrast-normalizes the pattern of layer 4 activation via the recurrent 4→2/3→5→6^I→4 loop. V1 activates the bottom-up V1→V2 corticocortical pathways from V1 layer 2/3 to V2 layers 6^I and 4, as well as the bottom-up corticothalamocortical pathway from V1 layer 5 to the PULV, which projects to V2 layers 6^I and 4. In V2, as in V1, the layer 6^I→4 pathway provides divisive contrast normalization to V2 layer 4 cells. Corticocortical feedback from V2 layer 6^{II} reaches V1 layer 1, where it activates apical dendrites of layer 5 cells. Layer 5 cells, in turn, activate the modulatory 6^I→4 pathway in V1, which projects a V1 top-down expectation to the LGN. TRN cells of the two thalamic sectors are linked via gap junctions, which synchronize activation across the two thalamocortical sectors when processing bottom-up stimuli. The nonspecific thalamic nucleus receives convergent bottom-up excitatory input from specific thalamic nuclei and inhibition from the TRN, and projects to layer 1 of the laminar cortical circuit, where it regulates mismatch-activated reset and hypothesis testing in the cortical circuit (see text). Corticocortical feedback connections from layer 6^{II} of the higher cortical area terminate in layer 1 of the lower cortical area, whereas corticothalamic feedback from layer 6^{II} terminates in its specific thalamus and on the TRN. This corticothalamic feedback is matched against bottom-up input in the specific thalamus.

As noted above, the model predicts that the reset event is expressed in the deeper layers of cerebral cortex, such as layers 4 to 6, and may thereby initiate slower beta oscillations in these layers. The more superficial cortical layers (e.g., layers 2/3) may, in contrast, express more fast gamma oscillations. The model supports its proposal about how match-sensitive differences in oscillation frequency can enable or disable learning by quantitatively simulating data about single cell biophysics, pharmacology, and neurophysiology; laminar neuroanatomy; aggregate cell recordings, such as current-source densities and local field potentials; large-scale oscillations at beta and gamma frequencies; and functionally links them all to requirements about how to achieve fast attentive learning and stable memory.

Many authors have examined synchronous oscillations within and across brain regions as one way in which behaviorally significant brain states are organized (Engel et al., 2001). Aggregate and single-cell recordings from multiple thalamic and cortical levels of mammals have shown high-frequency and low-frequency rhythmic synchronous activity correlated with cognitive, perceptual and behavioral tasks. In addition, large-scale neuronal population models have been proposed to model oscillatory dynamics (Bazhenov et al., 1998; Lumer et al., 1997; Destexhe *et al.*, 1999; Siegel et al., 2000). However, these models do not link brain spikes, oscillations, and self-stabilizing STDP, with the brain states that subserve attentive cognitive information processing.

The SMART model fills this gap. It clarifies data about how bottom-up processing and learned tuning of adaptive filters is modulated by top-down attentive learned expectations that embody predictions or hypotheses that focus attention on expected bottom-up stimuli (Salin and Bullier, 1995; Engel et al., 2001; Gao and Suga, 1998; Krupa et al., 1999; Desimone, 1998; Ahissar and Hochstein, 2002; Hermann et al., 2004). These data support predictions of Adaptive Resonance Theory, or ART (Grossberg, 1980, 2003; Carpenter and Grossberg, 1987, 1993) that top-down expectations regulate predictive coding and matching and thereby help to focus attention, synchronize and gain-modulate attended feature representations, and trigger fast learning that is dynamically buffered against catastrophic forgetting. The goal of achieving fast stable learning without catastrophic forgetting is often summarized as the *stability-plasticity dilemma* (Grossberg, 1980).

Recent ART models, called LAMINART, have begun to show how ART predictions may be embodied in laminar cortical circuits (Grossberg, 1999, 2003; Raizada and Grossberg, 2003). The SMART model goes further in three directions, two of them already mentioned: anatomically, it explains and simulates how laminar cortical circuits may interact with specific primary and higher-order thalamic nuclei and nonspecific thalamic nuclei; neurophysiologically, it incorporates spiking dynamics that clarify how synchronous oscillations and their oscillation frequencies can provide an additional degree of freedom for controlling cognitively-mediated operations such as matching and learning processes; and neuropharmacologically, it proposes how acetylcholine-based processes may embody predicted properties of *vigilance control* that regulate the generality of learned recognition categories in a way that is sensitive to changing environmental statistics, using only locally computed signals in the network.

What is vigilance and why is it needed? It is not enough to just regulate the stability of learned memories in a changing world. Survival requires that a human or animal learn to correctly discriminate, recognize, and predict important objects and events. An effective learner must thus be sensitive to changing environmental statistics and feedback that determine how specific or general our learned knowledge needs to be for us to effectively control and predict its environment. How does the brain determine how specific (concrete) or general (abstract) a learned recognition category should be in a given situation? If matches trigger learning, then a flexible, situationally-sensitive, criterion of matching is needed to control specific vs. general learning. Such a criterion has been called *vigilance* (Carpenter and Grossberg, 1987, 1991), corresponding to the intuition that higher vigilance enables finer discriminations to be made. In all ART models, including SMART, high vigilance triggers reset and search for a new category when even small mismatches occur, thereby leading to concrete learning. Low vigilance allows even coarse matches to trigger resonance, and to thereby learn abstract categories that respond to many input variations. What is new in SMART is the prediction that neuromodulation by acetylcholine (ACh) may regulate the level of vigilance through time.

1.2 Specific and nonspecific interactions control attention, learning, reset, and memory search

The remainder of this section specifies in greater detail how SMART model circuits work. SMART clarifies how retinal inputs activate the thalamus, and from there, the cortex, through two separate pathways, a *specific* pathway targeting middle cortical layers (LGN core cells to layers 4 and 6¹ cells, a subdivision of layer 6, see Table 1), and a *nonspecific* pathway targeting superficial layers (LGN matrix cells and nonspecific thalamic nucleus to layer 1 of V1). These two pathways are treated separately due to the different functional roles that were outlined in the previous section.

1.2.1 The specific pathway. The SMART specific pathway includes both specific first-order and second-order thalamic nuclei projecting to the middle layers of the cerebral cortex (Jones, 2002). Specific thalamic nuclei are often divided into first-order relays, such as the LGN, which receive inputs from the sensory periphery, and second-order relays, which receive their main inputs from the cerebral cortex (Sherman and Guillery, 2002). Although the largest part of the thalamus consists of second-order relays, the most widely studied structures are the first-order thalamic nuclei. As a consequence, thalamic nuclei are usually seen as relay stations of information from the sensory periphery to the cerebral cortex. This picture is misleading. For instance in the LGN, a first-order relay nucleus, the retina contributes only 5-10% of the total afferents (Sherman and Guillery, 2001). The pulvinar (PULV), one of the largest second-order thalamic nuclei, receives only minimal afferents from the sensory periphery. Most of its inputs originate from the cerebral cortex and the superior colliculus (SC). The LGN receives a massive cortical projection from V1 cortical layer 6, and the PULV receives afferents from layers 5 and 6 of several cortical areas (Rockland, 1998; Wang et al., 2002; Shipp, 2003).

Model connections	Type	Functional interpretation	References
First order thalamic relay cells → Layer 4 cells V1	D	Primary thalamic relay cells drive layer 4.	Blasdel and Lund (1983)
First order thalamic relay cells → Layer 6 ^I cells V1	D	Primary thalamic relay cells prime layer 4 via the 6 → 4 modulatory circuit.	Blasdel and Lund (1983) for LGN → 6; LGN input to 6 is weak (Callaway, 1998, pag 56); Layer 5 projects to 6 [Note 1]
First order thalamic relay cells → TRN	D	Recurrent inhibition to primary and secondary thalamic relay cells.	Sherman and Guillery (2001); Jones (2002)
TRN → First order thalamic relay cells	I	Off-surround to primary and secondary thalamic relay cells, synchronization of thalamic relay cells.	Pinault and Deschenes (1998); Sherman and Guillery (2001)
TRN → TRN	I	Normalization of inhibition.	Jones (2002); Sohal and Huguenard (2003)
TRN → TRN	GJ	Synchronize TRN and thalamic relay cells.	Landisman et al. (2002)
TRN → Nonspecific thalamic cells	I	Inhibition of nonspecific thalamic cells, participates in the reset mechanism.	Kolmac and Mitrofanis (1997); van der Werf et al. (2002)
Nonspecific thalamic cells → Layer 5 cells V1	M	To 5 through apical dendrites in 1, participates in the reset mechanism.	van der Werf et al. (2002)
Layer 4 cells V1 → Layer 4 inhibitory interneurons V1	D	Lateral inhibition in layer 4.	Markram et al. (2004)
Layer 4 inhibitory interneurons V1 → Layer 4 cells V1	I	Lateral inhibition in layer 4.	Markram et al. (2004)
Layer 4 inhibitory cells V1 → Layer 4 inhibitory interneurons V1	I	Normalization of inhibition in layer 4.	Ahmed et al. (1997), Markram et al. (2004)
Layer 4 cells V1 → Layer 2/3 cells V1	D	Feedforward driving output from 4 to 2/3.	Fitzpatrick <i>at al.</i> (1985); Callaway and Wiser (1996)
Layer 2/3 cells V1 → Layer 2/3 cells V1	D	Recurrent connections (grouping) in 2/3.	Bosking et al. (1997); Schmidt et al. (1997); Raizada and Grossberg (2003)
Layer 2/3 cells V1 → Layer 2/3 inhibitory interneurons V1	D	Avoid outward spreading (bipole) in 2/3.	McGuire et al. (1991); Raizada and Grossberg (2003)
Layer 2/3 inhibitory cells V1 → Layer 2/3 inhibitory interneurons V1	I	Normalization of inhibition.	Tamas et al. (1998); Raizada and Grossberg (2003)
Layer 2/3 cells V1 → Layer 4 cells V2	D	Feedforward output from cortical Area A to cortical Area B.	Van Essen et al. (1986)
Layer 2/3 cells V1 → Layer 6 ^{II} cells V2	D	Feedforward output from cortical Area A to cortical Area B.	Van Essen et al. (1986)
Layer 2/3 cells V1 → Layer 5 cells V1	D	Conveys layer 2/3 output to layer 5.	Callaway and Wiser (1996)
Layer 2/3 cells V1 → Layer 6 ^{II} cells V1	D	Conveys layer 2/3 output to layer 6 ^{II} .	Callaway (1998)
Layer 5 cells V1 → Pulvinar	D	Feedforward connections from cortical Area A to cortical Area B through secondary thalamic relay neurons.	Sherman and Guillery (2001).
Layer 5 cells V1 → Layer 6 ^I cells V1	D	Delivers corticocortical feedback to the 6 ^I → 4 circuit from higher cortical areas, sensed at the apical dendrites of 5	Callaway (1998); Callaway and Wiser (1996, “class B” cells) [Note 2]

		branching in 1.	
Layer 6 ^I cells V1 → Layer 4 cells V1	M	On-center to 4. Mediated by habituated synapses.	Stratford et al. (1996); Callaway (1998); Raizada and Grossberg (2003)
Layer 6 ^I cells V1 → Layer 4 inhibitory interneurons V1	D	Off-surround to 4.	McGuire et al. (1984); Ahmed et al. (1997); Callaway (1998);
Layer 6 ^{II} cells V1 → First order thalamic relay cells	M	On-center to primary thalamic relay cells.	Sillito et al. (1994); Callaway (1998);
Layer 6 ^{II} cells V1 → TRN	D	Off-surround to primary thalamic relay cells mediated by thalamic TRN.	Guillery and Harting (2003); Sherman and Guillery (2001).
Layer 6 ^{II} cells V2 → Layer 5 cells V1 → Layer 6 ^{II} cells V1→ Layer 4 cells V1	M	Intercortical feedback from 6 ^{II} Area B to 1 area A, where it synapses on layer 5 cells apical dendrites branching in 1, resulting in subliminal priming of layer 4 cells via 5 → 6 ^I → 4 on-center/off-surround circuit.	Rockland and Virga (1989); Salin and Bullier (1995)

Table 1 Major simulated anatomical pathways. Abbreviations: **TRN** = thalamic reticular nucleus; **D** = driving connections; **M** = modulatory connections; **I** = inhibitory connections; **GJ** = gap junctions. **[Note 1]:** Callaway (1998) subdivides cortical layer 6 neurons in 3 classes: *Class I*: project to 4C, also receive input from LGN, and project to LGN; *Class IIa*: dendrites in layer 6, receive projections from 2/3, project back to 2/3 with modulatory connections; *Class IIb*: dendrites in 5, project exclusively to deep layers (5 and 6) and claustrum. In the model, these populations are clustered in 2 classes, layer 6^I and 6^{II}, which provide feedback to thalamic relay cells and layer 4, respectively. **[Note 2]:** Callaway (1998) subdivides Layer 5 neurons in 3 classes: *Class A*: dendrites in 5, axons from 2/3, project back to 2/3 with modulatory connections; *Class B*: dendrites in 5, axons from 2/3, project laterally to 5 and the pulvinar; *Class C*: dendrites in 1, project to SC. In the model, layer 5 neurons receive input from 2/3 (Classes A and B), as well modulatory input from nonspecific thalamic nucleus (Class C, apical dendrites in layer 1), and provides output to 6^I and second-order thalamic nuclei.

In the primate, synaptic terminals in the thalamus can be roughly subdivided into two classes (Rockland, 1996; Sherman and Guillery, 2001): (a) round-large (RL) synapses, such as retinogeniculate synapses. These synapses are believed to be driving; (b) round-small (RS) terminations, such as the corticothalamic synapses from V1 layer 6 to the LGN. These synapses are believed to be modulatory. Terminations arising from layer 5 to a second-order thalamic nucleus are similar to retinogeniculate RL synapses, or driving, connections, often found in more proximal segments of the dendrites. This dual pattern of connectivity seems to be constant across species (Rouiller and Welcher, 2000). A functional correlate of the distinction between RL and RS synapses is that, whereas lesioning a cortical area that innervates the thalamus through layer 6 alone does not change the receptive field property of the thalamic cell, lesioning an area that innervates the thalamus through layer 5 *does* abolish the receptive field of the cell (in, for example, areas 17, 18 and 19; Sherman and Guillery, 2002). In addition, the observed receptive fields in the PULV resemble those of complex cells in visual cortex (binocular and direction selective).

In the SMART specific pathway, LGN core cells are driven by bottom-up sensory inputs and excite both layer 4 and layer 6^I (Figure 2a). Layer 6^I, in turn, contrast-normalizes layer 4 cell activities in response to bottom-up input patterns (Grossberg, 1980; Heeger, 1992) via a modulatory on-center, driving off-surround network (Carpenter and Grossberg, 1987; Grossberg, 1980, 2003) whose off-surround is mediated by layer 4 inhibitory interneurons (Grieve and Sillito, 1991). The direct pathway from LGN to layer 4 enables the cortex to fire despite the modulatory nature of the on-center from layer 6^I to 4. The on-center off-surround of the LGN→6^I→4 pathway biases the emergence of orientation sensitivity in layer 4 cells that spike after the arrival of the LGN input within the STDP learning window (see Section 2.1).

Top-down feedback pathways coexist with bottom-up pathways in the brain. SMART proposes that top-down feedback from layer 6^{II} of V1 to the LGN controls attention and plasticity in both the

bottom-up adaptive filter pathways from LGN to V1 and in the top-down expectation pathways (Figure 2b). As in previous ART models, SMART corticothalamic feedback is realized by a top-down, modulatory on-center, driving off-surround circuit whose on-center helps to create an attentional focus that selects and enhances behaviorally relevant, bottom-up sensory inputs (match), and whose off-surround suppresses inputs that are irrelevant (mismatch).

The processing that goes on between LGN and V1 has homologs in the processing by PULV and V2, and beyond. Bottom-up driving inputs to higher-order specific thalamic nuclei, such as the PULV, arise from layer 5 of V1, as indicated in Figure 3a (Salin and Bullier, 1995; Callaway, 1998). Top-down feedback from layer 6^{II} (see Table 1) of V2 to PULV can match the bottom-up input pattern from V1 layer 5 in a manner similar to how top-down feedback from layer 6^{II} of V1 matches retinal input in the LGN (Figures 3a and 2a, respectively).

Accumulating experimental evidence supports the ART prediction (Carpenter and Grossberg, 1987; Grossberg 1980, 1999, 2003) that that top-down attentional signals are mediated by a modulatory on-center, off-surround network. Both V2→V1 feedback (Bullier et al., 1988) and V1→LGN feedback (Sillito et al., 1994) possess this structure. A similar modulatory on-center, off-surround architecture has been observed in feedback interactions from auditory cortex to the medial geniculate nucleus (MGN) and the inferior colliculus (IC) (Zhang et al., 2004; Gao and Suga, 1998). Consistent with the ART prediction of the role of attention in controlling adult plasticity, Gao and Suga (1998) found that acoustic stimuli caused plastic changes in the IC of bats only when the IC received top-down feedback from auditory cortex. Moreover, plasticity is enhanced with behaviorally relevant auditory stimuli, consistently with the ART proposal that top-down feedback allows matched, and therefore attended, critical feature patterns to be learned, while suppressing mismatched, and thus unattended, features. Nicolelis and colleagues have shown that cortical feedback also controls thalamic plasticity in the somatosensory system (Krupa et al., 1999).

ART also predicted that matching synchronizes the firing patterns of cells coding matched stimuli and thereby facilitates fast stable learning (cf., Engel et al., 2001; Fries et al., 2001; Grossberg, 1976, 1980, 1999; Pollen, 1999; Usrey, 2002). SMART further develops that proposal to include spiking neurons and the role of the higher-order specific and nonspecific thalamic nuclei.

SMART clarifies how the thalamic reticular nucleus (TRN) mediates the off-surround that helps to select thalamic cells during the matching process (Figure 2b). The TRN forms a shell around the lateral and dorsal portions of the thalamus, lying in the axonal path connecting the specific and nonspecific thalamus and the cortex (Guillery and Harting, 2003). Afferents to the TRN are mainly branches of bottom-up axons from a specific thalamus to its target cortex, or branches of top-down axons from cortical layer 6 to its specific thalamic nucleus. Notably, the TRN does not receive projections from layer 5. The TRN has a rather uniform local structure. TRN cells are GABAergic, and are reciprocally linked both by chemical inhibitory projections and by electrical synapses (Landisman et al., 2002). Top-down inhibitory feedback from the TRN to specific thalamic nuclei helps to balance top-down cortical layer 6 excitatory signals at their shared target cells (Figures 2b and 3a), and thereby enables the excitatory signals to have only a modulatory effect on these cells (Guillery and Harting, 2003) when these are the only active inputs. In addition to projecting to first-order and higher-order specific thalamic nuclei (Guillery and Harting, 2003), the TRN also projects to the nonspecific intralaminar and midline thalamic nuclei (Kolmac and Mitrofanis, 1997); see Figures 2e and 3c. TRN projections to the intralaminar and midline nuclei are more diffuse than the reticular projection to the specific dorsal thalamic nuclei. The TRN influences the sleep/wake cycle (Steriade et al., 1993), the efficacy of thalamic inputs to the cortex (Nicolelis and Fanselow, 2002; Swadlow et al., 2002), and attention (Sherman and Guillery, 2001).

Both V1 layer 2/3 and PULV inputs are required to fully activate the SMART V2 area. V1 layer 2/3 and PULV can drive V2 layer 4, which in turns activates V2 layers 2/3, 5 and 6^{II}, whose axons project to the PULV, where V1 input from layer 5 is attentively matched against the layer 6^{II} feedback (Figures 3a and 3c). Layer 5 of V1 excites the matrix cells (see below), whose input is necessary for V2 layer 5 cells to close the intracortical resonant loop in V2 that is capable of driving fast self-stabilizing learning in V2; see Section 1.2.2.

V2 layer 6^{II} can also influence attentive top-down corticocortical feedback to layer 4 of V1 via layer 1 apical dendrites of layer 5 cells that project to layer 6^I and then to 4 via a modulatory on-center, off-surround circuit (Figure 3b). See Section 2.2 for simulation results.

In summary, the SMART specific pathway is responsible for attentively matching bottom-up and top-down information in the specific thalamus, and creating attentive resonant states that can support fast stable learning of bottom-up oriented filters and top-down oriented modulatory expectations. When the specific pathway interacts with the nonspecific pathway, it can also experience reset and memory search for better matching filters and expectations, as the following section clarifies.

1.2.2 The nonspecific pathway. The thalamic nonspecific pathway includes both the “matrix” cells in the specific thalamic nuclei (Figure 2a; Jones, 2002) and the nonspecific thalamic nuclei (Figures 2d-2f). Both pathways project to the superficial layers of the cerebral cortex. The term *nonspecific*, as opposed to *specific*, thalamic nuclei (both first-order and second-order nuclei), refers to the midline thalamic and the intralaminar nuclei. The term *nonspecific* derives from three characteristics of these nuclei, namely: (1) their diffuse innervation from pontine, medullary and mesencephalic reticular formation; (2) the signature of their stimulation in the cortical mantle (somnolence for low-frequency stimulation, arousal for high-frequency); and (3) the anatomical observation that they project to cerebral cortex in a fairly uniform fashion (Van der Werf et al., 2002). Most of the nonspecific thalamic nuclei are characterized by a high degree of convergent cortical input, widespread projections to large portions of neocortical layer 1, inhibition from the thalamic reticular nucleus (TRN), and strong neuromodulatory input from several brainstem centers (Van der Werf et al., 2002).

Neuropsychological and neurological evidence has demonstrated the importance of the intralaminar and midline nuclei for cortical functioning (Llinas and Pare, 1991; Llinas et al., 2002). Midline lesions of the thalamus affect general cognition, resulting in lethargy or coma (Facon et al., 1958) or unilateral hemineglect (Heilman et al., 1993), despite the fact that the specific sensory stimuli are relayed to the cortex.

Recent studies have shed additional light on the dichotomy between specific and nonspecific thalamic nuclei, showing how the distinction between patterns of cortical termination (superficial vs. deep layers) not only characterizes cells between nuclei, but also cells within specific thalamic nuclei. Cytological studies on thalamocortical relay cells in monkeys conducted with the use of immunoreactivity for the calcium binding proteins parvalbumin and calbindin have shown a “core” of parvalbumin-rich cells projecting to the middle layers of their cortical targets, surrounded by a “matrix” of calbindin-rich cells projecting to the superficial layers (Jones, 2002). This matrix extends to all specific thalamic nuclei irrespective of nuclear borders, and differs from the core also by the nature of its input.

Core cells receive subcortical afferents that are highly ordered topographically, and a similarly ordered pattern is maintained at the site of cortical terminations of core cell axons at layer 4 (Jones 2002). Matrix cells receive subcortical input which tends to terminate in multiple thalamic nuclei, show a less precise stimulus-response relationship, have receptive fields that are not easily definable, and project to superficial cortical layers. For instance, in the medial geniculate complex, core cells receive tonotopically-ordered inputs from the central nucleus of the inferior colliculus, representing the most direct ascending pathway from the cochlea. Matrix cells are instead innervated by a less direct

auditory pathway which ascends in the midbrain tegmentum and terminates diffusely in most of the nuclei that form part of the medial geniculate complex. Similar patterns of terminations are repeated in somatosensory and visual sections of the thalamus (ventral posterior complex and dorsal lateral geniculate nucleus, respectively). The results of Jones (2002) suggest that a functional microarticulation similar to the one observed in the specific and nonspecific thalamic nuclei may be mirrored by the core/matrix cell dichotomy in the specific thalamic nuclei.

As noted above, in the SMART model, the matrix cells in the nonspecific pathway provide a priming input that allows the cortical hierarchy to fully process a bottom-up input (Figure 2a). Both the matrix cells and nonspecific thalamic cells in the nonspecific pathway terminate on apical dendrites of layer 5 cells, mirroring the anatomical and functional similarities between matrix cells in specific nuclei and nonspecific thalamic cells (Jones, 2002).

The SMART nonspecific thalamic nucleus is responsible for generating reset signals and memory search during predictive mismatch episodes. The model cell population in this nucleus is excited by converging bottom-up input (Figure 2d), and sends excitatory connections to layer 1 of the cerebral cortex (Jones, 2002; Miller and Benevento, 1979), where its collaterals contact apical dendrites of layer 5 pyramidal cells (Vogt, 1991; Cauller, 1995; Cauller and Connors, 1994, 2001; Larkum et al., 2002, 2004). The nonspecific thalamus is also inhibited by the thalamic reticular nucleus, or TRN (Figure 2e), and the balance between bottom-up excitation and TRN inhibition is controlled by the matching process. If a mismatch is large enough, the decrease of excitation in the LGN due to the misalignment of bottom-up and top-down input will decrease LGN firing and, thus, TRN inhibition to the nonspecific thalamus, while the excitatory bottom-up input will remain unchanged. The total excitatory input to the TRN from layer 6^{II} and LGN is, all else being equal, larger in cases of match, where LGN cells are excited, than in cases of mismatch, where only a subset or no LGN cells are allowed to fire. The net result is an increase in firing rate in the nonspecific thalamus (see Section 2.3) that causes a spatially diffuse arousal burst to layer 1 of the cortex.

How does a spatially diffuse arousal burst from the nonspecific thalamic nucleus *selectively* reset the cortical codes that caused a mismatch? At the moment when a mismatch occurs, the brain does not know which cortical areas caused the predictive failure (Grossberg, 1980). Despite this lack of information in the nonspecific thalamus, the mismatch there needs to be able to selectively reset active representations throughout the cortical hierarchy. SMART proposes, in accord with known anatomical and physiological data both *in vivo* and *in vitro* (Larkum et al., 1999; Larkum and Zhu, 2002), that layer 5 pyramidal cell firing rate is jointly controlled by nonspecific thalamic inputs *and* specific layer 2/3 inputs, thus explaining how layer 5 cells exhibit two distinct firing modes (Williams and Stuart, 1999): Layer 5 cells that receive layer 2/3 inputs *and* nonspecific thalamic inputs during a mismatch episode fire in bursts at high rates (see Section 2.6 for experimental and simulation results). Active 2/3 cells represent cortical codes that caused the mismatch. In contrast, single spikes are produced in layer 5 cells when only one of these sources is activated, either during a match, or during a mismatch when layer 2/3 cells are inactive.

As noted above, layer 5 pyramidal cells send *driving* inputs directly to higher cortices through the thalamus (e.g., the pulvinar; Sherman and Guillery, 2002; Shipp, 2003; see Figure 3a), indirectly control corticothalamic feedback at their own cortical level through layer 6^{II} (Figures 2b and 3a), and also control corticocortical feedback to layer 4 at their own cortical level via layer 6^I (Figure 2c and 3c). Layer 5 can hereby generate widespread bursts of synchronized activity throughout the neocortex mediated by driving layer 5 terminations on higher-order thalamic nuclei (including pathological epileptogenic activity; Williams and Stuart, 1999), and selectively reset multiple cortical areas by relaying from the nonspecific thalamus layer 5 bursts to layer 4 via the 6^I→4 pathway. In particular,

model layer 6^I cells are predicted to respond to a thalamic mismatch with selective cortical reset and search for a more predictive cortical code in layers 4 and 2/3 (see Section 2.6 for simulation results).

The nonspecific pathway may also help to regulate modality-specific attention during reset episodes (Crick, 1984; Guillery et al., 1998; Montero, 1997; Weese et al., 1999). In particular, Crabtree and Isaac (2002) have shown that nonspecific thalamic nuclei which subserve different modalities are linked by mutually inhibitory interactions. SMART simulates how TRN-mediated (van Der Werf et al., 2002) inhibitory interactions (Crabtree and Isaac, 2002) between nonspecific thalamic nuclei can cause a pause in firing of one nonspecific thalamic nucleus that can transiently down-regulate layer 5 pyramidal cells of the competing cortical area (see simulations in Section 2.9). This may allow cortical areas that experience strong predictive mismatches in a given modality to reduce priming of the cortical area of a competing modality by inhibiting the corresponding nonspecific thalamic nucleus. SMART further predicts that competing *specific* nuclei, not only nonspecific nuclei as shown by Crabtree and Isaac (2002), might be inhibited by the TRN in cases of strong mismatches, therefore being a possible thalamic substrate for competitive allocation of attention.

How is the generality of recognition categories regulated to represent statistical properties of the environment? As noted above, ART predicts that resonance and learning occur when the degree of match between bottom-up and top-down representations is greater than a gain parameter, called *vigilance*. Vigilance can change due to internal factors, such as fatigue, or external factors, such as predictive mismatch or punishment. A baseline vigilance determines how big a mismatch is initially tolerated before cortical representations are reset. When a predictive error causes a mismatch to occur, the vigilance level is predicted to increase just enough to drive a memory search for a new recognition code. This process is called *match tracking* (Carpenter and Grossberg, 1987; 1991; Carpenter et al., 1992). Match tracking realizes a kind of minimax learning rule; namely, it enables a learning system to minimize predictive error while maximizing generalization. Choosing a low baseline vigilance leads to the learning of general categories and thus a minimum use of memory resources. Match tracking increases this baseline vigilance just enough to learn the most general categories that are consistent with predictive success.

The SMART model predicts that one way to control vigilance may be to modify the excitability of layer 5 cells during mismatch episodes. Anatomical studies in monkeys, cats and rats have established that the nonspecific thalamus (in particular, the midline and central lateral thalamic nuclei), whose activation is sensitive to the degree of mismatch, projects to the cholinergic nucleus basalis of Meynert (van Der Werf et al., 2002), one of the main source of cholinergic innervations of the cerebral cortex. The nucleus basalis of Meynert is also influenced by noxious stimulation and cortical control (Zhang et al., 2004). Saar et al. (2001) have shown that ACh release reduces the after-hyperpolarization (AHP) current and increases cell excitability in layer 5 cortical cells (see Section 2.8). In SMART, this increased layer 5 excitability due to predictive mismatch may cause reset via the layer 5-to-6^I-to-4 circuit, even in cases where top-down feedback may earlier have partially matched bottom-up input, which is a key property of vigilance control. The increase of ACh might therefore promote search for finer recognition categories in response to environmental feedback, even when bottom-up and top-down signals have a pretty good match in the nonspecific thalamus based on similarity alone.

Figure 3c summarizes all of the simulated SMART circuitry. Table 1 summarizes the main anatomical features simulated, their functional interpretation, and supportive experimental literature. The Methods section provides a detailed description of the model equations and parameters.

2. RESULTS

2.1 Learning bottom-up oriented filters in the specific pathway. In both the brain and the model, LGN parvalbumin-rich “core” cells receive topographically highly ordered bottom-up sensory input and project to layers 6^I and 4 of cortical area V1 (Jones 2002, Figure 1b) in a manner that is sensitive to stimulus orientation (Reid and Alonso, 1995). SMART simulates how adaptive synapses may become orientationally tuned in the pathways from LGN core relay cells to V1 layer 4 and layer 6^I cortical neurons (Figure 2a) via postsynaptically gated STDP (Figure 4a) during synchronous match-mediated gamma oscillations.

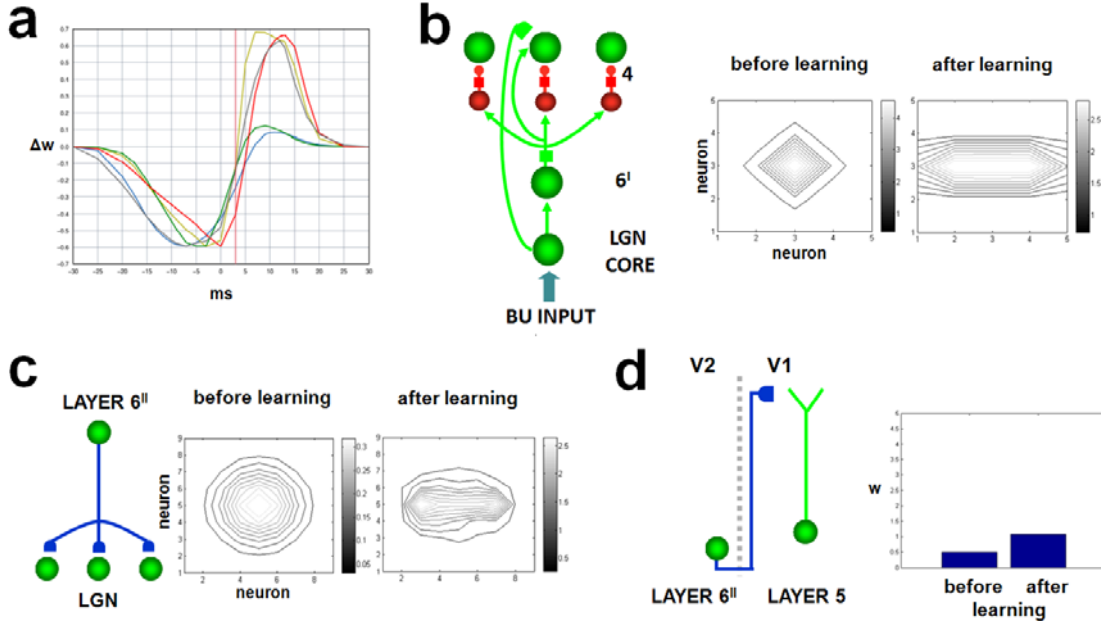


Figure 4 (a) STDP curves obtained by varying the time interval between presynaptic and postsynaptic spikes between $[-30, 30]ms$ for five gating functions: grey (no gating), blue (dual OR gating), red (presynaptic gating), green (postsynaptic gating), yellow (dual AND gating), modified from Gorchetnikov et al. (2005b). For a discussion of all gating functions, see Methods section and Gorchetnikov et al. (2005a). (b) Presentation of a horizontal bar to a untrained thalamocortical circuit causes changes in the bottom-up synaptic weights of LGN→layer 4 synapses (postsynaptic gating, 100ms episode). (c) At the same time, TD layer 6^{II} →LGN weights change by adapting to the BU input shape (presynaptic gating). (d) Top-down synaptic weights at the connections from V2 layer 6^{II} to the layer 1 apical dendrites of layer 5 cells change during learning when layer 6^{II} feedback is active (dual AND gating). Episodes of asynchronous activities can occur at learnable synaptic stages in different cortical areas. Dual AND gating prevents learning when only V2 layer 6^{II} cells are active and no activity is present in V1 layer 5.

Figure 4b illustrates the development of orientation sensitivity in a layer 4 cell that wins the competition with its neighboring cells. It spikes within a few milliseconds after the arrival of the LGN input, while nearby cells are suppressed and their spiking delayed by the on-center off-surround layer 6^I →4 network. This delay reduces or completely suppresses learning in cells other than the winning neurons. The gamma oscillations (see Section 2.10) during match episodes allow layer 4 cells to fire a few ms after LGN cells, and thus within the STDP window. The orientation selectivity is expressed in terms of LGN→4 synaptic weights (cf., Alonso et al., 2001) before and after a 100ms exposure to a horizontally-oriented stimulus. Orientationally selective cells in layer 4 of V1 excite layer 2/3 cells, which in turn project to layer 5 of V1. Layer 5 projects to layers 6^I and 6^{II} of the same area (Callaway, 1998). Layer 6^I closes the layer 2/3→ 6^I →4→2/3 intracortical modulatory excitatory loop that helps select the most activated cells in layer 4, while strongly suppressing less active cells and noise. Layer

6^{II} closes the thalamocorticothalamic loop by projecting with top-down modulatory connections to the specific (Figures 2b, 3a, and 3c) and nonspecific (Figures 2e and 3c) thalamic nuclei, and with driving connections to the TRN (Figures 2b, 3a, and 3c), as detailed below.

2.2 Top-down attention and STDP learning. V1 layer 6^{II} cells send top-down modulatory excitatory glutamatergic signals to thalamic relay cells in LGN (Sherman and Guillery, 2001; Murphy et al., 1999; Ichinohe et al., 2003). Although LGN neurons respond to unoriented visual stimuli, oriented spatial arrays of LGN neurons can respond to oriented contours in an image or scene, and corticothalamic feedback comes from oriented cortical cells. SMART simulates how top-down feedback signals from V1 layer 6^{II} are matched and mismatched in LGN, and thereby help to stabilize learning in both bottom-up adaptive filters and top-down modulatory expectations. Learning during a match state encodes top-down orientation sensitivity, which has also been reported in neurophysiological experiments (Murphy et al., 1999). Figure 4c illustrates the learned oriented shaping of model corticothalamic synaptic weights using an STDP rule with presynaptic gating (see Methods) before and after 100ms presentation of a horizontal bar. The oriented synaptic weights are learned in a gamma oscillation regime (see Figure 12b below) and allow subsequent attentive top-down signals to subliminally prime the consistent learned bottom-up stimulus, and match it or mismatch it with incoming bottom-up inputs. In particular, the oriented top-down expectation supports competitive selection, synchronization, and gain modulation of matched LGN cells, which has been reported in neurophysiological experiments (Sillito et al., 1994).

2.3 Attentive matching in the specific thalamus. The SMART model proposes functional roles for both the specific and nonspecific projections of the TRN (Figures 2b and 2e). The specific inhibitory projections of the TRN to the LGN (Guillery et al. 1998; Guillery and Harting, 2003) provide a detailed anatomical realization of the ART matching process that suppresses bottom-up inputs that mismatch cortical top-down excitatory expectations. In particular, the top-down excitatory on-center, adaptive pathway from layer 6^{II} to LGN core cells is supplemented by a TRN-mediated inhibitory off-surround (Figures 2b and 5). Cells that receive only bottom-up or top-down excitatory inputs are inhibited by the model TRN (balanced excitation and inhibition; one-against-one), whereas cells that receive sufficiently large simultaneous bottom-up and top-down excitatory inputs can offset TRN inhibition and fire (two-against-one). A perfect match occurs when the same subset of LGN cells receives bottom-up excitation and top-down excitatory modulatory priming signals from cortical layer 6^{II}; e.g., they both represent the same horizontal bar, as in Figure 5a. These matched LGN cells fire tonic action potentials that activate layers 4 and 6^I of the target cortical area. The tonic firing mode preserves a linear input-output relationship in LGN cells, and relays information better than burst firing (Sherman and Guillery, 2002). A sufficiently big mismatch, such as the top-down horizontal bar expectation matched against the vertical bar bottom-up input in Figure 5b, hyperpolarizes LGN cells via layer 6^{II}→TRN→LGN feedback, and then voltage-dependent T (transient) type Ca⁺⁺ currents causing burst firing (Sherman and Guillery, 2001). The model exhibits both the tonic and the burst firing modes that are found in the data (Figure 6).

Consistent with Sherman and Guillery (2002), SMART clarifies how burst firing might help to switch attention to a modality where a sudden bottom-up stimulus occurs, as when a sudden visual cue occurs while paying attention to an auditory stimulus.

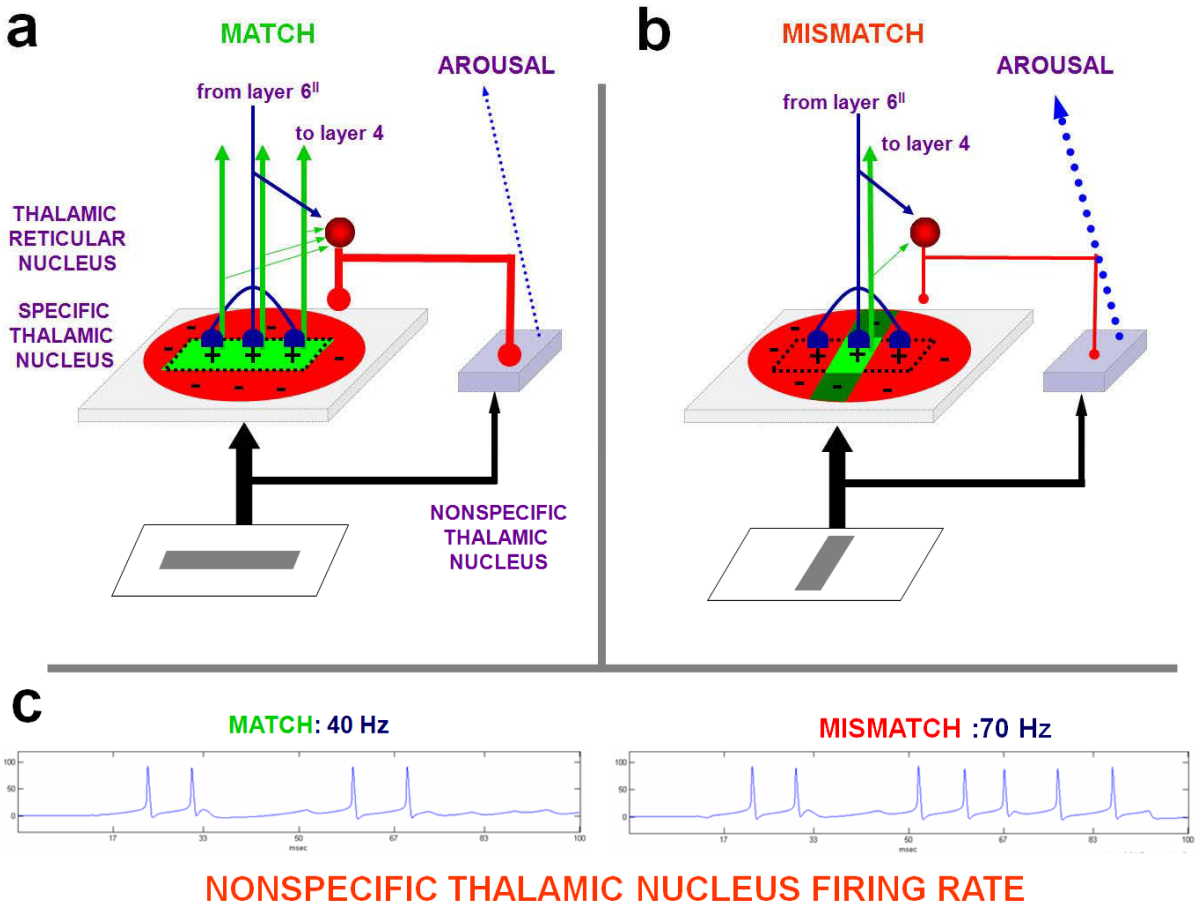


Figure 5 Regulation of nonspecific thalamic nucleus firing rate by the amount of match in the specific thalamic nucleus. **(a)** A bottom-up input pattern (horizontal bar, in green) is matched with a top-down expectation from layer 6^{II} (dotted horizontal bar) in the on-center (layer 6^{II} → specific thalamus) off-surround (layer 6^{II} → TRN → specific thalamus) corticothalamic loop. The convergent bottom-up excitation to the nonspecific thalamus is (partially or totally) cancelled by convergent TRN inhibition to the nonspecific thalamus. A spatial match (green horizontal area) allows specific thalamic cells to fire, excite their cortical target, and inhibit the nonspecific thalamus via the TRN. **(b)** A spatial mismatch between a bottom-up input pattern (vertical bar) and a top-down expectation (horizontal dotted bar) causes only a subset of specific thalamic cells to fire (bright green square area), excite their cortical target, and inhibit the nonspecific thalamus via the TRN. **(c)** Since the total, convergent bottom-up input to the nonspecific thalamus does not change in a match vs. a mismatch episode, the lower TRN firing rate during a mismatch triggers a higher firing rate in the nonspecific thalamus.

This mechanism complements the nonspecific thalamus-mediated mismatch, which can use vigilance control to cause mismatches across multiple modalities. Indeed, using vigilance control, even if a modality experiences a match that is good enough to predict an outcome elsewhere in the brain (e.g., seeing a visual object predicts its name), a mismatch with this outcome can raise vigilance enough to drive a search within the original modality for a recognition category that can predict the outcome better in the future (see Section 2.8).

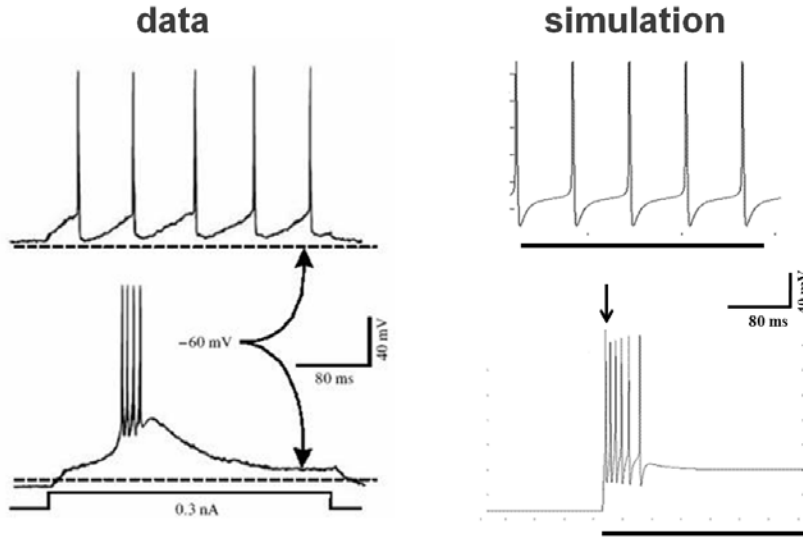


Figure 6 Burst and tonic firing in thalamic relay cells. *Data*: intracellularly *in vitro* recording illustrating the voltage dependency of the low threshold spike for a geniculate relay cell. The same depolarizing current pulse administered at two different initial holding potentials causes either tonic firing (top, cell depolarized, I_T inactivated) or burst firing (bottom, cell hyperpolarized, I_T de-inactivated). Modified and reprinted with permission from Sherman and Guillery, 2002. *Simulation*: a 0.3 nA current (horizontal bar) is injected in a simulated LGN cell in the absence (top) or presence (bottom) of a hyperpolarizing voltage clamp. The hyperpolarization of the cell and the presence of low-threshold Ca^{++} currents (see Equations (21)-(27) in Methods) causes the de-inactivation of the I_T current, inducing burst firing.

2.4 Attentive priming via corticocortical and corticothalamic feedback connections. As noted above, the STDP rule (Figure 4a; see Methods) is used to learn the top-down corticocortical attentive connection from V2 layer 6^{II} cells to layer 1 apical dendrites of V1 layer 5 cortical cells during presentation of a bottom-up input (Figure 4d). This learning correlates V2 layer 6^{II} cell outputs with *retrograde dendritic spikes* from V1 layer 5 cells to their layer 1 dendrites (Johnston et al., 1999). Such learning subsequently allows the V2 layer 6^{II} cell to fire the associated V1 layer 5 cell, and from there the corresponding V1 layer 6^I cell, which in turn primes V1 layer 4 via the modulatory on-center, off-surround layer 6^I→4 network. This top-down circuit mediates attention in the network. It embodies the concept of “folded feedback” whereby top-down signals are folded into the bottom-up flow of information from layer 6^I to 4, where they can attentionally enhance or suppress bottom-up signals (Grossberg, 1999).

A key prediction of the model is that the excitatory on-center of the 6^I→4 pathway is modulatory, or subthreshold. This prediction is consistent with the data showing that layer 4 excitatory post-synaptic potentials (EPSPs) elicited by layer 6 stimulation are much weaker than those caused by stimulation of LGN axons (Stratford et al., 1996), and also with the finding that binocular layer 6 neurons synapse onto monocular layer 4 cells without reducing the monocularity of the target layer 4 cells (Callaway, 1998).

The modulatory corticothalamic feedback provides excitatory priming of target thalamic cells. Figure 7a (top left panel) shows neurophysiological data illustrating modulatory priming in the specific somatosensory thalamus caused by layer 6 stimulation (Jones, 2002), and simulated model thalamic cell modulation (bottom left panel) during top-down layer 6^{II} priming of the model LGN. Figure 7b shows simulated subthreshold activation of a V1 layer 4 cell after learning top-down feedback from a V2 layer 6^{II} cell to the apical dendrites of V1 layer 5 cells. In the figure, the effect of top-down feedback is simulated by direct layer 5 stimulation. These experimental and modeling results are

consistent with ART predictions that top-down attentive signals are typically, by themselves, modulatory and insufficient to fully activate their target cells. (See Grossberg (2000) for an analysis of how top-down signals can elicit suprathreshold responses during percepts of visual imagery and hallucinations when the excitatory and inhibitory signals become imbalanced.)

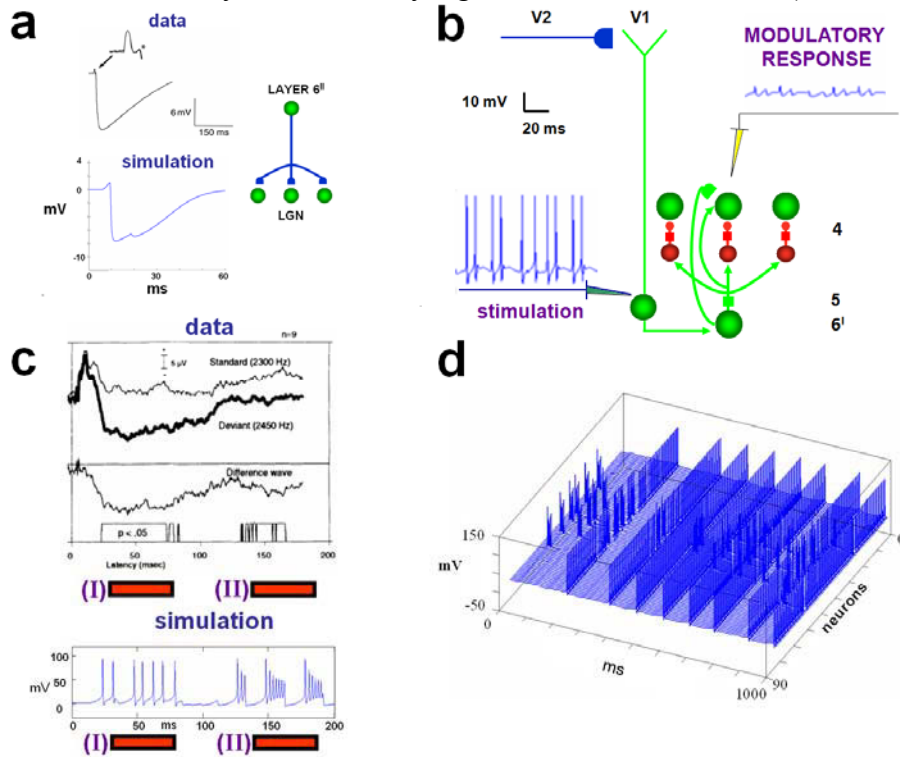


Figure 7 (a) Top-down corticothalamic feedback exerts a subthreshold excitatory effect on the membrane potential of thalamic relay cells. *Data* (upper left panel): whole-cell recording from a relay neuron in the somatosensory ventral posterior nucleus of a mouse thalamocortical slice *in vitro*. A single weak electrical stimulus (arrow) applied to a corticothalamic fiber elicits a small monosynaptic EPSP (asterisk in enlarged inset) followed by a deep and long-lasting disynaptic IPSP resulting from collateral corticothalamic excitation of the TRN (Jones, 2002). *Simulation* (lower left panel): a complete corticothalamic module is used in this simulation. Stimulation via current injection is provided to a central layer 6^{II} neuron, which has previously learned a bottom-up stimulus, until a single spike is produced, and the somatic membrane potential of the cell which coded the learned bottom-up stimulus is recorded in the absence of external stimulation. (b) Electrical stimulation of model layer 5 apical dendrites, simulating the top-down feedback excitation exerted by layer 6^{II} of V2, induces layer 4 priming via the 6^I modulatory on-center, off-surround network. (c) The nonspecific thalamic nucleus, not the specific nuclei, is involved in novelty detection in an auditory mismatch negativity (MMN) paradigm. *Data*: Extracellular recordings to standard stimulus (2300Hz, thin line) and deviant stimulus (2450Hz, thick line) obtained from the caudomedial portion of the nonspecific medial geniculate body (MGcm) in guinea pigs (Kraus et al., 1994). Significant differences between the responses to the standard and deviant stimuli are indicated in the box under the difference wave. Significant negative deflections (at 30-80ms and 135- 170ms) were identified in the nonspecific MGcm but not in the specific medial geniculate body (MGv). *Simulation*: a complete corticothalamic module was used in 300ms simulation epochs, and the potential of the nonspecific thalamic nucleus cell was recorded. Stimulation of a layer 6^{II} cell that has previously learned a horizontal stimulus provides top-down feedback to the thalamus, where it mismatches a vertically-oriented bottom-up input. The mismatch corresponds to the MMN condition, in which a repetitive stimulus builds up top-down expectations that are mismatched when a novel stimulus is presented. The first increase in the nonspecific nucleus firing rate is caused by the release from inhibition from the TRN due to the reduced firing of the primary thalamic nucleus, whereas the second increase in firing rate is caused by thalamocortical layer 6^{II} feedback, in turn caused by the synchronized layer 5 firing that is caused by activation of the nonspecific thalamus during a mismatch, followed by widespread activation of cortical layer 1, including the dendrites of layer 5 cells. (d) Simulation of all layer 5 cells firing synchronously in response to the increased nonspecific thalamic input. In these simulations the top-down feedback (stimulation of a layer 6^{II} cell with horizontal top-down thalamocortical receptive field) is kept on for one second, during which the top-down feedback mismatches the vertically oriented bottom-up input.

2.5 Nonspecific thalamic nucleus and cortical arousal regulation. The matching process in the specific thalamic nuclei is predicted to regulate the activity of the nonspecific thalamic nucleus. In particular, a match decreases the firing rate, or cortical arousal, from the nonspecific nucleus, whereas a mismatch increases it (Figure 5). How does the nonspecific thalamus become sensitive to the degree of match in the specific thalamus?

The total convergent bottom-up excitatory input to a nonspecific thalamic nucleus is unchanged by the matching process (van der Werf et al., 2002; Jones, 2002; Figure 5). When a match occurs, the TRN receives stronger excitation via bottom-up thalamocortical collaterals than during a mismatch (Sherman and Guillery, 2001, 2002; Figure 5a vs. 5b). During a match, this leads to strong, convergent inhibition to the nonspecific thalamic nucleus that can balance the total excitatory input that it receives. During a mismatch, reduced specific thalamus spiking causes decreased inhibition by TRN of the nonspecific thalamus, and a consequent increase in nonspecific thalamus firing rate, or arousal, that is proportional to the degree of mismatch (Figure 5c).

The human mismatch negativity (MMN) event-related potential has features that are consistent with these predicted properties. Physically deviant stimuli trigger a MMN roughly 200ms after stimulus onset (Näätänen et al., 1978). Kraus et al. (1994) demonstrated involvement of nonspecific, but not specific, thalamic nuclei in the MMN (Figure 7c), with differences between novel and standard stimuli at 30-80ms and 135-170ms after stimulus onset. The late latency suggests a cortical contribution, which involves superficial cortical layers (Karmos et al., 1986).

The SMART model explains and simulates these earlier thalamic and later cortical components using the following properties: Mismatch increases nonspecific thalamic nucleus firing at around 50ms and 150ms after stimulus onset (Kraus et al., 1994; Figure 7c), reaching cortical layer 1 and causing synchronized firing in layer 5 (Figure 7d). Layer 5 then excites layer 6^{II} (Figure 3c), which in turn reactivates the nonspecific thalamic nucleus. The nonspecific thalamic nucleus cell generates an additional burst of activation mediated by low threshold Ca^{++} spikes (see Equations (21)-(27) in the Methods). This spiking pattern occurs when a hyperpolarized thalamic cell with low-threshold Ca^{++} T-current is activated by an excitatory stimulus (Sherman and Guillery, 2001, 2002; Shipp, 2003).

2.6 Layer 5 regulation of cortical reset. Larkum et al. (1999) found that layer 5 cell dendrites can produce action potentials that actively propagate to layer 5 cell bodies and cause somatic action potentials (Figures 8a and 8b). Until now, there has been no functional explanation of these regenerative dendritic potentials. Figures 8b and 8c compare *in vitro* recordings of layer 5 pyramidal apical dendrites and soma, and model layer 5 cell simulations during match and mismatch episodes.

2.7 Predictive search using mismatch-mediated arousal and habituating synapses. How does a mismatch-mediated layer 5 reset signal choose a new cortical representation that can lead to a better match, and thus a better prediction? How can reset do this without an external teacher? A proposed solution to this problem (Grossberg, 1980) is herein realized using known laminar corticocortical and thalamocortical circuits. This solution predicts that the pathway which mediates reset utilizes habituating transmitter gates, also called depressing synapses (Grossberg, 1976, 1980; Carpenter and Grossberg, 1990; Abbott et al., 1997; Tsodyks and Markram, 1997). In particular, when a bottom-up input activates a layer 6^I cell, or a layer 6^I-to-4 inhibitory interneuron, a fraction of its neurotransmitter is released to activate layer 4 target cells (Figure 9; see Methods). The transmitter recovery rate is slow relative to its release rate, and thus the net EPSP recorded at a post-synaptic site decreases through time to a habituated level of firing after an initial burst of activation (Beierlein et al., 2002). Despite this reduction, synaptic transmission remains unbiased and stronger inputs produce bigger steady-state EPSPs even as the corresponding transmitters habituate (Grossberg, 1980; Figure 8d(I)). When a layer 5-mediated reset wave later hits layer 6^I (Figure 8d(II)), this arousal burst changes the balance of total input to layer 4 cells. Simulations (Figure 8e) and mathematical proofs (Grossberg, 1980; Grossberg

and Seidman, 2006) show how layer 4 cells reset based on their prior activation and the reset wave size, to favor previously inactive or weakly active layer 4 cells (Figure 8d(III)).

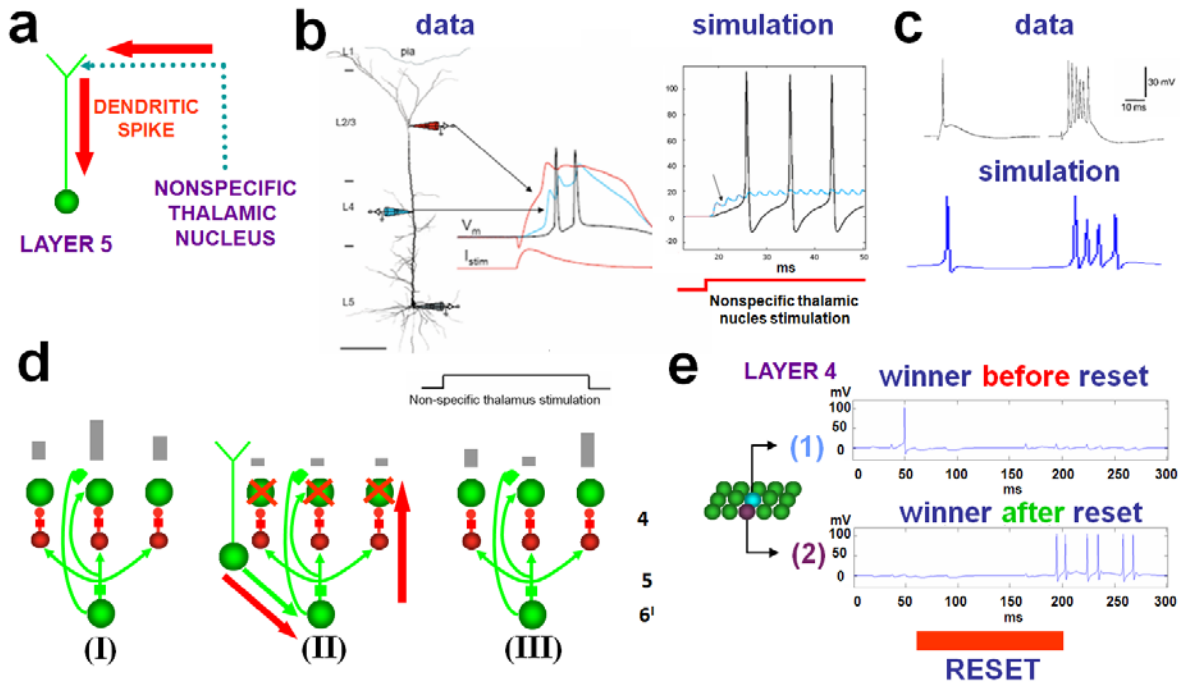


Figure 8 (a) In the model, an increase in nonspecific thalamic firing rate during a mismatch nonspecifically activates layer 1, including apical dendrites of layer 5 cells, where dendritic spikes are triggered that can cause layer 4 somatic action potentials. (b) Input to the apical dendrite of layer 5 pyramidal neurons results in action potentials recorded at the soma. *Data*: recordings of a layer 5 pyramidal neuron (rats, *in vitro*) show apical (red), proximal (blue) dendritic and somatic (black) potentials during stimulation of the apical dendrite (modified with permission from Larkum et al., 1999). *Simulation*: stimulation of the apical dendrites of an isolated simulated layer 5 pyramidal cell via the nonspecific thalamic nucleus produces a stream of action potentials at the soma. The arrow indicates the recording from the intermediate section of the dendrite of the simulated neuron, located at 400 μm from the soma, which is equivalent to the L4 recording electrode in the data. The voltage oscillations recorded at the proximal dendrite are caused by dendritic spikes occurring at the cell's apical dendrite, and propagated towards the soma. (c) *Data*: *in vitro* (rat) recordings of layer 5 pyramidal cells show that neuronal firing in response to extracellular synaptic excitation can consist of single spikes or burst firing (modified from Williams and Stuart, 1999). *Simulation*: recordings from a layer 5 pyramidal neuron during a mismatch episode. Depending on the presence of a layer 2/3 input, the cell can either respond with a single spike (no layer 2/3 input) or a burst of spikes (layer 2/3 input). (dI) Layer $6^1 \rightarrow 4$ on-center off-surround network normalizes and primes layer 4 cells activities. Neurotransmitter depletion (green squares) does not bias the competition in layer 4 until a reset occurs. (dII) A reset is driven by mismatch-mediated layer 6^1 firing in response to a burst of layer 1 nonspecific activation. (dIII) The reset unmasks previously inactive cells that are favored by higher levels of neurotransmitters which have accumulated in non-depleted layer $6^1 \rightarrow 4$ synapses. (e) Before a reset occurs, a "wrong" winning layer 4 cell spikes (1). Reset (red bar) favors the activation of previously inhibited cells (2).

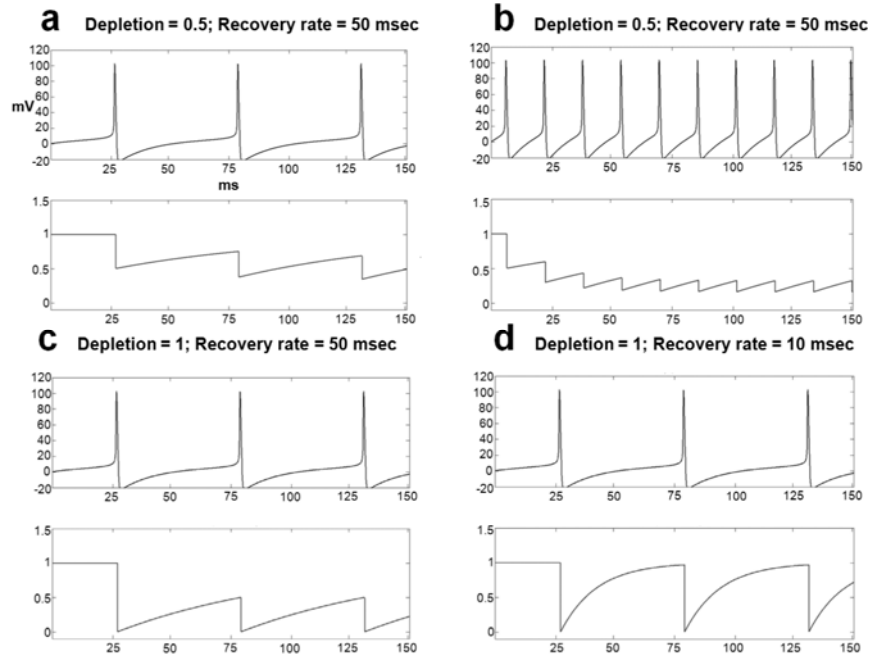


Figure 9 Neurotransmitter dynamics with different values of depletion (inactivation, habituation) and recovery rate (ε and τ , respectively, see Equation 7 in Methods) and different pre-synaptic firing frequencies in an isolated layer 6^I cell. Stimulation was induced by current injection until firing rates of 23Hz (panels a, c) or 70Hz (panels b, d) were generated. Each panel shows the pre-synaptic cell membrane potential (top) and the level of neurotransmitter at the synapse (bottom). **(a, b)** Higher firing rates cause larger and quicker neurotransmitter depletion due to the mass action (Equation 7 in Methods), all else being equal. **(c)** Increasing the depletion rate ε from 0.5 to 1 results in larger neurotransmitter depletion. **(d)** A faster recovery rate τ counterbalances the effect of depletion.

2.8 Acetylcholine neuromodulation controls vigilance, learning, and generalization. How is the concreteness or abstractness of recognition categories controlled in a task-sensitive manner? A clue is provided by the fact that the nonspecific thalamic nucleus controls the excitability of layer 5, and therefore when reset and search for a new recognition category occurs. If the sensitivity of layer 5 to arousal bursts from nonspecific thalamus can be modulated by predictive success, then the concreteness or abstractness of learned recognition categories can be controlled.

In particular, suppose that increased ACh release occurs in the cortex from the nucleus basalis of Meynert following a predictive mismatch (Figure 10b). Figure 10a summarizes data showing interactions between nonspecific thalamic glutamatergic transmission, ACh innervations of cortical layer 5, and its regulation of after-hyperpolarization (AHP). In both *in vitro* data (Saar et al., 2001) and isolated model layer 5 pyramidal cells, ACh regulates AHP currents and cell excitability in layer 5 cortical cells.

Figure 10a (top) shows that a steady depolarization current causes rat pyramidal cell firing to rapidly habituate, whereas injection of the ACh agonist carbachol reduces the adaptation (Saar et al., 2001). Figure 10a (bottom) shows the simulation results for an isolated layer 5 pyramidal cell which include AHP currents in its somatic compartment, before and after ACh stimulation. Data and simulations show that the release of ACh can modulate, through the reduction of AHP and the prevention of spike adaptation, the excitability of layer 5 pyramidal neurons, and consequently the amount of thalamic mismatch that can be tolerated by the cortical area. High levels of ACh may increase vigilance by reducing spiking adaptation, facilitating reset and therefore requiring a higher degree of match between bottom-up and top-down representations.

Given this mechanism, suppose that bottom-up and top-down information are well enough matched in one cortical area to activate a category which generates a prediction elsewhere in the brain. If this prediction causes a predictive mismatch with, say, environmental feedback, then increased ACh release can trigger reset and search throughout the cortex, including the cortical region that accepted the previous match as sufficient to make the prediction. Reset can rapidly shut off the previously active recognition category before it can become engaged in erroneous new learning, and the ensuing search can discover either a new recognition category, or a familiar one, that makes a good enough mismatch to prevent prediction disconfirmation. The new recognition category will be learned, or the familiar category will be refined, to incorporate the new constraints imposed by the bottom-up data. ACh hereby makes the cortex more “vigilant.” High vigilance forces learning of more precisely matched, and thus more concrete, categories than low vigilance.

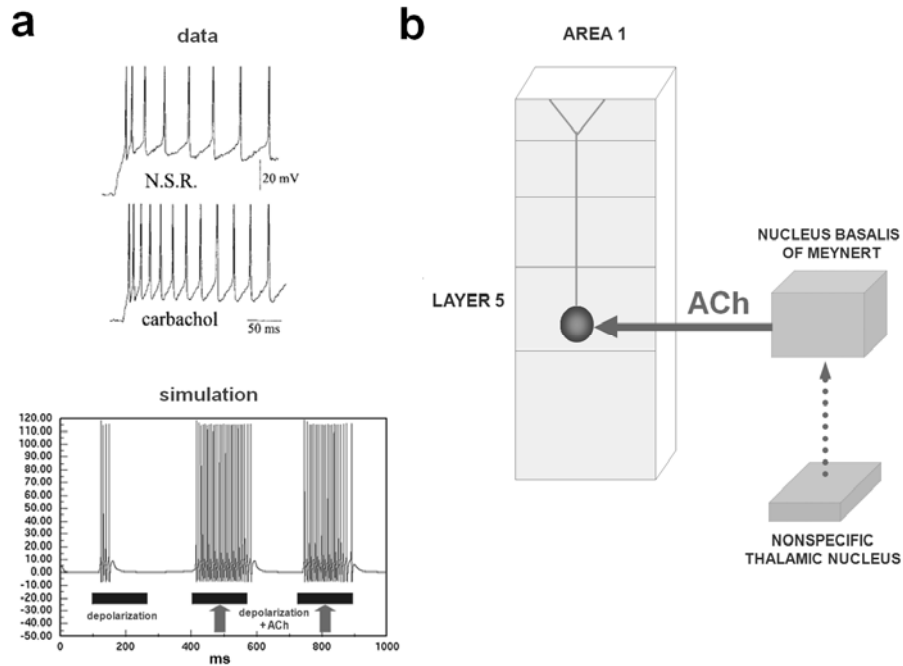


Figure 10 Interactions between nonspecific thalamic glutamatergic transmission, ACh and afterhyperpolarization (AHP) (a) ACh may modulate reset by regulating AHP currents and cell excitability in layer 5 cortical cells. *Data:* Intracellular recordings *in vitro* show that the ACh agonist carbachol reduces firing adaptation in layer 2 neurons in response to a constant current step injection (modified with permission from Saar et al., 2001). *Simulation:* an isolated, 3-compartment-layer 5 pyramidal cell is simulated, and a constant current injection is provided to the soma in order to produce a stream of action potentials at 80Hz. The AHP current at the soma is characterized by a long-lasting hyperpolarizing K^+ current, which slows down and eventually prevents spiking activity. ACh activation is represented as the 100ms stimulation of a single cholinergic neuron terminating on the soma of the layer 5 pyramidal cell. The activation of the cholinergic nucleus opens a conductance (multiplicative gating variable, Equation 7 in Section 3.3) which reduces the conductance of the AHP current, therefore reducing spiking adaptation. (b) The nonspecific thalamic nucleus may control the cortical release of ACh via its terminations in the Nucleus Basalis of Meynert (van Der Werf et al., 2002).

2.9 Intramodal attention and nonspecific thalamus. Crabtree and Isaac (2002) have shown that activation of cells in one nonspecific thalamic nucleus leads to a TRN-mediated IPSP that temporarily switches off tonic firing of action potentials in cells of another nonspecific thalamic nucleus (Figure 11a). A simulation of these results was carried out in an isolated circuit comprising two nonspecific thalamic cells and a TRN cell (Figure 11b). Constant stimulation of a nonspecific thalamic nucleus cells caused a tonic stream of action potentials (Figure 11c) which was interrupted by the stimulation

of a competing nonspecific thalamic cell (Figure 11d). Crabtree and Isaac (2002) suggested that this effect is due to the TRN, as confirmed by our simulation results in Figure 11e.

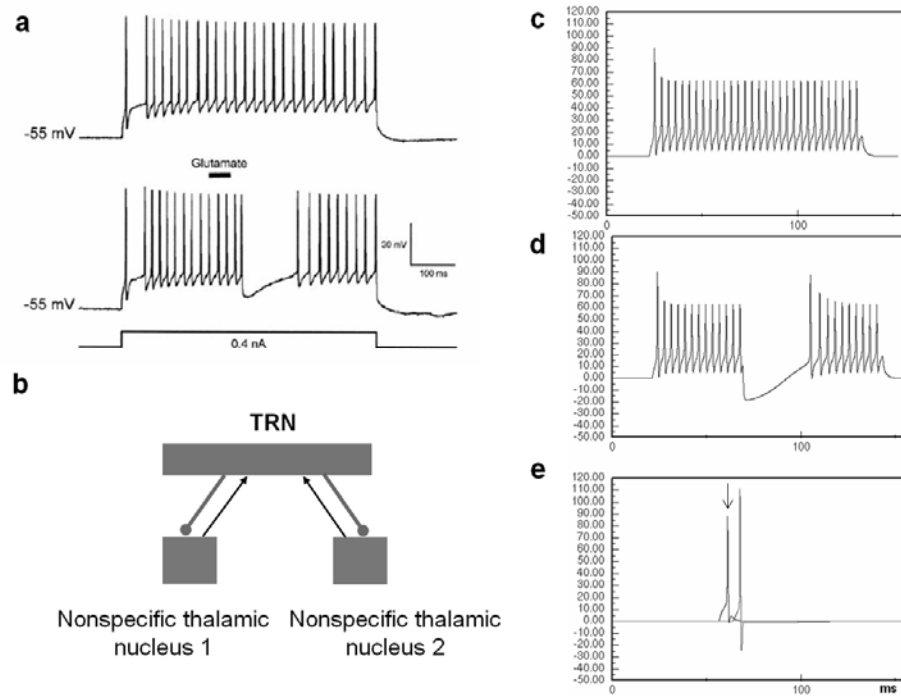


Figure 11 (a) Stimulation of one nonspecific thalamic nucleus interrupts a train of action potentials in another nonspecific thalamic nucleus. When held close to -55mV , a rostral intralaminar nucleus (RIL) cell responds with a train of action potentials (top recording) to a depolarizing 0.4nA current pulse (bottom, square wave). A train of action potentials (bottom recording) in the RIL cell in response to the depolarizing current pulse was interrupted by glutamate stimulation (black bar) in the caudal intralaminar nucleus (CIL, modified with permission from Crabtree and Isaac, 2002). **(b)** Model simulation includes two nonspecific thalamic nuclei and a TRN, all simulated as 1-neuron populations, with the TRN receiving excitation from the nonspecific thalamic nuclei, and inhibiting them with GABA projections. Cell activation was recorded at the nonspecific thalamic nucleus 2. **(c)** Constant stimulation of the nonspecific thalamic nucleus 2 gives rise to a train of action potentials (tonic firing) at 187Hz . **(d)** Stimulation of nonspecific thalamic nucleus 1 causes a TRN-mediated IPSP in the nonspecific thalamic nucleus 2. **(e)** Stimulation of the nonspecific thalamic nucleus 1 (blue) causes a spike in the TRN (red), which in turn inhibits the nonspecific thalamic nucleus 2.

2.10 Synchronous oscillation frequency reflects match and mismatch. Gamma (γ , $20\text{--}70\text{Hz}$) and beta (β , $12\text{--}30\text{Hz}$) oscillations are observed in visual cortex during various cognitive, perceptual and attentive states (Singer, 1999; Engel et al., 2001; Hermann et al., 2004; Grossberg, 1976, 2003). Beta oscillations often correlate with long-range synchronous activity of neocortical regions (Roelfsema et al., 1997), and gamma is restricted to sites within an area (Friedman-Hill et al., 2000) or between two areas with strong monosynaptic connections (Von Stein et al., 2000). Gamma and beta oscillation frequencies in the model reflect match and mismatch dynamics, respectively. Gamma oscillations are amplified between cells of an input population, and between cells of an input and a receiving population, when a top-down expectation matches its bottom-up input pattern (Figures 12a and 12c). During mismatch within lower cortical layers, beta oscillations prevail (Figures 12b and 12d) due to the low frequency, widespread synchronized firing of layer 5 cells, as illustrated in Figure 7. Layer 1 apical dendritic potentials slowly depolarize layer 5 cell bodies, causing the low frequency, synchronized spikes of layer 5 cells. This frequency component dominates the power spectrum of the cumulative spike histogram in cases of mismatches, as illustrated in Figures 12b and 12d.

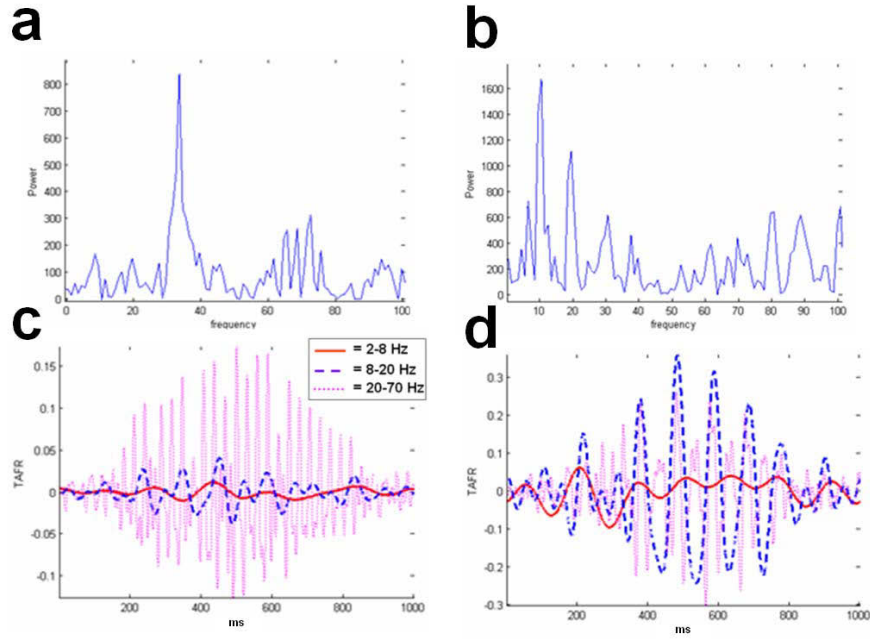


Figure 12 Power spectra of cumulative spike histograms of a laminar primary sensory cortical area during presentation of a stimulus (horizontal bar, 5 thalamic relay nuclei activated for 1000ms) during match **(a)** and mismatch **(b)** conditions show a peak in the slow γ frequency band (20-70Hz) in case of match, and lower frequencies in case of mismatch. The histograms were analyzed into three frequency bands (δ and θ , 2-8Hz; α and β , 8-20Hz; γ , 20-70Hz) to highlight the separate contribution of different oscillation frequencies in a match **(c)** and mismatch **(d)**. Notably, γ oscillations are drastically reduced in a mismatch in favor of lower-frequency oscillations.

The SMART model also simulates data about short and long-range synchrony. Friedman-Hill et al. (2000) showed gamma synchronization between two adjacent macaque V1 cells with overlapping receptive fields in response to a preferred stimulus (Figure 13 top). Model V1 layer 4 cells during match of a learned stimulus (Figure 13 bottom) show a similar cross-correlation power spectrum. These results are consistent with the intuition that cells with a shared bottom-up input would tend to spike in close temporal proximity, and therefore express high gamma synchronization when no strong low-frequency synchronization is imposed by mismatch-mediated, synchronized layer 5 discharges. Von Stein et al. (2000) showed (Figure 14, top) that synchronization between distant cortical areas (middle layers of cortical area 17 and lower layers of area 7 in cats) is prevalent in the lower and middle frequency ranges, whereas local interactions (within areas 17 and 7) show gamma band dominance. The model simulates these properties (Figure 14, bottom), showing that synchrony between distant cortical areas is mediated mostly by slower frequency oscillations. These simulations support the hypothesis that monosynaptically connected cells, such as cells within an area or between nearby areas, can synchronize at gamma frequency bands (Figure 13), which is compatible with STDP. Top-down interactions between lower layers of higher-order and upper levels of lower-order cortical areas are mostly modulatory. Therefore, upper pyramidal layers of lower-order areas should *not necessarily* fire in response to a top-down modulatory influence from higher cortical areas, and should *not necessarily* express gamma frequency synchronization, unless bottom-up and top-down signals match.

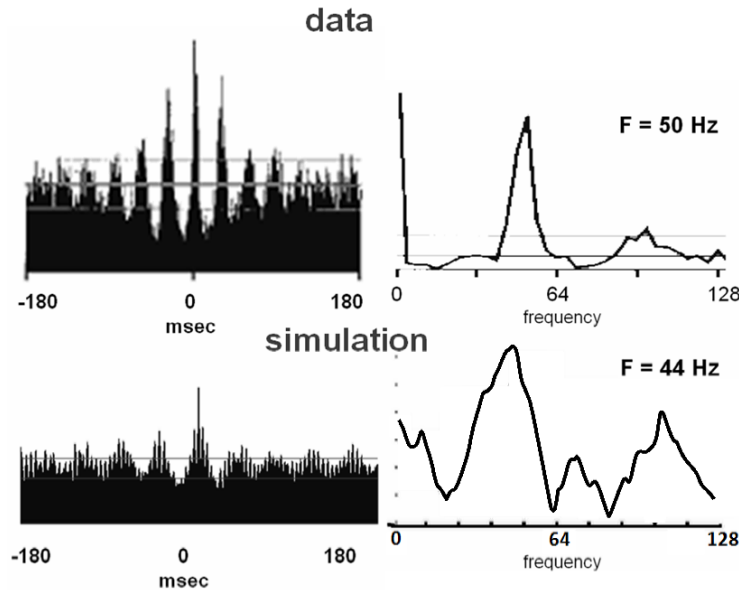


Figure 13 Example of short range ($300\mu\text{m}$), single unit–single unit correlation of cells with overlapping receptive fields and similar orientation preference in V1; *top, left*: cross-correlation computed from the two spike trains during the response to the stimulus. *top, right*: power spectrum of the cross-correlation shown on the left, which shows a peak around 50Hz. Modified from Friedman-Hill et al. (2000). *Bottom, left*: cross-correlation computed from the spike trains of two nearby simulated layer 4 cells during stimulation of a learned stimulus (lines show the 95% confidence limit). *Bottom, right*: power spectrum of the cross-correlogram shown on the left.

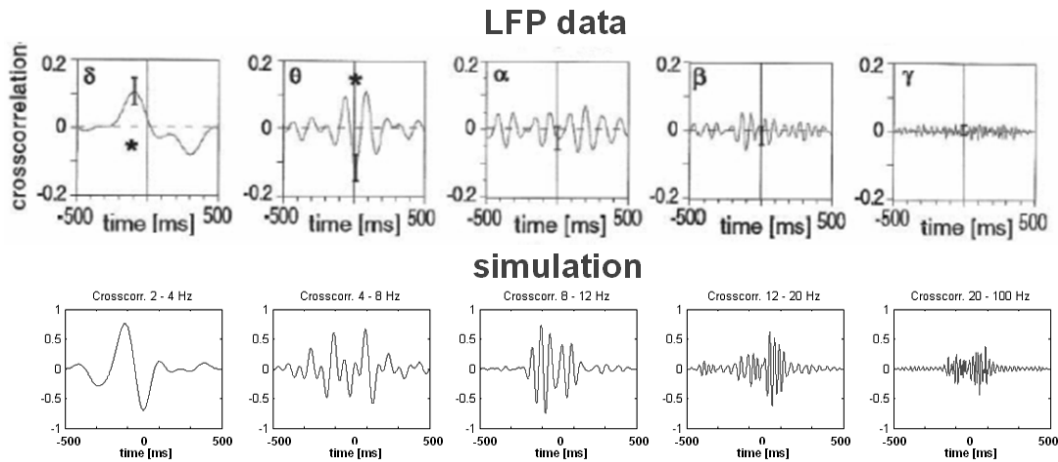


Figure 14 *Data*: Cross-correlation functions of local field potentials (LFP) from the middle layer of area 17 (primary visual cortical area) and lower layers of area 7 (higher-order visual area) during presentation of a no-go stimulus in behaving cats (reprinted with permission from Von Stein et al., 2000). *Simulation*: The activity of two thalamocortical loops was simulated, with a synaptic delay between layer 2/3 of the first-order cortical area and layer 4 of the second-order cortical area set at 10ms. Epochs of 1000ms were aligned to onset of a learned bottom-up stimulus that was presented for 1s prior to the beginning of the recording. Analysis was performed on a LFP recorder from two simulated 54-tip-electrodes from the two cortical areas, and data were separated in five different frequency ranges in accordance with classical electroencephalogram conventions: 2–4, 4–8, 8–12, 12–20, and 20–100Hz. The data were Fourier transformed and multiplied with the complex conjugate, and the inverse transformation was performed for selected frequency bins (corresponding to one “band”) to obtain cross-correlation functions for separate frequency ranges. Cross-correlation functions at different frequency bands was performed between LFP produced in the lower 0.3mm of the higher cortical area and the upper 0.3mm of the lower cortical area (both areas are 1.2mm thick).

3. DISCUSSION

This article describes a model that functionally links single cell properties, such as spiking dynamics, STDP, and ACh modulation; detailed laminar thalamic and cortical circuit designs and their interactions; aggregate cell recordings, such as current-source densities and local field potentials; and single cell and large-scale inter-areal oscillations in the gamma and beta frequency domains, as an expression of the cognitive processing requirements that are needed to regulate fast learning and stable memory of brain representations. As a result of this wide descriptive range, the model proposes many testable predictions that link these various levels of brain organization as manifestations of how bottom-up adaptive filters and top-down expectations may be learned, matched, and stably remembered during thalamocortical and corticocortical STDP learning. In particular, the model simulates how specific and nonspecific thalamic nuclei regulate learning via temporal cycles of match/resonance and mismatch/reset, wherein learning is facilitated during match/resonance states and reduced during mismatch/reset states. The predicted involvement of the nonspecific thalamus in learning is consistent with lesion studies showing a role for the nonspecific intralaminar/midline thalamic nuclei in declarative memory (van Der Werf et al., 2003). Moreover, Kraus et al. (1994) have shown that the nonspecific thalamic nuclei, but not the specific thalamic nuclei, show significant differential activation in states of match vs. mismatch, consistently with the model prediction that the nonspecific pathway is sensitive to the degree of mismatch between bottom-up and top-down cortical signals.

Simulations (Figures 11c-e) and experimental results (Crabtree and Isaac, 2002; Figure 11a) show that the nonspecific thalamic nuclei innervating different cortical areas compete via TRN-mediated inhibitory interactions. The model predicts that competition in the nonspecific pathway does not interfere with bottom-up processing in the specific pathway, but rather transiently decreases the activation of some layer 5 cells, therefore preventing the corresponding cortical area from further influencing thalamic and cortical areas in the cortical hierarchy. The model suggests that this mechanism might be a subcortical substrate of cross-modality switching and competitive deployment of attentional resources. This prediction complements the observation (Zeki and Shipp, 1988; Sillito et al., 1994) that top-down, layer 6-mediated attention has similar modulatory effects on target cortical and subcortical areas even in the absence of bottom-up input (Grossberg, 1999; Raizada and Grossberg, 2003). In particular, simulation results (Figures 7a and 7b) show how layer 6-mediated top-down corticothalamic feedback causes both fast priming excitation and slower inhibitory effects, as has been reported in experimental data (Jones, 2002).

A novel role for the neurotransmitter acetylcholine is postulated, linking levels of cortical ACh release to layer 5 excitability and layer 4 reset. Experimental results (Singer and Rauschecker, 1982; Kilgard and Merzenich, 1998) and modeling work (Hasselmo, 1993; Sánchez-Montañés et al., 2000) have shown that cholinergic modulation is an essential ingredient in cortical plasticity. The model predicts how strong ACh release, such as during repeated mismatches, or as a consequence of an environmental stressor, can influence the sharpness of the neural code, by altering the degree of match required for bottom-up and top-down matches to prevent reset. Lower levels of ACh favors coarser codes, because higher levels of mismatch can be tolerated by the system, thereby enabling more variable bottom-up input patterns to be associated with the same active recognition category without causing recoding.

The model for the first time mechanistically links cognitive mechanisms with brain oscillations, notably in the gamma (γ) and beta (β) frequency ranges, recorded from a variety of cortical and subcortical structures. Kopell et al. (2000) proposed that γ and β oscillations might subserve different functional roles. Their simulations showed that β oscillations are more robust in synchronizing areas separated by larger transmission delays, whereas γ oscillations tend to be dispersed when significant

delays are interposed. Olufsen et al. (2003) have shown that β oscillations allow a different separation between “leading” and “suppressed” cell assemblies than do γ oscillations. Gamma oscillations promote a sharp dichotomy between active/inactive assemblies, a situation similar to a “choice”. The SMART model shows how β oscillations can become a signature of modulatory top-down feedback and reset. Top-down processing, in both experimental and model results (Figure 14), shows prevalence of lower frequency oscillations, consistent with their modulatory nature (Olufsen et al., 2003) and their computational role of priming (Raizada and Grossberg, 2003; Siegel et al., 2000). In accordance with the present results, a computational study by Siegel et al. (2000) has shown that top-down feedback is accompanied by an overall increase of power in the low-frequency domain in the target neural population.

The SMART model extends previous modeling work by explaining how gamma oscillations emerge when modulatory top-down expectations are matched by consistent bottom-up input patterns. Such a match allows cells to more efficiently cross their spiking threshold to fire action potentials, leading to an overall increase in local gamma-frequency synchronization among cells sharing common top-down priming modulation.

The SMART model also links the role of different oscillation frequencies with STDP. Learning episodes tend to be restricted to match conditions, when on average presynaptic and postsynaptic cells spike within 10-20ms, namely within the STDP learning window, consistent with experimental results (Wespatat et al., 2004). The model predicts that STDP further reinforces synchronous activation of related cortical and subcortical areas, and that the effect of spurious synchronizations on long-term memory weights in a fast learning regimen can be prevented or rapidly reversed by a synchronous resonance during a match state. Gamma oscillations, amplified in case of a match, may favor propagation of spikes through the cortical hierarchy by packing pre-synaptic spikes within a narrow temporal window. This prediction is consistent with the observation that the efficacy of pairs of pre-synaptic LGN spikes on generating post-synaptic activation in the visual cortex falls off rapidly in time with the increase of the interspike interval (Usrey, 2002).

Finally, the SMART model advances a computational framework that allows testing and further development of how computations on multiple organizational levels in cortical and subcortical networks of spiking neurons may provide additional insights into how the brain learns to predict and control an increasingly complex and changing environment in a stable way through time.

4. METHODS

4.1 Model overview. The SMART model (Figures 2 and 3) includes two hierarchically-organized thalamocortical loops: a first-order primary loop (analogous to the LGN-V1) and a higher-order loop (analogous to the PULV-V2). Each thalamocortical loop simulates a 1.2mm thick, 6-layered-cortical module with cortical excitatory and inhibitory neurons, a thalamic nucleus composed of core and matrix cells (Jones, 2002) and local inhibitory interneurons, and a GABAergic thalamic reticular nucleus (TRN). The primary thalamocortical loop also includes a nonspecific thalamic nucleus. All cortical and subcortical layers are organized in 9x9 neural sheets, with the exception of the nonspecific thalamic nucleus and matrix thalamic cells that are simulated as single populations. Units are implemented as multi-compartment neurons obeying Hodgkin–Huxley-type dynamics (Hodgkin and Huxley, 1952). The minimal numbers of compartments and currents needed to produce the desired network properties is used in each neuron’s unbranched cable sections (Rall, 1962). The model implements online spike-timing-dependent plasticity (STDP) learning (Gorchetnikov et al., 2005a), and the plastic synaptic weights, as well as each neuron’s compartmental currents, are recorded to allow off-line local-field potentials (LFP), current-source densities (CSD), and oscillation

frequency/synchrony analysis (Versace et al., 2007). Stimuli are horizontally or vertically oriented bars that enable testing of model hypotheses about match/mismatch dynamics and learning.

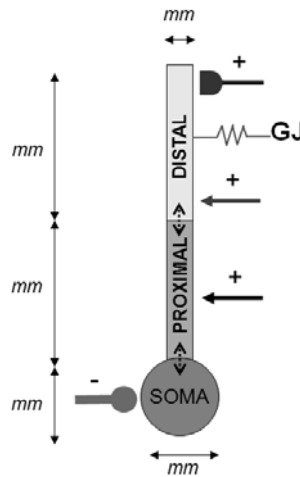


Figure 15 The generic neuron model. The neuron depicted above is a 3-compartment-cell with a soma, a proximal and a distal dendrite. Excitatory driving (arrow terminating in the proximal dendrite, +), modulatory (arrow terminating in the distal dendrite, +), plastic (half-ellipse terminating in the distal dendrite, +), as well as inhibitory (rounded arrow terminating in the soma, -) connections can terminate in each cell compartment, which are in turn linked by passive leakage currents (vertical dotted arrows). Electrical coupling between different cell compartments (gap junctions, GJ) can also be present (in the figure, in the distal dendrite).

4.2 Neuron description. Excitatory neurons (thalamic core, matrix, and nonspecific, cortical layers 4, 2/3, 5 and 6) and inhibitory interneurons (TRN and thalamic interneurons, cortical layers 4 and 2/3 interneurons), as well as their connections, were constructed according to known anatomical and biophysical data from primarily rats and cats. When unavailable, cell parameters were chosen in order to obtain the desired functional properties. Each of the two simulated thalamocortical loops consists of 732 multi-compartmental neurons (Figure 15), 2,106 compartments, and is described by 17,415 differential equations. Figure 16 shows the spatial arrangement and cell sizes of the populations composing the simulated 1.2mm thick laminar cortical sheet.

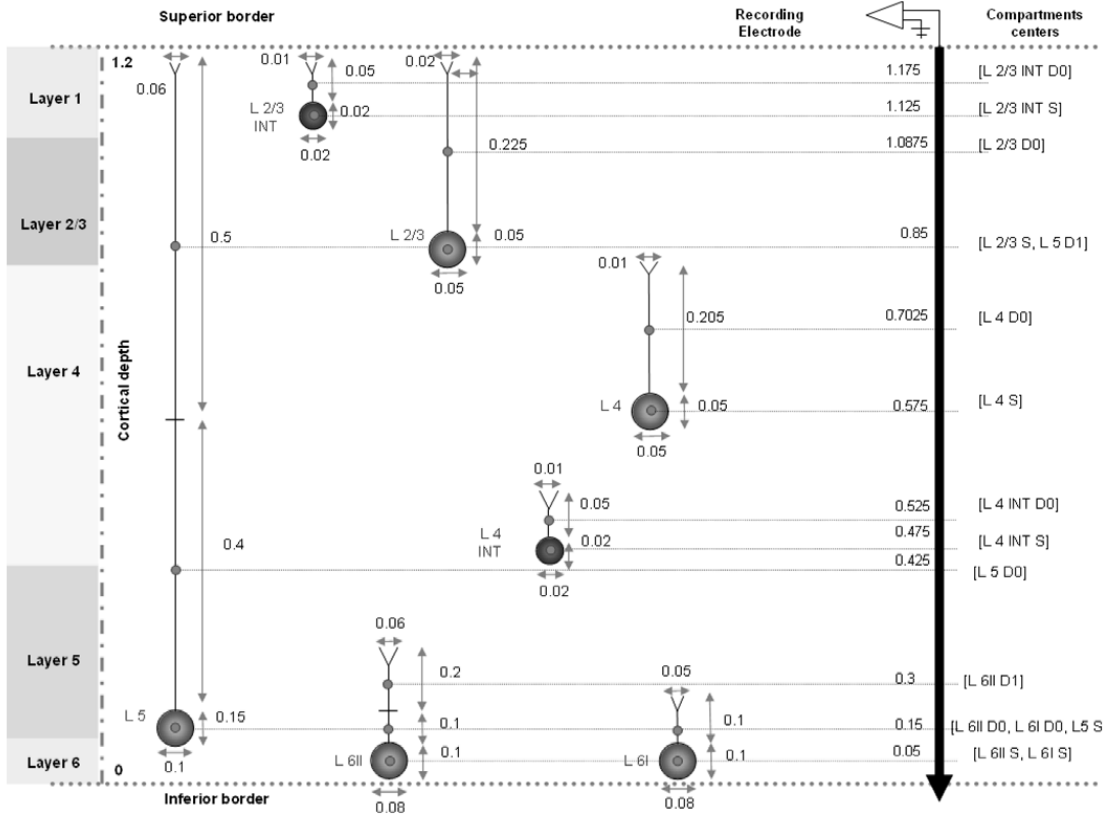


Figure 16 Spatial arrangement and cell sizes of the populations composing the 1.2mm thick laminar cortical sheet. A multi-compartment model with a spatially explicit structure allows to calculate transmembrane currents, which can be employed to derive aggregate cell recordings such as Local Field Potentials (LFP) and Current Source Densities (CSD). The activity of dendrites and cell somas of the populations can be recorded by an electrode with variable number of tips (black thick downward arrow, right). Since each compartment is treated as electrically uniform, the center of the compartment is the physical point at which the current source/sink is calculated (thick dot at the center of soma/dendrite). Cell bodies and dendrites are vertically aligned parallel to the recording electrode. For each layer, cells are displaced at random distance from the recording electrode. The distance of the electrode to the selected cell in the population is drawn from a uniform distribution on the interval $[10 - 200] \mu m$, whereas the distance to all other cells in the population is drawn from a uniform distribution on the interval $[10 - 1000] \mu m$. In the figure, only one cell for each population is shown. Abbreviations: L = layer; S = soma; D = dendrite (D0 = proximal dendrite; D1 = distal dendrite), INT = interneurons. All measurements are in mm.

Each compartmental membrane potential $V [mV]$ is described by:

$$C_M \frac{dV}{dt} = \sum_i I_i. \quad (1)$$

In (1), $C_M [\mu F \cdot cm^2]$ is the membrane capacitance. Ionic or chemically-gated channels and inter-compartmental currents are described by the current density $I_i [\mu A/cm^2]$ equation:

$$I_i = g_{Ch} (V^{EQ} - V), \quad (2)$$

where the channel conductance g_{Ch} and the equilibrium voltage $V^{EQ} [mV]$ change according to the nature of the current. Inter-compartmental currents from compartment m to compartment l are described by (2), where $g_{Ch} = g_{ml} D_l / 4 L_l^2 [k\Omega cm]$, g_{ml} is the conductance between compartments m and l , $D_l [mm]$ and $L_l [mm]$ are the diameter and length of membrane compartment l , respectively, and $V^{EQ} = V_m$ and $V = V_l$ are potentials of the neighboring compartments. Table 2 lists dimensions, passive

cable properties, and ionic channels (such as sodium (Na^{++}), potassium (K^+) and leakage channels) parameters.

CELL	Compartment diameter	Compartment length	Axial resistance	E_L	g_L	g_{Na}	g_K	g_{Ca}
<i>Units</i>	<i>mm</i>	<i>mm</i>	<i>KΩ·cm</i>	<i>mV</i>	<i>mS/cm²</i>	<i>mS/cm²</i>	<i>mS/cm²</i>	<i>mS/cm²</i>
First order thalamic relay								
Soma	0.05	0.06	8	-60	0.01	100	100	-
Dendrite 0	0.005	0.008	8	-60	0.01	-	-	10
Dendrite 1	0.005	0.008	8	-60	0.01	-	-	10
First order thalamic (matrix)								
Soma	0.05	0.06	8	-60	0.01	100	100	-
Dendrite 0	0.005	0.008	8	-60	0.01	-	-	10
Dendrite 1	0.005	0.008	8	-60	0.01	-	-	10
First order thalamic interneurons								
Soma	0.02	0.02	60	-49	0.01	50	30	-
Dendrite 0	0.001	0.1	60	-49	0.01	-	-	-
TRN								
Soma	0.05	0.05	10	-69	0.1	100	100	-
Dendrite 0	0.01	0.05	10	-69	0.1	-	-	10
Dendrite 1	0.01	0.05	10	-69	0.1	-	-	10
Thalamic nonspecific								
Soma	0.08	0.08	10	-64	0.09	100	100	-
Dendrite 0	0.015	0.1	10	-64	0.1	-	-	250
Dendrite 1	0.015	0.1	10	-64	0.1	-	-	250
Layer 4 Excitatory								
Soma	0.05	0.05	40	-65	0.01	50	30	-
Dendrite 0	0.01	0.25	40	-65	0.01	-	-	-
Layer 4 inhibitory								
Soma	0.02	0.02	100	-50	0.01	50	30	-
Dendrite 0	0.01	0.05	100	-50	0.01	-	-	-
Layer 2/3 excitatory								
Soma	0.05	0.05	100	-65	0.05	50	30	-
Dendrite 0	0.02	0.225	100	-65	0.05	-	-	-
Layer 2/3 inhibitory								
Soma	0.02	0.02	60	-49	0.01	50	30	-
Dendrite 0	0.01	0.05	60	-49	0.01	-	-	-
Layer 5								
Soma	0.1	0.15	5	-72	0.1	50	30	-
Dendrite 0	0.06	0.4	5	-72	0.03	-	-	-
Dendrite 1	0.06	0.5	5	-72	0.03	50	30	-
Layer 6^I								
Soma	0.08	0.1	80	-70	0.15	50	30	-
Dendrite 0	0.05	0.1	80	-70	0.9	-	-	-
Layer 6^{II}								
Soma	0.06	0.1	25	-64	0.1	50	30	-
Dendrite 0	0.08	0.1	25	-64	0.03	-	-	-
Dendrite 1	0.08	0.2	25	-64	0.03	-	-	-

Table 2 Dimensions, passive cable properties and ionic channels parameters of each cellular stage of the thalamocortical circuit. E_L and g_L represent the leakage currents equilibrium potential and conductance, respectively. Cell morphologies are the same for cells in the first order and second order thalamocortical loop.

In chemically-gated channels (AMPA, GABA, etc.) between neurons j and k , $V^{EQ} = E_i[mV]$ is the reversal potential of the channel, and the conductance $g_{Ch} = w_{jk} \bar{g}_{jk} g(t)$, where w_{jk} is the synaptic weight connecting neurons j and k , and \bar{g}_{jk} [pS] is the maximal channel conductance of the synaptic weight w_{jk} . The synaptic weight $w_{jk} = \frac{N_i}{\pi DL} \left[\frac{10^6}{cm^2} \right]$ corresponds to the density of receptors (millions of

channels per membrane cm^2). The conductance $g(t)$ is defined as a dual exponential factor describing the time course of the excitatory or inhibitory post-synaptic potentials (EPSP and IPSP, respectively) triggered by the pre-synaptic spike:

$$g(t) = \begin{cases} \frac{p}{\tau_f - \tau_r} (e^{-\frac{t}{\tau_f}} - e^{-\frac{t}{\tau_r}}) & \text{if } \tau_f \neq \tau_r \\ \frac{t}{\tau_f} e^{-(1 - \frac{t}{\tau_f})} & \text{if } \tau_f = \tau_r \end{cases}, \quad (3)$$

where t is the time since the onset of a pre-synaptic spike, p is a normalizing coefficient that ensures:

$$\max(\frac{p}{\tau_f - \tau_r} (e^{-\frac{t}{\tau_f}} - e^{-\frac{t}{\tau_r}})) = 1, \quad (4)$$

and τ_r and τ_f are the EPSP and IPSP rise and fall time constants, respectively. See Supplementary Table 3 online for parameters of chemically gated channels.

Unless otherwise specified, simulations were implemented in a full first-order thalamocortical sector including a six-layered cortical structure (V1), a TRN sector, a first-order thalamic nucleus (LGN), and a nonspecific thalamic nucleus. Equations (1)-(27) and (29) below describe the cell properties of the first-order thalamocortical sector, whereas Equation 28 is used only in producing the results illustrated in Figures 10 and 17. The passive properties of the cells describing each cellular stage in the first-order thalamocortical sector are listed in Table 2, whereas chemical and electrical synapses properties are listed in the Supplementary Table 3 online. Simulations of isolated cells in the network are performed by preserving all passive electrical properties of the simulated cell as listed in Table 2, whereas all synaptic conductances of other cell stages are set to zero to prevent any interaction with the isolated cell. More details on the simulation methods for isolated cells are provided in the pertinent figure captions.

4.3 Synaptic plasticity. Plasticity in the synaptic weight w_{jk} modulates the post-synaptic conductance $\bar{g}_{jk} g(t)$ by varying the density of post-synaptic channels, therefore influencing the impact of a spike on the magnitude of the current I_i . Learning in synaptic weights obeys a gated learning law (Grossberg, 1980; Gorchetchnikov et al., 2005a):

$$\frac{dw_{jk}}{dt} = \lambda f_G(V_k, g_{jk}) (g_{jk} f_N(V_k) (\bar{w} - \check{w}) + w_0 - w_{jk}), \quad (5)$$

where λ is the learning rate, $f_G(V_k, g_{jk})$ is a gating signal that turns learning on and off, \bar{w} and \check{w} are the minimum and maximum weight, and w_0 stands for the baseline weight achieved when there is no correlation between presynaptic and postsynaptic firing. The gating function $f_G(V_k)$ is described as:

$$f_G(V_k) = \begin{cases} D+1 & \text{if } V_k \geq V_k^\theta \\ -10(t-s) + D+1 & \text{if } s < t < s+0.1 \text{ ms} \\ \frac{-D}{25}(t-s-0.1 \text{ ms}) + D & \text{if } s+0.1 \text{ ms} \leq t < s+25.1 \text{ ms} \\ 0 & \text{otherwise} \end{cases}, \quad (6)$$

where V_k^θ is the spiking threshold potential, t is time, s is the moment of the postsynaptic spike, and $D = (\check{w} - w_0)/(\bar{w} - \check{w})$. This scaling function is a non-negative function of pre- and postsynaptic

activity and allows synaptic change to occur only when pre- and postsynaptic cell are simultaneously active. See Gorchetchnikov et al. (2005a) for the derivation and the detailed discussion of the rule.

Two forms of gating are used: post-synaptic and dual-AND gating. Post-synaptic gating, where $f_G(V_k, g_{jk}) = (V_k)^2$, is implemented in specific thalamic projections terminating in layer 4 (bottom-up adaptive weights) and allows the winning layer 4 cells to learn the LGN spatio-temporal pattern of activation. Dual-AND gating, where $f_G(V_k, g_{jk}) = g_{jk}(V_k)^2$, is implemented in layer 6^{II} projections terminating in the specific thalamus and in layer 1 apical dendrites of layer 5 cells of a previous cortical stage (top-down adaptive weights). This gating allows V2 layer 6^{II} cells sending feedback projections to V1 layer 5 cells to prime, and then learn the activation pattern of, active layer 5 cells.

4.4 Neurotransmitter release. The neurotransmitter released by the pre-synaptic terminal scales the EPSP or IPSP triggered at the post-synaptic site. The accumulation and depletion (inactivation, habituation) of neurotransmitter z_{jk} at a synapse between neurons j and k is described by (Grossberg, 1980):

$$\frac{dz_{jk}}{dt} = \frac{(B - z_{jk})}{\tau} - \varepsilon \delta(t) z_{jk}, \quad (7)$$

where $B = 1$ is the target level of neurotransmitter at rest, $0 < \varepsilon < 1$ is the depletion coefficient that can scale the amount of neurotransmitter released at every spike, and $0.1 < \tau < 500$ is the recovery rate (in *ms*) regulating the rate of neurotransmitter accumulation. A spike $\delta(t)$ is defined as:

$$\delta(t) = \begin{cases} 1 & \text{if } V(t) < 0 \quad \text{and} \quad V(t - \Delta t) > V^\theta \\ 0 & \text{otherwise} \end{cases}, \quad (8)$$

where $V(t)$ is the soma membrane voltage at time t , V^θ is the voltage threshold that is invariably crossed during spikes (30 *mV*), $V(t - \Delta t)$ is the soma membrane voltage at time $t - \Delta t$ that precedes the soma voltage crossing 0*mV*. In (7), the neurotransmitter z_{jk} accumulates towards B at a rate inversely proportional to the recovery rate τ , and habituates, or is depleted, by $-\varepsilon \delta(t) z_{jk}$ every time a spike occurs. Neurotransmitter depletion allows the EPSP and IPSP to be multiplicatively gated by the amount of neurotransmitter available, while still ensuring that $0 < g_{jk} z_{jk} < B$ (for all simulations, $B = 1$). Figure 9 shows how neurotransmitter level varies with different values of ε and τ and different pre-synaptic firing frequencies.

4.5 Ionic currents. Potassium (K^+) and Sodium (Na^{++}) currents I_K and I_{Na} in (1) are derived from Traub and Miles (2001), and are described as:

$$I_K = \bar{g}_K n^4 (E_K - V), \quad (9)$$

where

$$\frac{dn}{dt} = \alpha(1 - n) - \beta n, \quad (10)$$

$$\alpha = \frac{.032(15 - V)}{e^{\frac{15 - V}{5}} - 1}, \quad (11)$$

$$\beta = .5e^{\frac{10 - V}{40}}, \quad (12)$$

and

$$I_{Na} = m^3 h \bar{g}_{Na} (E_{Na} - V), \quad (13)$$

where

$$\frac{dm}{dt} = \alpha(1-m) - \beta m, \quad (14)$$

$$\alpha = \frac{.032(13-V)}{e^{\frac{13-V}{4}} - 1}, \quad (15)$$

$$\beta = \frac{-.28(40-V)}{e^{\frac{40-V}{-5}} - 1}, \quad (16)$$

$$\frac{dh}{dt} = \alpha(1-h) - \beta h, \quad (17)$$

$$\alpha = .128e^{\frac{27-V}{18}}, \quad (18)$$

and

$$\beta = \frac{4}{e^{\frac{40-V}{5}} + 1}. \quad (19)$$

For all neurons, $E_K = -90mV$ and $E_{Na} = 50mV$. Leakage current I_{leak} is defined as:

$$I_{leak} = -\frac{g_{leak} N_{leak}}{\pi DL} V, \quad (20)$$

where g_{leak} is the conductance of the leakage channel, $\frac{N_{leak}}{\pi DL}$ is the channel density, and $E_{leak} = 0mV$.

4.6 Calcium currents in thalamic cells. Low Threshold *T-Type current* (Desthene, 2000) are implemented in thalamic matrix, core, TRN and nonspecific thalamic cells, and are described as:

$$I_{Ca} = \bar{g}_{Ca} m^3 h (E_{Ca} - V), \quad (21)$$

where

$$\frac{dm}{dt} = \frac{1}{\tau_m} (m_{\infty} - m), \quad (22)$$

$$\tau_m = \frac{1}{e^{\frac{-63-V}{7.8}} + 1}, \quad (23)$$

$$m_{\infty} = 2.44 + 2.506 \cdot 10^{-2} e^{-9.84 \cdot 10^{-2} V}, \quad (24)$$

$$\frac{dh}{dt} = \frac{1}{\tau_h} (h_{\infty} - h), \quad (25)$$

$$\tau_h = \frac{1}{\frac{-83-V}{6.3} + 1}, \quad (26)$$

and

$$h_{\infty} = 19.5 + 7.171 \cdot 10^{-2} e^{-10.54 \cdot 10^{-2} V}. \quad (27)$$

For all neurons with Ca^{++} currents, $\bar{g}_{Ca} = 250 mS/cm^2$, and $E_{Ca} = 180 mV$.

4.7 Cholinergic modulation and after-hyperpolarization currents (AHP). Pharmacological and physiological studies have demonstrated that ACh has facilitatory effects on cortical pyramidal

neurons (McCormick and Prince, 1985), and rat cortical layer 5 cells seem to be a preferential target for cholinergic innervation (Turrini et al., 2001). The known electrophysiological excitatory action is thought to be mediated by binding of ACh to muscarinic and/or nicotinic receptors on pyramidal neurons. This causes a reduction of membrane K^+ conductance in cortical neurons, enhancing depolarization in response to glutamatergic input (McCormick and Prince, 1985) and reducing spike adaptation due to the after-hyperpolarization current (AHP, Hille, 2001) based on a slow and long-lasting increase in K^+ conductance.

AHP and its modulation by acetylcholine are modeled by:

$$I_i = g_{Ch}(V^{EQ} - V),$$

where the AHP current conductance $g_{Ch} = g^* \bar{g}_{AHP} g(t)$ is modulated by the conductance g^* controlled by the cholinergic presynaptic spike, and \bar{g}_{AHP} [nS] is the maximal K^+ conductance of the AHP channel. The AHP conductance $g(t)$ is described by (3):

$$g(t) = \begin{cases} \frac{p}{\tau_f - \tau_r} (e^{-\frac{t}{\tau_f}} - e^{-\frac{t}{\tau_r}}) & \text{if } \tau_f \neq \tau_r \\ \frac{t}{\tau_f} e^{-(1 - \frac{t}{\tau_f})} & \text{if } \tau_f = \tau_r \end{cases},$$

where t is time since the action potential of a modulatory cell; p is the scaling coefficient described in (4). For the AHP used in these simulations τ^r and τ^f , namely the rise and fall time constants, respectively, are $\tau^r = 80ms$ and $\tau^f = 100ms$. The K^+ channels responsible for the AHP are opened by any cell's axonal output. If there is no spike, $t = \infty$, therefore $g = 0$. If there is a spike, $t = 0$, causing g to rise. The effect of a cell's spike on the soma membrane potential in the presence of AHP is illustrated in Figure 17.

The cholinergic modulation conductance g^* is described by

$$g^* = \begin{cases} 1 - \frac{p}{\tau_f - \tau_r} (e^{-\frac{t}{\tau_f}} - e^{-\frac{t}{\tau_r}}) & \text{if } \tau_f \neq \tau_r \\ 1 - \frac{t}{\tau_f} e^{-(1 - \frac{t}{\tau_f})} & \text{if } \tau_f = \tau_r \end{cases}, \quad (28)$$

where $\tau^r = 5ms$ and $\tau^f = 6ms$, and t is the time since the pre-synaptic cholinergic cell spikes (nucleus basalis of Maynert). These simulations investigate only the fast cholinergic dynamics, and do not address longer-lasting effect of ACh on target neural populations (Hasselmo, 1995). The cholinergic input acts by closing the normally open gate g^* , therefore limiting the total AHP conductance when ACh modulation is active.

4.8 Network connectivity. Connections between and within cell populations link a presynaptic cell with a given postsynaptic cell compartment target of the axonal projection, and can be categorized as: 1-to-1, 1-to-many, or many-to-1 projections. Synaptic weights w_{ij} can be defined between and within layers according to:

$$w_{ij} = \frac{1}{\sqrt{2\pi\sigma^2}} e^{-(x-\mu)^2 / 2\sigma^2}, \quad (29)$$

where μ is the mean and σ is the standard deviation. Each axonal pathway can be considered as a delay line, which adds an additional component of delay between pre- and post-synaptic spike, aside from

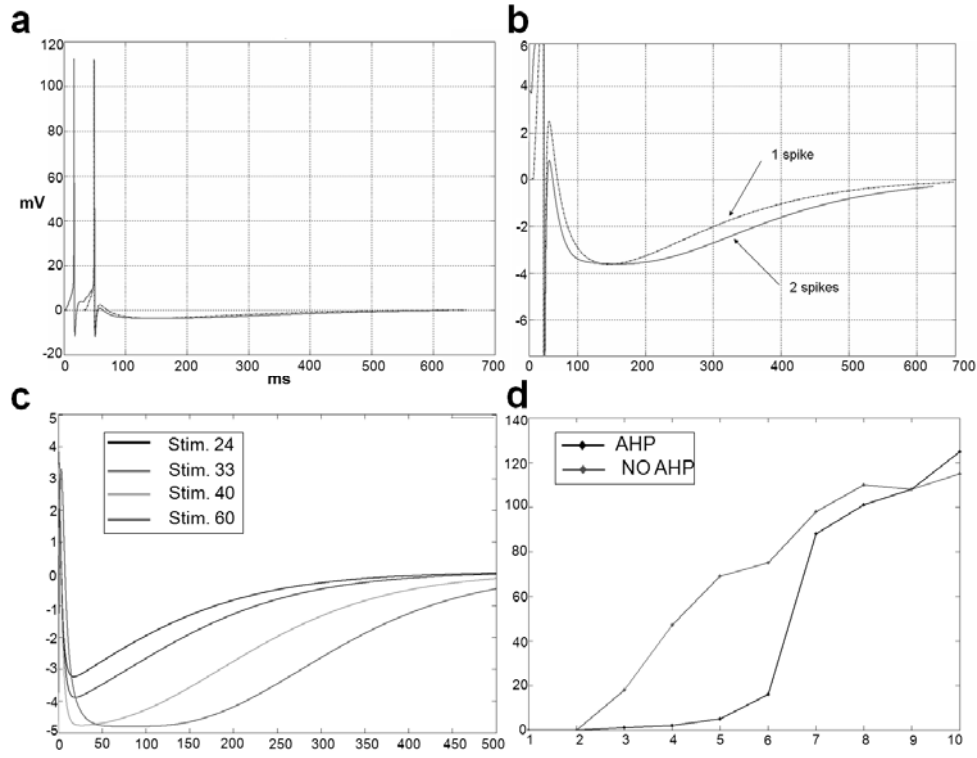


Figure 17 AHP-controlled inhibitory currents are spike-dependent. **(a)** Effect of cell spiking frequency on the membrane potential in the presence of AHP. The membrane potential of an isolated layer 5 pyramidal cell is plotted after emitting one (dotted trace) or two (continuous trace) spikes. Stimulation was induced by a 10ms current injection until one or two spikes were generated. In order to allow direct comparison of the membrane voltage, the second spike in the “two-spikes” condition and the only spike in the “one-spike” condition were aligned for comparison. **(b)** Magnification of **(a)** shows the different time course and amplitude of the membrane potential in the two conditions. **(c)** Higher firing rates, caused by higher currents injections of 24, 33, 40, and 60mV cause longer-lasting and deeper cell hyperpolarization, almost fully recovering after 500ms . **(d)** Firing rate (output) vs. input intensity (voltage clamp of 3, 9, 15, 24, 33, 40, 60, 72, 77mV) in a pyramidal cell with (black) and without (red) AHP. Firing rates of cells with active AHP are generally lower from those with blocked AHP. Cells with active or inactive AHP also differ on the shape by their input/output function.

the time required by EPSPs to trigger an action potential. Axonal delays were chosen to be consistent with both known transmission delays in cortical and subcortical areas, and with the spatial conformation of the model, and are summarized in Supplementary Table 3 online. In general, inhibitory to excitatory connections have small delays, intra-cortical feedforward connections have longer delays (Dinse and Kruger, 1994), and feedback connections (both corticocortical and corticothalamic) have even longer delays (Schmolesky et al., 1998; Miller, 1996).

The model accounts for the driving vs. modulatory nature of synaptic connections by exploiting both the magnitude of the synaptic weight *and* the passive neuron cable properties. An EPSP occurring at the distal dendrite tends to be attenuated with respect to the one occurring at the proximal dendrite or the soma depending on compartmental length and diameter. Inter-compartmental currents are described by (2), where $g_{Ch} = g_m r D / 4 L_l^2$ [$k\Omega \cdot \text{cm}$], and where V^{EQ} and V represent the voltage of neighboring compartments. The longer and smaller the dendrite, the more attenuated the post-synaptic current will be at the soma. Differential dendritic termination and synaptic weight magnitudes can be used to simulate the proposed functional differentiation between driving, large, round (R-type) thalamic vesicles occurring at retinothalamic and thalamocortical synapses, and elongated, small vesicles that characterize many corticothalamic terminations (Rockland, 1998; Sherman and Guillery,

2001). Elongated and round-type synapses also widely occur at the level of corticocortical synapses (Rockland, 2002). Besides the different morphology of synaptic boutons, inputs to thalamic relay cells are not distributed evenly on their dendrites (Guillery, 1969; Wilson et al., 1984; Erisir et al., 1997). Retinal and parabrachial inputs are limited to proximal dendrites, while cortical inputs are located more distally. The SMART model captures these morphological and functional characteristics by concentrating driving connections in proximal dendrites, and modulatory connections with smaller synaptic weights in distal dendrites of the target cell. These characteristics are realized between neurons in the on-center/off-surround architecture implemented by inhibitory interneurons in cortical and thalamic areas.

4.9 Stimuli. Bottom-up stimuli consist of static vertical or horizontal bars centered on the 9 x 9 receptor grid, and implemented via fixed intensity current injection to 5 vertically or horizontally aligned thalamic specific relay neurons until a stream of action potential is induced at a firing rate of 40 Hz. When indicated, top-down feedback is induced by injecting a stimulating current to the soma of a layer 6^{II} cortical cell. A typical run of the model consists of 100ms epoch, or 1000ms in recording of neural synchrony, with the membrane potentials of all neuronal compartments recorded along with the plastic synaptic weights configuration before and after the run.

4.10 Oscillations analysis. Power analysis of single or collective neural signals allows the extraction of information contained in different frequency ranges. Where indicated, analysis of 1000ms epochs is performed separately in three different frequency ranges: 2–8 (delta and theta, δ and θ), 8–10 (alpha and beta, α and β) and 20–70Hz (gamma, γ). The mean firing rate is subtracted from the data, and a Hamming window of 200ms is applied to smooth the resulting values. The results are then Fourier transformed and multiplied with the complex conjugate (cross- and auto-components), and the inverse transformation is performed for selected, continuous frequency bins (corresponding to one “band”). In this way, it is possible to reconstruct a time-averaged firing rate for selected frequency ranges. These values can then be used to compute cross- and auto-correlations at different frequency ranges (von Stein et al., 2000).

4.11 Local Field Potential and Current Source Density analysis. Cortical LFP and CSD are recorded via a simulated 54-tip-electrode. The distance of the electrode to the selected cell in the population is drawn from a uniform random distribution in the interval [10 - 200] μm , whereas the distance to all other cells in the layer is drawn from a uniform random distribution in the interval [10 - 1000] μm . An extracellular inward current flow towards the interior of the cell creates a current *sink*, while an outside flow creates a current *source* in a particular membrane section. Assuming an extracellular fluid with constant conductance, the potential generated by such current dipole is:

$$V_e = \frac{1}{4\pi\sigma} \left(\frac{I^+}{r^+} + \frac{I^-}{r^-} \right), \quad (30)$$

where I -s and r -s are currents and distances between the electrode and the point where the respective current flows through the membrane (approximated by the center of the compartment), respectively, + and - mark the attributes of source and sink, respectively, and $\sigma = 15$ [mS/cm] is the extracellular conductivity. In the case of more complex cells with many possible sources and sinks, V_e becomes:

$$V_e = \frac{1}{4\pi\sigma} \sum_l \frac{I_l}{r_l}. \quad (31)$$

Compartmental trans-membrane currents I_l [μA] are expressed in terms of:

$$I_l = J_l S_l = -\frac{g_l D_l}{4L_l^2} (V_l - V_{l\pm 1}) \left(2\frac{\pi D_l^2}{4} + \pi D_l L_l \right) = -\frac{g_l \pi D_l^2}{4L_l^2} (V_l - V_{l\pm 1}) \left(\frac{D_l}{2} + L_l \right). \quad (32)$$

Since CSD and LFP can be measured with multiple electrodes, for each electrode tip the distance r_l to the compartment center is different. CSD is calculated both in experimental studies and in the present work by linear approximation of the second derivative of the voltage:

$$CSD = \frac{V_{e+1} + V_{e-1} - 2V_e}{\Delta x}, \quad (33)$$

where Δx is the distance between neighboring electrode tips.

4.12 Simulation environment. The model is implemented in KInNeSS (KDE Integrated NeuroSimulation Software, www.kinness.net), a software package that allows the simulation of single neurons with multiple compartments as well as large networks of such elements (Versace et al., 2007). All off-line data analysis is implemented in Matlab (Mathworks Inc.). Simulations are run on 2.80 GHz Intel CPU, 1GB of RAM, under Linux operating system. The network is described in Neuro Markup Language code (NeuroML, <http://www.neuroml.org/>). NeuroML is a variation of XML designed for modeling different aspects and levels of neural systems, from intracellular mechanisms and ion channel kinetics to the dynamics of networks of reconstructed neurons. The code is downloadable in the Research section at <http://www.kinness.net/>.

REFERENCES

- Abbott L.F., Sen, K., Varela, J.A., Nelson, S.B., 1997. Synaptic depression and cortical gain control. *Science*, 275, 220-222.
- Ahissar, M., and Hochstein, S., 2002. View from the Top: Hierarchies and Reverse Hierarchies in the Visual System. *Neuron*, 36, 791-804.
- Ahmed, B., Anderson, J.C., Martin, K.A.C., and Nelson, J.C., 1997. Map of the synapses onto layer 4 basket cells of the primary visual cortex of the cat. *J. Comp. Neurol.*, 380, 230-242.
- Alonso, J. M., Usrey, W. M., and Redi, R. C., 2001. Rules of connectivity between geniculate cells and simple cells in cat primary visual cortex. *J. Neurosci.*, 21, 4002-4015.
- Bazhenov, M., Timofeev, I., Steriade, M., and Sejnowski, T.J., 1998. Computational Models of Thalamocortical Augmenting Responses. *J. Neurosci.*, 18, 6444-6465.
- Beierlein, M., Fall, C.P., Rinzel, J., and Yuste, R., 2002. Thalamocortical Bursts Trigger Recurrent Activity in Neocortical Networks: Layer 4 as a Frequency-Dependent Gate. *J. Neurosci.*, 22, 9885-9894.
- Bi, G.Q., Poo, and M., 2001. Synaptic modification by correlated activity: Hebb's postulate revisited. *Annu. Rev. Neurosci.*, 24, 139-166.
- Blasdel, G.G., and Lund, J.S., 1983. Termination of afferent axons in macaque striate cortex. *J. Neurosci.*, 3, 1389-1413.
- Bosking, W., Zhang, Y., Schofield, B., and Fitzpatrick, D., 1997. Orientation selectivity and the arrangement of horizontal connections in tree shrew striate cortex. *J. Neurosci.*, 17, 2112-2127.
- Bullier, J., McCourt, M.E. and Henry, G.H., 1988. Physiological studies on the feedback connection to the striate cortex from cortical areas 18 and 19 of the cat. *Exp. Brain Res.* 70, 90-8.
- Callaway, E.M., 1998. Local circuits in primary visual cortex of the macaque monkey. *Annu. Rev. Neurosci.*, 21, 47-74.
- Callaway, E.M., and Wiser, A.K., 1996. Contributions of individual layer 2-5 spiny neurons to local circuits in macaque primary visual cortex. *Vis. Neurosci.*, 13, 907-922.
- Carpenter, G.A., and Grossberg, S., 1987. A massively parallel architecture for a self-organizing neural pattern recognition machine. *Computer, Vision, Graphics and Image Proc.*, 37, 54-115.
- Carpenter, G.A. and Grossberg, S., 1990. ART 3: Hierarchical search using chemical transmitters in self-organizing pattern recognition architectures. *Neural Netw.*, 3, 129-152.
- Carpenter, G.A., Grossberg, S., and Reynolds, J.H., 1991. ARTMAP: Supervised real-time learning and classification of nonstationary data by a self-organizing neural network. *Neural Netw.*, 4, 565-588.
- Carpenter, G.A., Grossberg, S., Markuzon, N., Reynolds, J.H., and Rosen, D.B., 1992. Fuzzy ARTMAP: A neural network architecture for incremental supervised learning of analog multidimensional maps. *IEEE Transactions on Neural Netw.*, 3, 698-713.
- Cauler, L.J., 1995. Layer I of primary sensory neocortex: where top-down converges upon bottom-up. *Behav. Brain Res.*, 71, 163-70.
- Cauler, L.J. and Connors, B.W., 2001. Synaptic Physiology of Horizontal Afferents to Layer I in Slices of Rat SI Neocortex. *J. Neurosci.*, 14, 751-762.
- Cauler, L.J., and Connors, B.W., 1994. Synaptic physiology of horizontal afferents to layer I in slices of rat SI neocortex. *J. Neurosci.*, 14, 751-62.
- Crabtree, J.W., and Isaac, J.T., 2002. New intrathalamic pathways allowing modality-related and cross-modality switching in the dorsal thalamus. *J. Neurosci.*, 22, 8754-61.
- Crick, F., 1984. Function of the thalamic reticular complex: the searchlight hypothesis. *Proc. Natl. Acad. Sci. USA.*, 81, 4586-4590.

- Desimone, R. and Duncan, J., 1995. Neural Mechanisms of Selective Visual Attention. *Annu. Rev. Neurosci.*, 18, 193-222.
- Desimone, R., 1998. Visual attention mediated by biased competition in extrastriate visual cortex. *Phil. Trans. R. Soc. Lond. B.* 353, 1245-1255.
- Destexhe, A., 2000. Modelling corticothalamic feedback and the gating of the thalamus by the cerebral cortex. *J. Physiol. Par.*, 94, 391-410.
- Destexhe, A., Contreras, D., and Steriade, M., 1999. Cortically-induced coherence of a thalamic-generated oscillation. *Neurosci.*, 92, 427-43.
- Dinse, H.R. and Kruger, K., 1994. The timing of processing along the visual pathway in the cat. *Neuroreport*, 5, 893-7.
- Engel, A.K., Fries, P., and Singer, W., 2001. Dynamic predictions: oscillations and synchrony in top-down processing. *Natl. Rev. Neurosci.*, 2, 704-16.
- Erişir, A., Van Horn, S.C., Bickford, M.E., and Sherman, S.M., 1997. Immunocytochemistry and distribution of parabrachial terminals in the lateral geniculate nucleus of the cat: a comparison with corticogeniculate terminals. *J. Comp. Neurol.*, 377, 35-49.
- Facon, E., Steriade, M., and Wertheim, N., 1958. Prolonged hypersomnia caused by bilateral lesions of the medial activator system; thrombotic syndrome of the bifurcation of the basilar trunk. *Rev. Neurolog. Par.*, 98, 117-33.
- Fitzpatrick, D., Lund, J.S., and Blasdel, G.G., 1985. Intrinsic connections of macaque striate cortex: afferent and efferent connections of lamina 4C. *J. Neurosci.*, 5, 3329-3349.
- Friedman-Hill, S., Maldonado, P.E., and Gray, C.M., 2000. Dynamics of Striate Cortical Activity in the Alert Macaque: I. Incidence and Stimulus-dependence of Gamma-band Neuronal Oscillations. *Cereb. Cortex*, 10, 1105-1116.
- Fries, P., Reynolds, J. H., Rorie, A. E., and Desimone, R., 2001. Modulation of oscillatory neuronal synchronization by selective visual attention. *Science*, 291, 1560-1563.
- Gao, E., and Suga, N., 1998. Experience-dependent corticofugal adjustment of midbrain frequency map in bat auditory system. *Proc. Natl. Acad. Sci. USA*, 95, 12663-70.
- Gorchetchnikov, A., Versace, M., and Hasselmo, M.E., 2005a. A model of STDP based on spatially and temporally local information: Derivation and combination with gated decay. *Neural Netw.*, 18, 458-466.
- Gorchetchnikov, A., Versace, M., and Hasselmo, M.E., 2005b. Spatially and temporally local spike-timing-dependent plasticity rule. *Proc. Internatl Joint Conf. on Neural Netw.*, 1568, 390-396.
- Gove, A. Mingolla, E., and Grossberg, S., 1995. Brightness perception, illusory contours, and corticogeniculate feedback. *Vis. Neurosci.*, 12, 1027-1052.
- Grieve, K.L., and Sillito, A.M., 1991. The length summation properties of layer VI cells in the visual cortex and hypercomplex cell end zone inhibition. *Exp. Brain. Res.*, 84, 319-325.
- Grossberg, S., 1976. Adaptive pattern classification and universal recoding, II: Feedback, expectation, olfaction, and illusions. *Biol Cybern.*, 20, 69-98.
- Grossberg, S., 1980. How does a brain build a cognitive code? *Psych. Rev.*, 87, 1-51.
- Grossberg, S., 1995. The attentive brain. *American. Scient.*, 83, 438-449.
- Grossberg, S., 1999a. How does the cerebral cortex work? Learning, attention, and grouping by the laminar circuits of visual cortex. *Spat. Vis.*, 12, 163-187.
- Grossberg, S., 1999b. The link between brain learning, attention, and consciousness. *Conscious. Cogn.*, 8, 1-44.
- Grossberg, S., 2000. How hallucinations may arise from brain mechanisms of learning, attention, and volution. *J. Int. Neuropsych. Soc.*, 6, 579-588.

- Grossberg, S., 2003. How does the cerebral cortex work? Development, learning, attention, and 3D vision by laminar circuits of visual cortex. *Behav. Cogn. Neur. Rev.*, 2, 47-76.
- Grossberg, S. and Seidman, D., 2006. Neural dynamics of autistic behaviors: Cognitive, emotional, and timing substrates. *Psych. Rev.*, 113, 483-525.
- Guillery, R.W., 1969. An abnormal retinogeniculate projection in Siamese cats. *Brain Res.* 3, 739-41.
- Guillery, R.W., Feig, S.L., and Lozsadi, D.A., 1998. Paying attention to the thalamic reticular nucleus. *Trends Neurosci.*, 21, 28 -32.
- Guillery, R.W., and Harting, J.K., 2003. Structure and Connections of the Thalamic Reticular Nucleus: Advancing Views over Half a Century. *J. Comp. Neurol.*, 463, 360-371.
- Hasselmo, M.E., 1993. Acetylcholine and learning in a cortical associative memory. *Neural Comput.*, 5, 32-44.
- Hasselmo, M.E., 1995. Neuromodulation and cortical function: modeling the physiological basis of behavior. *Behav. Brain Res.*, 67, 1-27.
- Heeger, D.J., 1992. Normalization of cell responses in cat striate cortex. *Vis. Neurosci.*, 9, 181-197.
- Heilman, K.M., Bowers, D., Valenstein. E., and Watson, R.T., 1993. Disorders of visual attention. *Baillière's Clinical Neurology*, 2, 389-413.
- Herrmann C.S., Munk, M.H.J., and Engel, A., 2004. Cognitive functions of gamma-band activity: memory match and utilization. *Trends Cognit. Sci.*, 8, 347-355.
- Hille, B., 2001. Ion Channels of Excitable Membranes. Third Edition, MA, USA: Sinauer Associates.
- Hodgkin, A.L., and Huxley, A.F., 1952. A quantitative description of membrane current and its application to conduction and excitation in nerve. *J. Neurophysiol.*, 117, 500-544.
- Ichinohe, N., Fujiyama, F., Kaneko, T., and Rockland, K.S., 2003. Honeycomb-like mosaic at the border of layers 1 and 2 in the cerebral cortex. *J. Neurosci.*, 23, 1372-82.
- Johnston, D., Hoffman, D.A., Colbert, C.M., and Magee, J.C., 1999. Regulation of back-propagating action potentials in hippocampal neurons. *Curr. Op. Neurob.*, 9, 288-292.
- Jones, E.G., 2002. Thalamic circuitry and thalamocortical synchrony. *Phil. Trans. R. Soc. Lond. B.*, 357, 1659-1673.
- Karmos, G., Molnár, M., Csépe, V., and Winkler, I., 1986. Evoked potential components in the layers of the auditory cortex of the cat. *Acta Neurobiologiae Experimentalis*, 46, 227-36.
- Kilgard, M.P., and Merzenich, M.M., 1998. Cortical map reorganization enabled by nucleus basalis activity. *Science*, 279, 1714-8.
- Kolmac, C.I., and Mitrofanis, J., 1997. Organisation of the reticular thalamic projection to the intralaminar and midline nuclei in rats. *J. Comp. Neurol.*, 377, 165-78.
- Kopell, N., Ermentrout, G.B., Whittington, M.A., and Traub, R.D., 2000. Gamma rhythms and beta rhythms have different synchronization properties. *P. Natl. Acad. Sci.*, USA.15, 1867-1872.
- Kraus, N., McGee, T., Littman, T., Nicol, T., and King, C., 1994. Nonprimary auditory thalamic representation of acoustic change. *J. Neurophysiol.*, 72, 1270-1277.
- Krupa, D.J., Ghazanfar, A.A., and Nicolelis, M.A.L., 1999. Immediate thalamic sensory plasticity depends on corticothalamic feedback. *P. Natl. Acad. Sci. USA*, 96, 8200-5.
- Landisman, C.E., Long, M.E., Beierlein, M., Deans, M.R., Paul, D.L. and Connors, B.W., 2002. Electrical Synapses in the Thalamic Reticular Nucleus. *J. Neurosci.*, 22, 1002-1009.
- Larkum, M.E., Senn, W., and Lusher, H.R., 2004. Top-down dendritic input increases the gain of layer 5 pyramidal neurons. *Cereb. Cortex*, 14, 1059-1070.
- Larkum, M.E., Zhu, J.J., and Sakmann, B.A., 1999. A new cellular mechanism for coupling inputs arriving at different cortical layers. *Nature*, 398, 338-341.

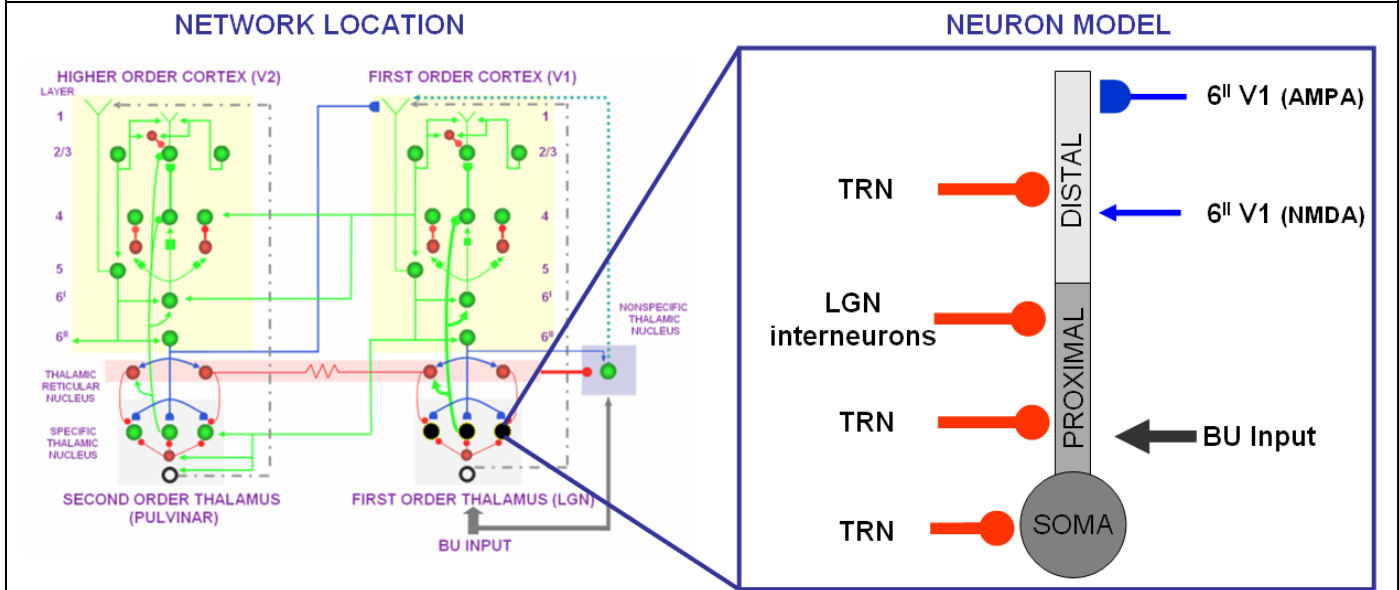
- Larkum, M.E., and Zhu, J.J., 2002. Signaling of Layer 1 and Whisker-Evoked Ca^{++} and Na^{++} Action Potentials in Distal and Terminal Dendrites of Rat Neocortical Pyramidal Neurons In Vitro and In Vivo. *J. Neurosci.*, 22, 6991-7005.
- Levy, W.B., and Steward, O., 1983. Temporal contiguity requirements for long-term associative potentiation/depression in the hippocampus. *Neurosci.*, 8, 791-797.
- Llinas, R.R., and Pare, D., 1991. Of dreaming and wakefulness. *Neurosci.*, 44, 521-35.
- Llinas, R.R., Leznik, E., and Urbano, F.J., 2002. Temporal binding via cortical coincidence detection of specific and nonspecific thalamocortical inputs: a voltage-dependent dye-imaging study in mouse brain slices. *P. Natl. Acad. Sci. USA*, 99, 449-454.
- Lumer, E.D., Edelman, G.M., and Tononi, G., 1997. Neural dynamics in a model of the thalamocortical system I. Layers, loops and the emergence of fast synchronous rhythms. *Cereb. Cortex*, 7, 207-227.
- Markram, H., Lubke, J., Frotscher, M., and Sakmann, B., 1997. Regulation of synaptic efficacy by coincidence of postsynaptic APs and EPSPs. *Science*, 275, 213-215.
- Markram, H., Toledo-Rodriguez, M., Wang, Y., Gupta, A., Silberberg, G., and Wu, C., 2004. Interneurons of the neocortical inhibitory system. *Nat. Rev. Neurosci.*, 5, 793-807.
- Maunsell, J.H.R., and Van Essen, D.C., 1983. Anatomical connections of the middle temporal visual area in the macaque monkey and their relationship to a hierarchy of cortical areas. *J. Neurosci.*, 3, 2563-2586.
- McCormick, D.A., and Prince, D.A., 1985 Two types of muscarinic response to acetylcholine in mammalian cortical neurones. *P. Natl. Acad. Sci. USA*, 82, 6344-6349.
- McGuire, B.A., Gilbert, C.D., Rivlin, P.K., and Wiesel, T.N., 1991. Targets of horizontal connections in macaque primary visual cortex. *J. Comp. Neurol.*, 305, 370-392.
- McGuire, B.A., Hornung, J.P., Gilbert, C.D., and Wiesel, T.N., 1984. Patterns of synaptic input to layer 4 of cat striate cortex. *J. Neurosci.*, 4, 3021-3033.
- Miller, J.M., and Benevento, L.A., 1979. Demonstration of a direct projection from the intralaminar central lateral nucleus to the primary visual cortex. *Neurosci. Lett.*, 14, 229-34.
- Miller, R., 1996. Corticothalamic interplay and the security of operation of neural assemblies and temporal chains in the cerebral cortex. *Biol Cybern.*, 75, 263-75.
- Montero, V.M., 1997. C-fos induction in sensory pathways of rats exploring a novel environment: shifts of active thalamic reticular sectors by predominant sensory cues. *Neurosci.*, 76, 1069 - 1081.
- Murphy, P.C., Duckett, S.G., and Sillito, A.M., 1999. Feedback connections to the lateral geniculate nucleus and cortical response properties. *Science*, 286, 1552-1554.
- Näätänen, R., Gaillard, A.W.K., and Mäntysalo S., 1978. Early selective attention effect on evoked potential reinterpreted. *Acta Psychologica*, 42, 313-329.
- Nicolelis, M.A., and Fanselow, E.E., 2002. Dynamic shifting in thalamocortical processing during different behavioural states. *Phil. Trans. R. Soc. Lond. B*, 357, 1753-8.
- Olufsen, M.S., Whittington, M.A., Camperi, M., and Kopell, N., 2003. New Roles for the Gamma Rhythm: Population Tuning and Preprocessing for the Beta Rhythm. *J. Comput. Neurosci.*, 14, 33-54.
- Pinault, D., and Deschenes, M., 1998. Anatomical evidence for a mechanism of lateral inhibition in the rat thalamus. *E. J. Neurosci.*, 10, 3462-9.
- Pollen, D.A., 1999. On the neural correlates of visual perception. *Cereb. Cortex*, 9, 4-19.
- Raizada, R.D.S., and Grossberg, S., 2003. Towards a Theory of the Laminar Architecture of Cerebral Cortex: Computational Clues from the Visual System. *Cereb. Cortex*, 13, 100-113.
- Rall, W., 1962. Theory of physiological properties of dendrites. *Ann. N. Y. Acad. Sci.*, 96, 1071-1092.

- Reid, R.C., and Alonso, J.M., 1995. Specificity of monosynaptic connections from thalamus to visual cortex. *Nature*, 378, 281-284.
- Rockland, K.S., 1996. Two types of cortico-pulvinar terminations: round , type 2 and elongate , type 1. *J. Comp. Neurol.*, 368, 57-87.
- Rockland, K.S., 1998. Convergence and Branching Patterns of Round, Type 2 Corticopulvinar Axons. *J. Comp. Neurol.*, 390, 515-536.
- Rockland, K.S., 2002. Visual cortical organization at the single axon level: a beginning. *Neurosci. Res.*, 42, 155-166.
- Rockland, K.S., and Virga, A., 1989. Terminal arbors of individual “feedback” axons projecting from area V2 to V1 in the macaque monkey: a study using immunohistochemistry of anterogradely transported Phaseolus vulgaris leucoagglutinin. *J. Comp. Neurol.*, 285, 54-72.
- Rockland, K.S., Andresen, J., Cowie, R.J., and Robinson, D.L., 1999. Single axon analysis of pulvinocortical connections to several visual areas in the macaque. *J. Comp. Neurol.*, 406, 221-50.
- Roelfsema, P.R., Engel, A.K., König, P. and Singer, W., 1997. Visuomotor integration is associated with zero time-lag synchronization among cortical areas. *Nature*, 385, 157-161.
- Rouiller, E.M., and Welker, E., 2000. A comparative analysis of the morphology of corticothalamic projections in mammals. *Brain Res. Bull.*, 53, 727-41.
- Saar, D., Grossman, Y., and Barkai, E., 2001. Long-Lasting Cholinergic Modulation Underlies Rule Learning in Rats. *J. Neurosci.*, 21, 1385-1392.
- Salin, P.A., and Bullier, J., 1995. Corticocortical connections in the visual system: structure and function. *Physiol. Rev.*, 75, 107-154.
- Sánchez-Montañés, M.A., Verschure, P.F.M.J., and König, P., 2000. Local and global gating of synaptic plasticity. *Neural Comput.*, 13, 543-552.
- Schmidt, K.E., Goebel, R., Löwel, S., and Singer, W., 1997. The perceptual grouping criterion of colinearity is reflected by anisotropies of connections in the primary visual cortex. *E. J. Neurosci.*, 9, 1083-1089.
- Schmolesky, M.T., Wang, Y., Hanes, D.P., Thompson, K.G., Leutgeb, S., Schall, J.D., and Leventhal, A.G., 1998. Signal timing across the macaque visual system. *J. Neurophysiol.*, 6, 3272-8.
- Sherman, S.M., and Guillery, R., 2001. Exploring the Thalamus. San Diego: Academic Press.
- Sherman, S.M., and Guillery, R.W., 2002. The role of the thalamus in the flow of information to the cortex. *Phil. Trans. R. Soc. Lond. B*, 357, 1695-708.
- Shipp, S., 2003. The functional logic of cortico-pulvinar connections. *Phil. Trans. R. Soc. Lond. B*, 358, 1605-24.
- Siegel, M., Kording, K.P., and König, P., 2000. Integrating top-down and bottom-up sensory processing by somato-dendritic interactions. *J. Comput. Neurosci.*, 8, 161-173.
- Sillito, A.M., Jones, H.E., Gerstein, G.L., and West, D.C., 1994. Feature-linked synchronization of thalamic relay cell firing induced by feedback from the visual cortex. *Nature*, 369, 479-482.
- Singer, W., 1999. Neuronal synchrony: A versatile code for the definition of relations? *Neuron*, 24, 49-65.
- Singer, W. and Rauschecker, J.P., 1982. Central core control of development plasticity in the kitten visual cortex. II: Electrical activation of mesencephalic and diencephalic projections. *Exp. Brain. Res.*, 47, 223-233.
- Soares, J.G.M., Diogo, A.C.M. Fiorani, M., Souza, A.P.B., and Gattass, R., 2004. Effects of inactivation of the lateral pulvinar on response properties of second visual area cells in cebus monkeys. *Clin. Exp. Pharmacol. Physiol.*, 31, 580-590.

- Sohal, V.S., and Huguenard, J.R., 2003. Inhibitory Interconnections Control Burst Pattern and Emergent Network Synchrony in Reticular Thalamus. *J. Neurosci.*, 23, 8978-8988.
- Steriade, M., Contreras, D., Curro Dossi, R., and Nunez, A., 1993. The slow, < 1 Hz oscillation in reticular thalamic and thalamocortical neurons: scenario of sleep rhythm generation in interacting thalamic and neocortical networks. *J. Neurosci.*, 13, 3284-99.
- Stratford, K.J., Tarczy-Hornoch, K., Martin, K.A.C., Bannister, N.J., and Jack, J.J.B., 1996. Excitatory synaptic inputs to spiny stellate cells in cat visual cortex. *Nature*, 382, 258-261.
- Swadlow, H.A., Gusev, A.G., and Bezdudnaya, T., 2002. Activation of a cortical column by a thalamocortical impulse. *J. Neurosci.*, 22, 7766-73.
- Tamas, G., Somogyi, P., and Buhl, E.H., 1998. Differentially interconnected networks of GABAergic interneurons in the visual cortex of the cat. *J. Neurosci.*, 18, 4255-4270.
- Tsodyks, M., and Markram, H., 1997. The neural code between neocortical pyramidal neurons depends on neurotransmitter release probability. *P. Natl. Acad. Sci. USA*, 94, 719-723.
- Traub, R.D., and Miles, R., 2001. Neuronal networks of the hippocampus., Cambridge, UK: Cambridge UP.
- Traub, R.D., Spruston, N., Soltesz, I., Konnerth, A., Whittington, M.A., and Jefferys, G.R., 1998. Gamma-frequency oscillations: a neuronal population phenomenon, regulated by synaptic and intrinsic cellular processes, and inducing synaptic plasticity. *Prog. Neurobiol.*, 55, 563-75.
- Turrini, P., Casu, M.A., Wong, T.P., De Koninck, Y., Ribeiro-da-Silva, A., and Cuello, A.C., 2001. Cholinergic nerve terminals establish classical synapses in the rat cerebral cortex: synaptic pattern and age-related atrophy. *Neurosci.*, 105, 277-285.
- Usrey, W.M., 2002. The role of spike timing for thalamocortical processing. *Curr. Op. Neurob.*, 12, 411-417.
- van Der Werf, Y.D., Scheltens, P., Lindeboom, J., Witter, M.P., Uylings, H.B., and Jolles, J., 2003. Deficits of memory, executive functioning and attention following infarction in the thalamus; A study of 22 cases with localised lesions. *Neuropsychologia*, 41, 1330-44.
- van Der Werf, Y.D., Witter, M.P., and Groenewegen, H.J., 2002. The intralaminar and midline nuclei of the thalamus. Anatomical and functional evidence for participation in processes of arousal and awareness. *Brain Res. Rev.*, 39, 107-40.
- Van Essen, D.C., Newsome, W.T., Maunsell, J.H., and Bixby, J.L., 1986. The projections from striate cortex, V1 to areas V2 and V3 in the macaque monkey: asymmetries, areal boundaries, and patchy connections. *J. Comp. Neurol.*, 244, 451-480.
- Versace, M., Ames, A., Leveille, J., Fortenberry, B., Mhatre, H., and Gorchetchnikov, A., 2007 KInNeSS: A modular framework for computational neuroscience. *BU Technical Report CAS/CNSTR-07-007*.
- Vogt, B.A., 1991. The role of layer I in cortical function. In: Cerebral Cortex, Peters A, and Jones E, (Eds.), 49-79. New York: Plenum.
- Von Stein, A., Chiang, C., and König, P., 2000. Top-down processing mediated by interareal synchronization. *P. Natl. Acad. Sci. USA*, 97, 14748-53.
- Wang, S., Eisenback, M.A., and Bickford, M.E., 2002. Relative Distribution of Synapses in the Pulvinar Nucleus of the Cat: Implications Regarding the "Driver/Modulator" Theory of Thalamic Function. *J. Comp. Neurol.*, 454, 482-494.
- Wespataat, V., Tegnigheit, F., and Singer, W., 2004. Phase sensitivity of synaptic modifications in oscillating cells of rat visual cortex. *J. Neurosci.*, 24, 9067-9075.
- Weese, G.D., Phillips, J.M., and Brown, V.J., 1999. Attentional Orienting is impaired by unilateral lesions of the thalamic reticular nucleus in the rat. *J. Neurosci.*, 19, 1035-10139.

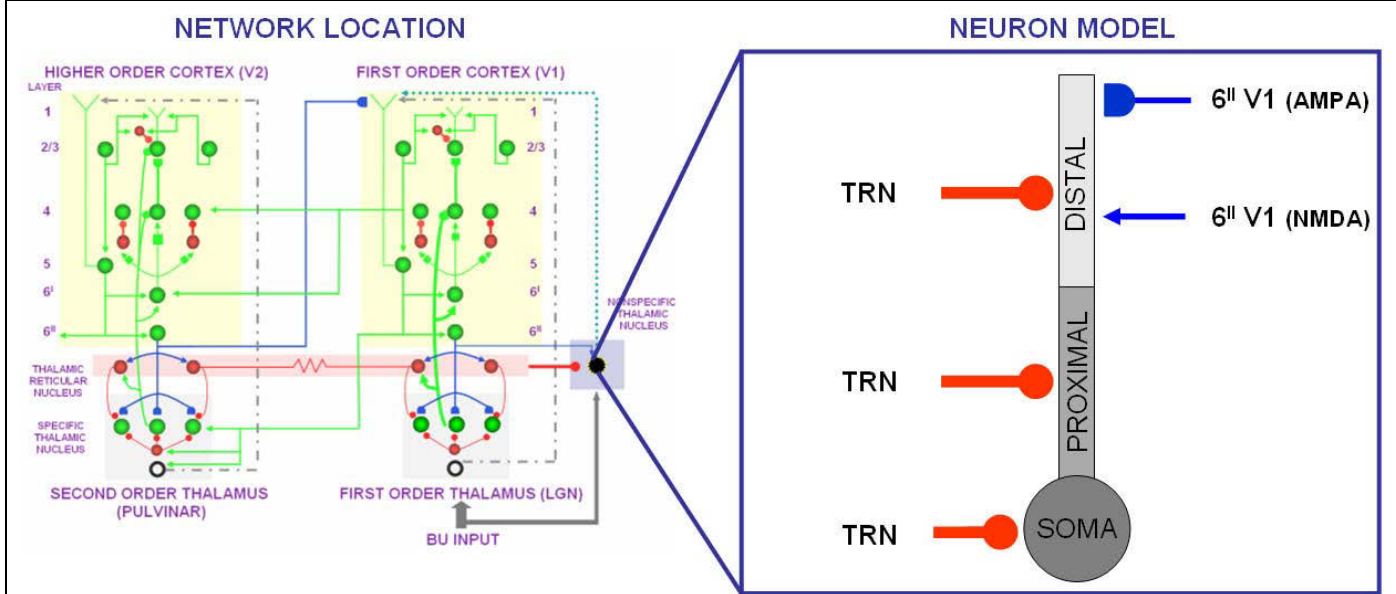
- Williams, S.R., and Stuart, G.J., 1999. Mechanisms and consequences of action potential burst firing in rat neocortical pyramidal neurons. *J. Neurophysiol.*, 521, 467-482.
- Wilson, J.R., Friedlander, M.J., and Sherman, S.M., 1984. Fine structural morphology of identified X- and Y-cells in the cat's lateral geniculate nucleus. *Phil. Trans. R. Soc. Lond. B*, 221, 411-36.
- Zeki, S., and Shipp, S., 1988. The functional logic of cortical connections. *Nature*, 335, 311-7.
- Zhang, Y.Q., Lu, S.G., Ji, J.P., Zhao, Z.Q., and Mei, J., 2004. Electrophysiological and pharmacological properties of nucleus basalis magnocellularis neurons in rats. *Acta Pharmacologica Sinica*, 25, 161-170.

THALAMIC RELAY (First Order Thalamus, LGN)



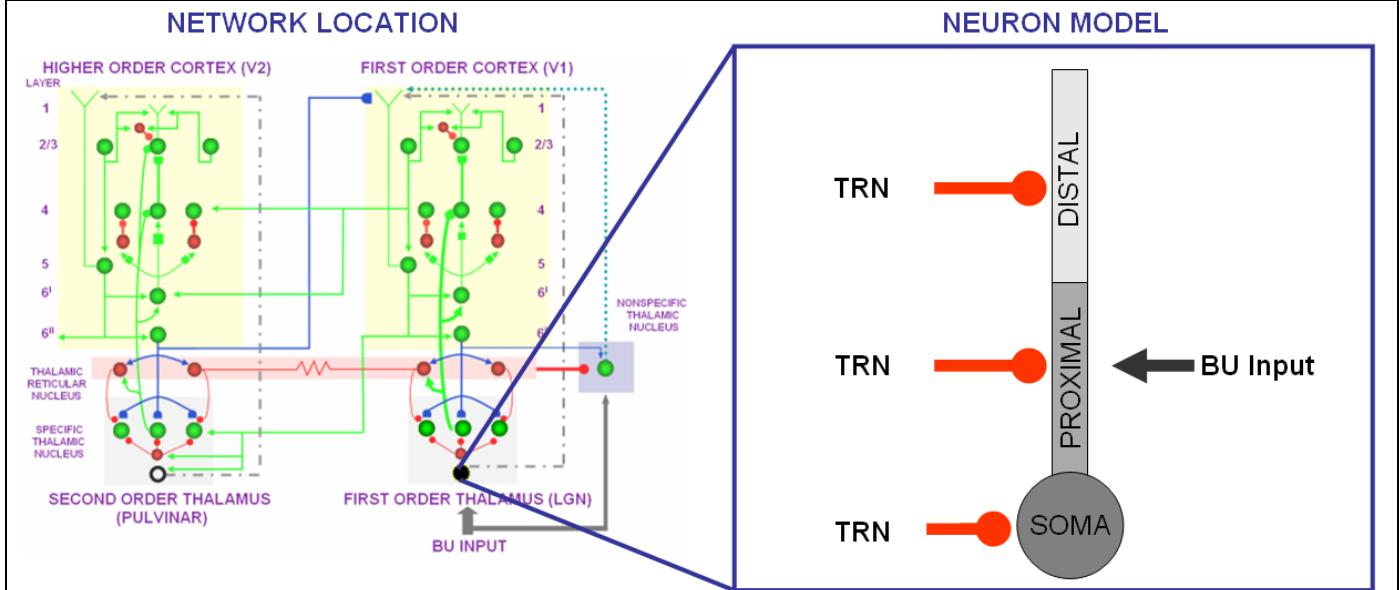
TO	FROM					
	Units	TRN	Thalamic interneurons	Layer 6 ^{II} V1	Layer 6 ^{II} V1	BU INPUT
SOMA						
Channel type		GABA				
Reverse potential	<i>mV</i>	-70				
Conductance	<i>pS</i>	2.5				
Synaptic weight	$10^6/\text{cm}^2$	0.19				
Gaussian Spread	σ	3.2				
Axonal delay	<i>ms</i>	0.1				
Channel τ' - τ''	<i>ms</i>	1 – 7				
PROXIMAL DENDRITE						
Channel type		GABA	GABA			INP.
Reverse potential	<i>mV</i>	-70	-70			0
Conductance	<i>pS</i>	2.5	2.0			1.1
Synaptic weight	$10^6/\text{cm}^2$	0.18	1.8			
Gaussian Spread	σ	3	0.35			1 to 1
Axonal delay	<i>ms</i>	0.1	0.1			
Channel τ' - τ''	<i>ms</i>	1 – 7	1 – 2			
DISTAL DENDRITE						
Channel type		GABA		AMPA (*)	NMDA	
Reverse potential	<i>mV</i>	-70		0	0	
Conductance	<i>pS</i>	2.5		1	0.5	
Synaptic weight	$10^6/\text{cm}^2$	0.19		1.5(0.05, 0.1)	0.3	
Gaussian Spread	σ	3		1.3	1.3	
Axonal delay	<i>ms</i>	0.1		2	2	
Channel τ' - τ''	<i>ms</i>	1 – 7		2 – 7	10 – 80	

THALAMIC NONSPECIFIC (First Order Thalamus)



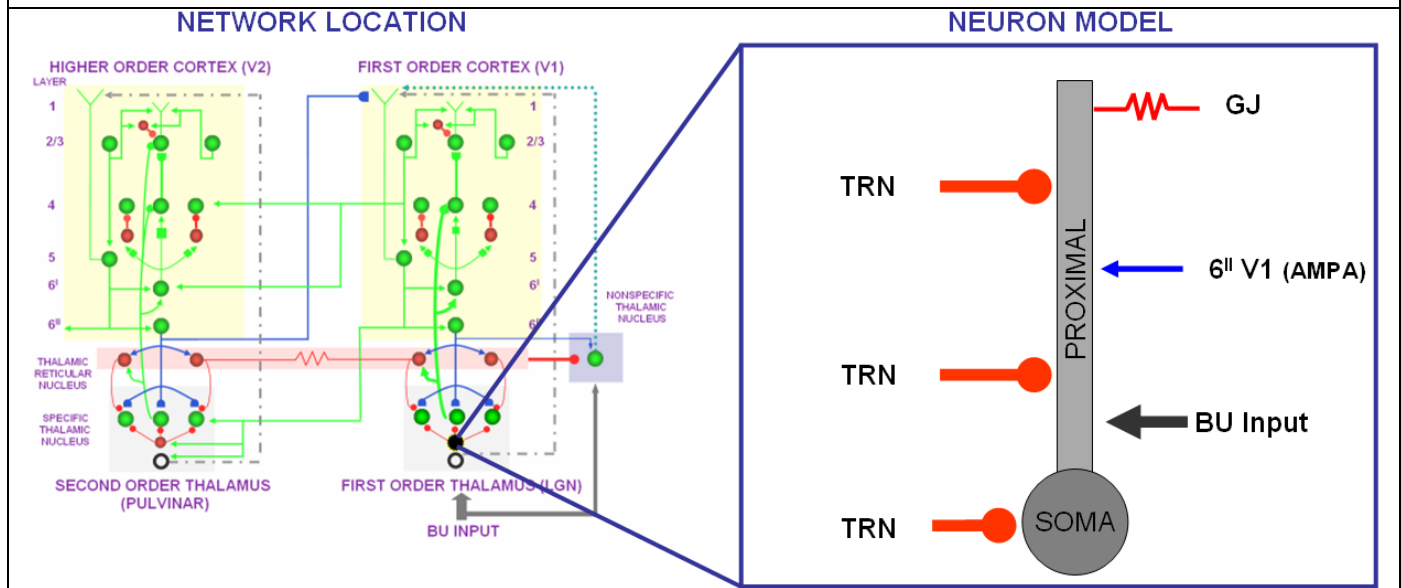
TO	FROM			
	Units	TRN	Layer 6 ^{II} V1	Layer 6 ^{II} V1
SOMA				
Channel type		GABA		
Reverse potential	<i>mV</i>	-70		
Conductance	<i>pS</i>	2.461		
Synaptic weight	$10^6/cm^2$	0.01		
Gaussian Spread	σ	all to 1		
Axonal delay	<i>ms</i>	0.1		
Channel $\tau^r - \tau^l$	<i>ms</i>	1 – 4		
PROXIMAL DENDRITE				
Channel type		GABA		
Reverse potential	<i>mV</i>	-70		
Conductance	<i>pS</i>	1.5		
Synaptic weight	$10^6/cm^2$	0.16		
Gaussian Spread	σ	all to 1		
Axonal delay	<i>ms</i>	0.1		
Channel $\tau^r - \tau^l$	<i>ms</i>	1 – 4		
DISTAL DENDRITE				
Channel type		GABA	AMPA	NMDA
Reverse potential	<i>mV</i>	-70	0	0
Conductance	<i>pS</i>	1.5	0.2	0.1
Synaptic weight	$10^6/cm^2$	0.16	1	1
Gaussian Spread	σ	all to 1	all to 1	all to 1
Axonal delay	<i>ms</i>	0.1	6	6
Channel $\tau^r - \tau^l$	<i>ms</i>	1 – 7	2 – 2	0.7 – 80

THALAMIC MATRIX (First Order Thalamus)



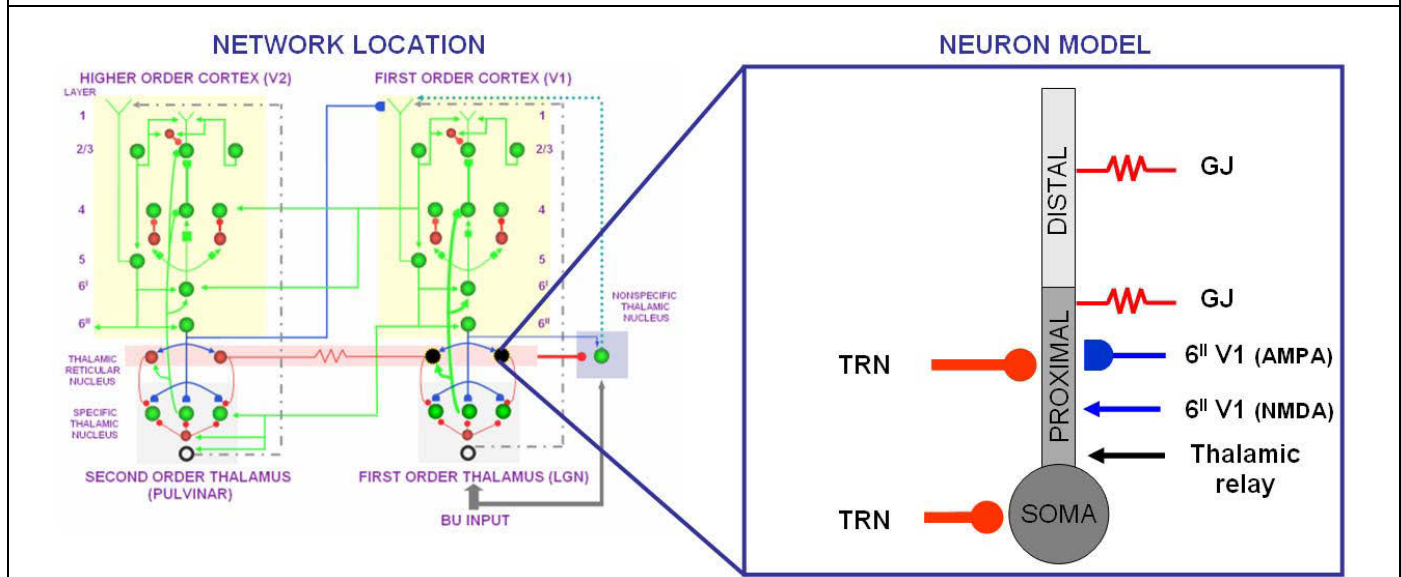
	FROM		
TO	Units	TRN	BU INPUT
SOMA			
Channel type		GABA	
Reverse potential	mV	-70	
Conductance	pS	2.461	
Synaptic weight	$10^6/cm^2$	0.5	
Gaussian Spread	σ	all to 1	
Axonal delay	ms	0.1	
Channel $\tau^r - \tau^l$	ms	1 – 4	
PROXIMAL DENDRITE			
Channel type		GABA	INP.
Reverse potential	mV	-70	0
Conductance	pS	1.5	1.1
Synaptic weight	$10^6/cm^2$	0.14	
Gaussian Spread	σ	all to 1	all to 1
Axonal delay	ms	0.1	
Channel $\tau^r - \tau^l$	ms	1 – 4	
DISTAL DENDRITE			
Channel type		GABA	
Reverse potential	mV	-70	
Conductance	pS	1.5	
Synaptic weight	$10^6/cm^2$	0.14	
Gaussian Spread	σ	all to 1	
Axonal delay	ms	0.1	
Channel $\tau^r - \tau^l$	ms	1 – 4	

THALAMIC INHIBITORY INTERNEURONS (First Order Thalamus)



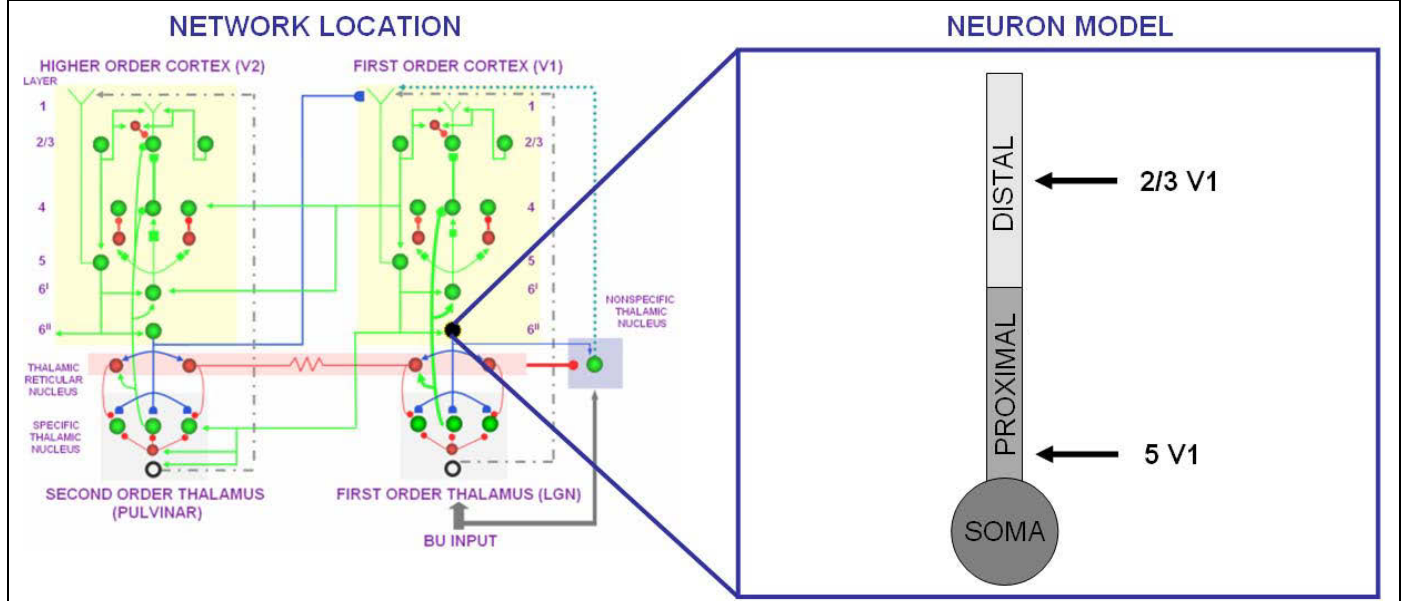
TO	FROM				
	Units	TRN	Thalamic interneurons	Thalamic interneurons (proximal dendrite)	Layer 6" V1
SOMA					
Channel type		GABA			
Reverse potential	mV	-70			
Conductance	pS	2.5			
Synaptic weight	$10^6/cm^2$	0.2			
Gaussian Spread	σ	0.8			
Axonal delay	ms	0.1			
Channel $\tau' - \tau$	ms	1 – 6			
PROXIMAL DENDRITE					
Channel type		GABA	GABA	GJ	AMPA
Reverse potential	mV	-70	-70		0
Conductance	pS	2.5	2.461	0.005	0.1
Synaptic weight	$10^6/cm^2$	0.2	0.08		1
Gaussian Spread	σ	0.8	0.9	0.3	1.2
Axonal delay	ms	0.1	0.1		4
Channel $\tau' - \tau$	ms	1 – 6	1 – 5		2 – 2

THALAMIC RETICULAR – TRN (First Order Thalamus)



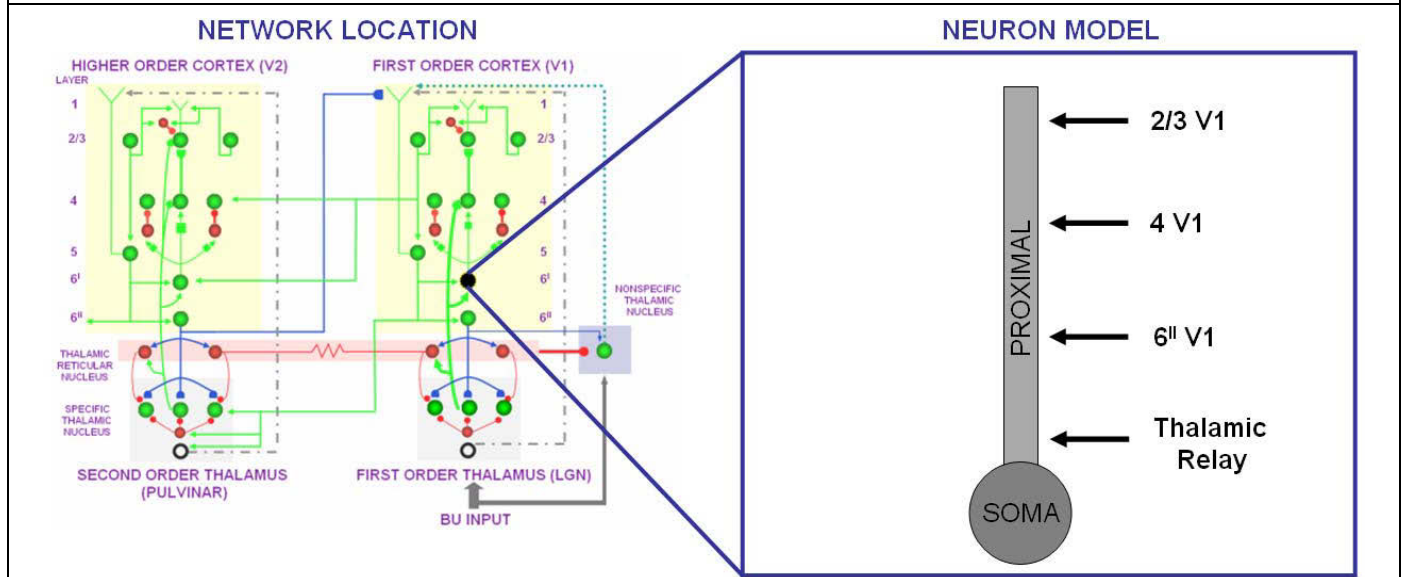
TO	FROM						
	Units	TRN	Layer 6 ⁱⁱ V1	Layer 6 ⁱⁱ V1	Thalamic relay	TRN (proximal dendrite)	TRN (distal dendrite)
SOMA							
Channel type		GABA					
Reverse potential	<i>mV</i>	-70					
Conductance	<i>pS</i>	2.461					
Synaptic weight	$10^6/cm^2$	0.3					
Gaussian Spread	σ	2					
Axonal delay	<i>ms</i>	0.1					
Channel $\tau^r - \tau^l$	<i>ms</i>	1 – 4					
PROXIMAL DENDRITE							
Channel type		GABA	AMPA	NMDA	AMPA	GJ	
Reverse potential	<i>mV</i>	-70	0	0	0		
Conductance	<i>pS</i>	2.461	0.3	0.2	0.4	0.015	
Synaptic weight	$10^6/cm^2$	0.2	4	0.3	5		
Gaussian Spread	σ	2	1.5	1.2	2.2	1	
Axonal delay	<i>ms</i>	0.1	4	4	0.1		
Channel $\tau^r - \tau^l$	<i>ms</i>	1 – 4	4 – 5	2 – 2	2 – 2		
DISTAL DENDRITE							
Channel type							GJ
Reverse potential	<i>mV</i>						
Conductance	<i>pS</i>						0.010
Synaptic weight	$10^6/cm^2$						
Gaussian Spread	σ						1
Axonal delay	<i>ms</i>						
Channel $\tau^r - \tau^l$	<i>ms</i>						

Layer 6^{II} (First Order Cortex, V1)



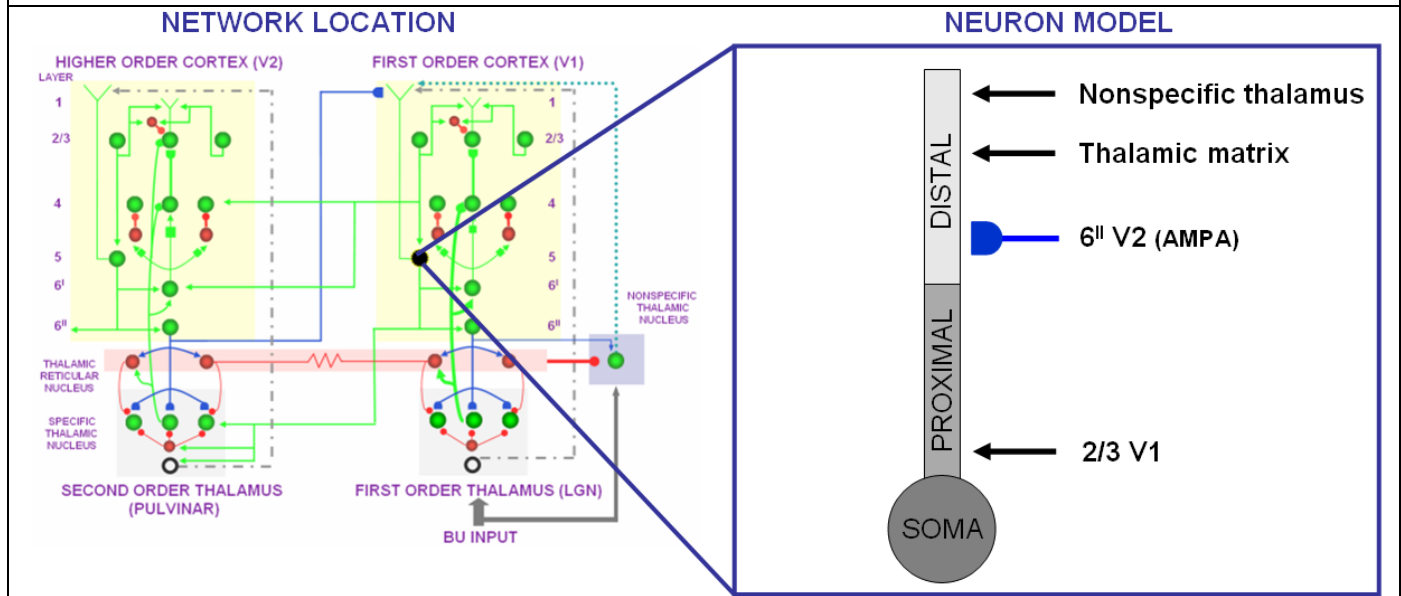
TO	FROM		
	Units	Layer 2/3 V1	Layer 5 V1
SOMA			
Channel type			
Reverse potential	mV		
Conductance	pS		
Synaptic weight	$10^6/cm^2$		
Gaussian Spread	σ		
Axonal delay	ms		
Channel $\tau^r - \tau^l$	ms		
PROXIMAL DENDRITE			
Channel type			AMPA
Reverse potential	mV		0
Conductance	pS		0.1
Synaptic weight	$10^6/cm^2$		2
Gaussian Spread	σ		1 to 1
Axonal delay	ms		0.1
Channel $\tau^r - \tau^l$	ms		2 – 2
DISTAL DENDRITE			
Channel type		AMPA	
Reverse potential	mV	0	
Conductance	pS	0.1	
Synaptic weight	$10^6/cm^2$	2	
Gaussian Spread	σ	1 to 1	
Axonal delay	ms	0.1	
Channel $\tau^r - \tau^l$	ms	2 – 2	

Layer 6^I (First Order Cortex, V1)



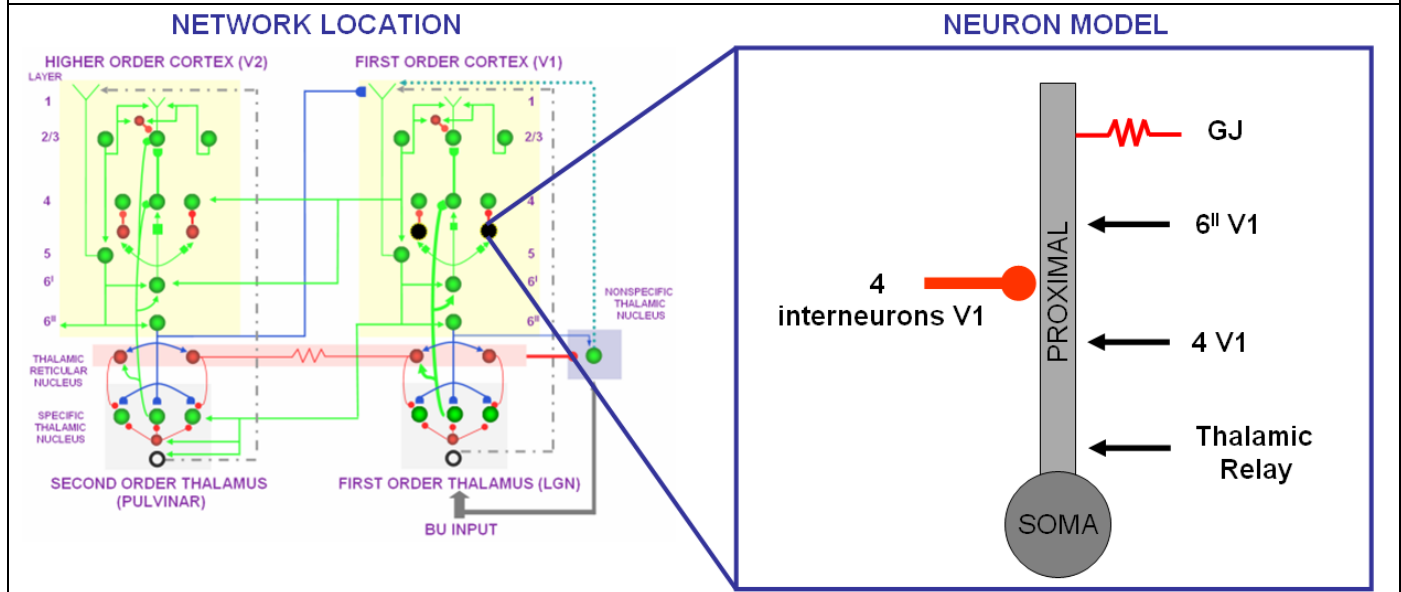
	FROM				
TO	Units	Thalamic relay	Layer 2/3 V1	Layer 4 V1	Layer 6 ^{II} V1
SOMA					
Channel type					
Reverse potential	<i>mV</i>				
Conductance	<i>pS</i>				
Synaptic weight	$10^6/cm^2$				
Gaussian Spread	σ				
Axonal delay	<i>ms</i>				
Channel $\tau^r - \tau^l$	<i>ms</i>				
PROXIMAL DENDRITE					
Channel type		AMPA	AMPA	AMPA	AMPA
Reverse potential	<i>mV</i>	0	0	0	0
Conductance	<i>pS</i>	0.9	0.1	0.1	0.1
Synaptic weight	$10^6/cm^2$	3	1	3	3
Gaussian Spread	σ	0.35	1 to 1	1 to 1	1 to 1
Axonal delay	<i>ms</i>	0.5	1	0.8	0.1
Channel $\tau^r - \tau^l$	<i>ms</i>	0.1 – 2	2 – 2	2 – 2	2 – 2

Layer 5 (First Order Cortex, V1)



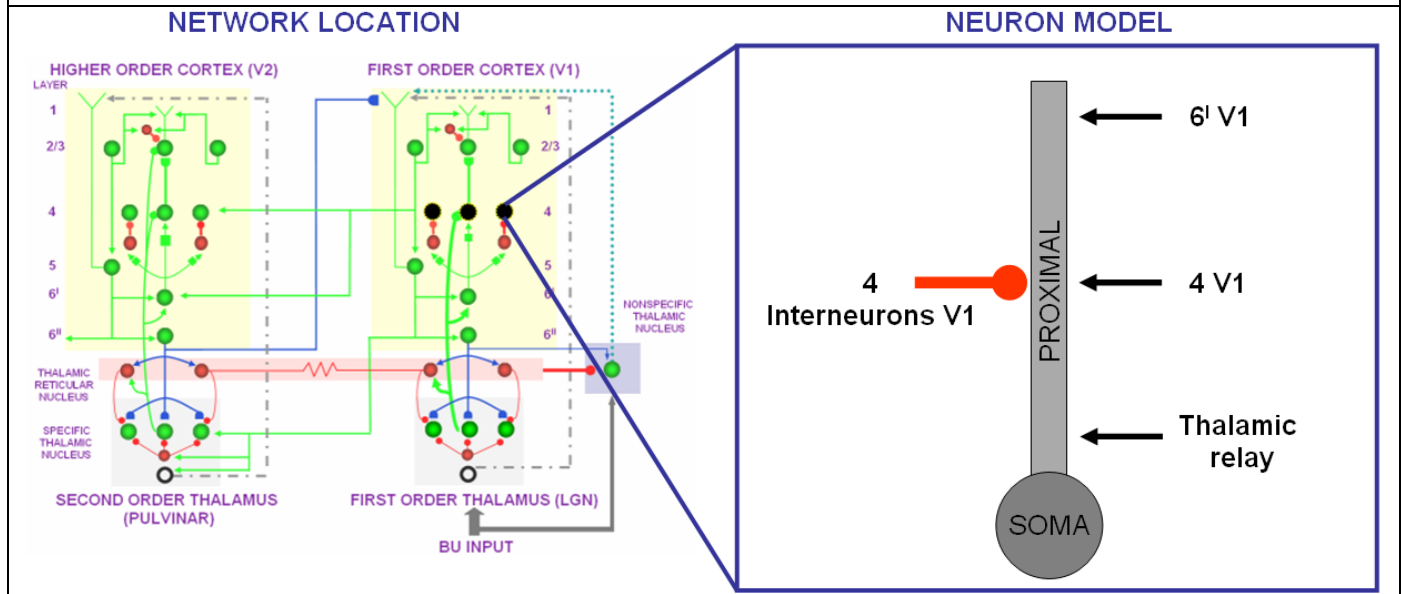
TO	FROM					
	Units	Layer 2/3 V1	Layer 6 ^{II} V2	Nonspecific thalamus	Nonspecific thalamus	Thalamic matrix
SOMA						
Channel type						
Reverse potential	<i>mV</i>					
Conductance	<i>pS</i>					
Synaptic weight	$10^6/cm^2$					
Gaussian Spread	σ					
Axonal delay	<i>ms</i>					
Channel $\tau^r - \tau^l$	<i>ms</i>					
PROXIMAL DENDRITE						
Channel type		AMPA				
Reverse potential	<i>mV</i>	0				
Conductance	<i>pS</i>	0.1				
Synaptic weight	$10^6/cm^2$	2.5				
Gaussian Spread	σ	0.35				
Axonal delay	<i>ms</i>	0.1				
Channel $\tau^r - \tau^l$	<i>ms</i>	2 – 2				
DISTAL DENDRITE						
Channel type			AMPA(*)	AMPA	NMDA	AMPA
Reverse potential	<i>mV</i>		0	0	-70	0
Conductance	<i>pS</i>		0.09	0.06	0.06	0.02
Synaptic weight	$10^6/cm^2$		5	0.06	0.01	0.01
Gaussian Spread	σ		1(0.5, 0.1)	all-to-1	all-to-1	all-to-1
Axonal delay	<i>ms</i>		0.1	3	3	3
Channel $\tau^r - \tau^l$	<i>ms</i>		2 – 2	2 – 2	2 – 10	2 – 2

LAYER 4 INTERNEURONS (First Order Cortex, V1)



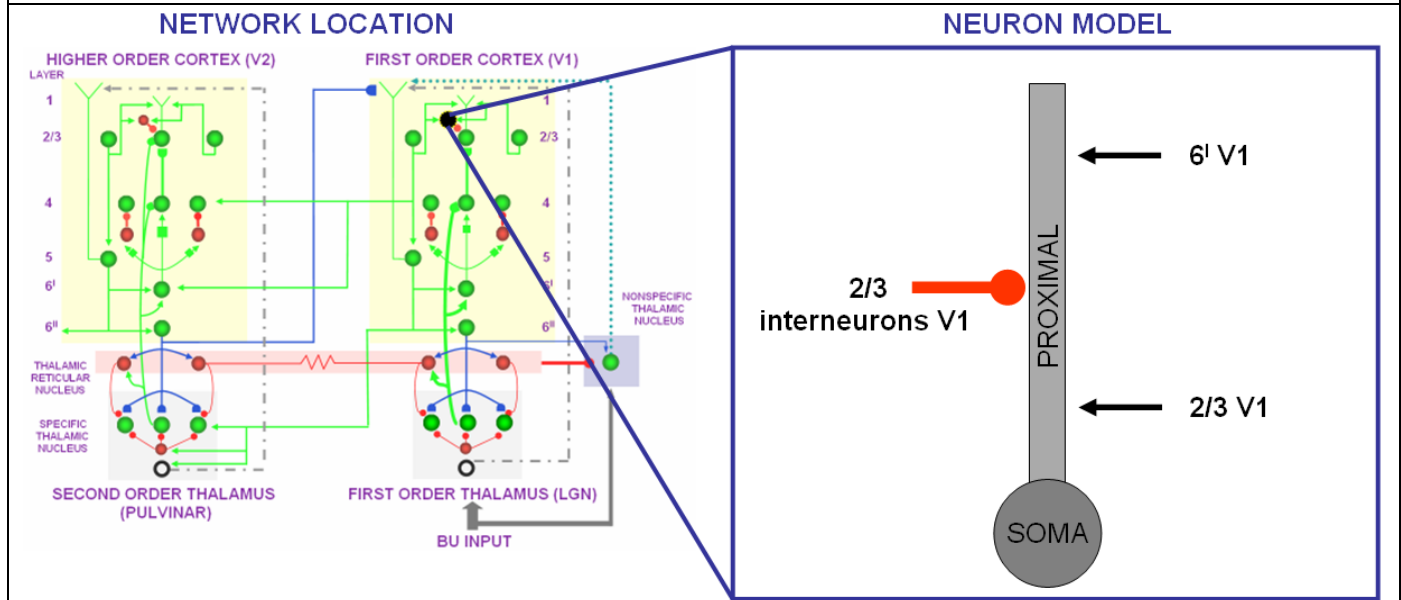
TO	FROM					
	Units	Thalamic relay	Layer 4 V1	Layer 6 ⁱ V1	Layer 4 interneurons V1	Layer 4 interneurons V1
SOMA						
Channel type						
Reverse potential	<i>mV</i>					
Conductance	<i>pS</i>					
Synaptic weight	$10^6/cm^2$					
Gaussian Spread	σ					
Axonal delay	<i>ms</i>					
Channel $\tau^r - \tau^l$	<i>ms</i>					
PROXIMAL DENDRITE						
Channel type		AMPA	AMPA	N	GABA	GJ
Reverse potential	<i>mV</i>	0	0	0	-70	
Conductance	<i>pS</i>	0.5	0.1	0.2	2.461	0.03
Synaptic weight	$10^6/cm^2$	6.5	5	(#)2 (1, 400)	0.11	
Gaussian Spread	σ	1	0.3	0.5	0.2	0.4
Axonal delay	<i>ms</i>	3	0.1	0.1	01	
Channel $\tau^r - \tau^l$	<i>ms</i>	0.1 – 0.2	0.1 – 2	0.1 – 3	1 – 2	

Layer 4 (First Order Cortex, V1)



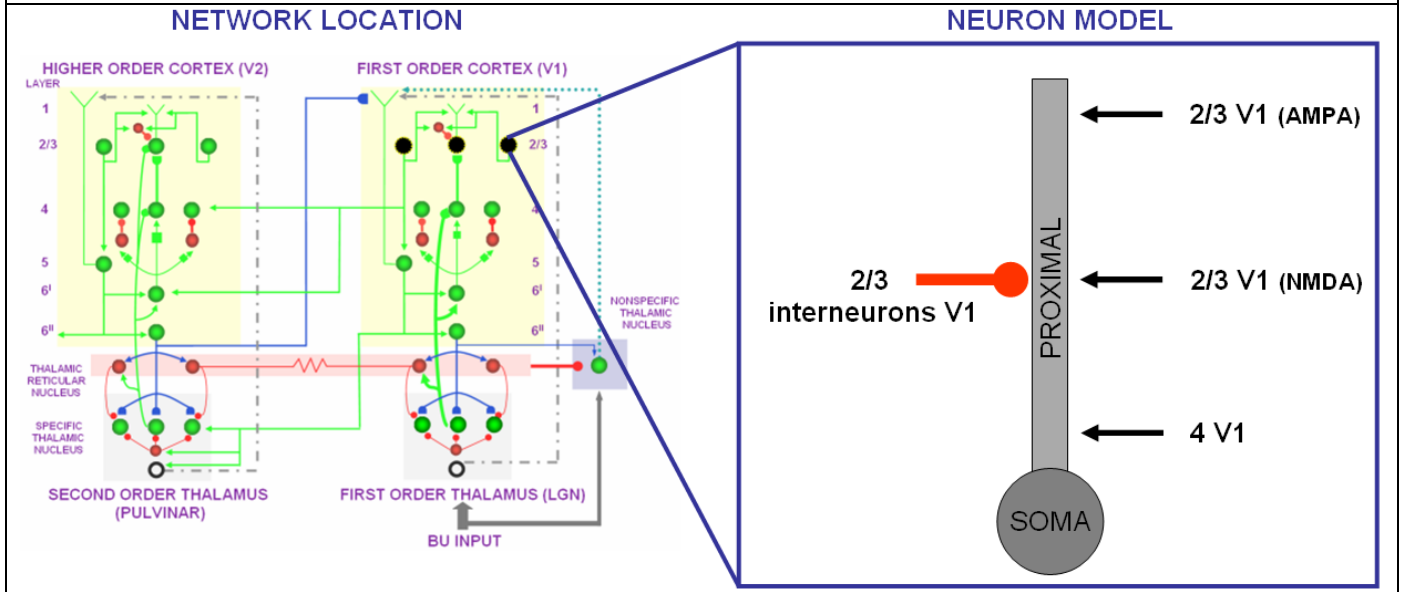
TO	FROM				
	Units	Thalamic relay	Layer 4 V1	Layer 6 ^I V1	Layer 4 interneurons V1
SOMA					
Channel type					
Reverse potential	<i>mV</i>				
Conductance	<i>pS</i>				
Synaptic weight	$10^6/cm^2$				
Gaussian Spread	σ				
Axonal delay	<i>ms</i>				
Channel $\tau^r - \tau^l$	<i>ms</i>				
PROXIMAL DENDRITE					
Channel type		AMPA (*)	AMPA	AMPA	GABA
Reverse potential	<i>mV</i>	0	0	0	-70
Conductance	<i>pS</i>	0.247	0.09	0.09	2.461
Synaptic weight	$10^6/cm^2$	6(0.3, 0.1)	0.15	(#) 0.7 (1, 400)	2
Gaussian Spread	σ	0.5	1 to 1	1 to 1	1.5
Axonal delay	<i>ms</i>	3	0.1	1	0.1
Channel $\tau^r - \tau^l$	<i>ms</i>	1 – 7	2 – 2	2 – 2	0.1 – 2

Layer 2/3 INTERNEURONS (First Order Cortex, V1)



TO	FROM			
	Units	Layer 2/3 V1	Layer 4 V1	Layer 2/3 interneurons V1
SOMA				
Channel type				
Reverse potential	mV			
Conductance	pS			
Synaptic weight	$10^6/cm^2$			
Gaussian Spread	σ			
Axonal delay	ms			
Channel $\tau^r - \tau^l$	ms			
PROXIMAL DENDRITE				
Channel type		AMPA	AMPA	GABA
Reverse potential	mV	0	0	-70
Conductance	pS	0.09	0.4	0.1
Synaptic weight	$10^6/cm^2$	0.15	1	1
Gaussian Spread	σ	1 to 1	0.3	1
Axonal delay	ms	0.1	0.1	0.1
Channel $\tau^r - \tau^l$	ms	2 - 2	2 - 2	2 - 2

Layer 2/3 (First Order Cortex, V1)



TO	FROM				
	Units	Layer 4 V1	Layer 2/3 V1	Layer 2/3 V1	Layer 2/3 interneurons V1
SOMA					
Channel type					
Reverse potential	mV				
Conductance	pS				
Synaptic weight	$10^6/cm^2$				
Gaussian Spread	σ				
Axonal delay	ms				
Channel $\tau^r - \tau^l$	ms				
PROXIMAL DENDRITE					
Channel type		AMPA	AMPA	NMDA	GABA
Reverse potential	mV	0	0	0	-70
Conductance	pS	0.09	0.09	0.1	2.461
Synaptic weight	$10^6/cm^2$	2	0.1	0.01	0.3
Gaussian Spread	σ	0.3	1.3	1.3	0.8
Axonal delay	ms	1	0.1	0.1	0.1
Channel $\tau^r - \tau^l$	ms	2 – 2	0.1 – 2	0.7 – 80	1 – 7

Supplementary Table 3. Connections of cellular stages of the first-order thalamocortical loop, and a description of synaptic currents parameters. In each table, (*) refers to modifiable weights, the first value indicating the maximal weight, and in parenthesis the baseline weight and learning rate, respectively (Equation 6 main paper), and (#) refers to depletable neurotransmitters, with in parenthesis the transmitter depletion ε and the transmitter recovery rate τ (in ms , Equation 7 main paper).